BETA-OXIDATION OF ADIPOSE-DERIVED FATTY ACIDS FUEL PTH-INDUCED BONE FORMATION

by
Nathalie Spita Alekos

A dissertation submitted to Johns Hopkins University in conformity with the requirements for the degree of Doctor of Philosophy

Baltimore, Maryland
June 2022

Abstract

The energetic costs of bone formation require osteoblasts to coordinate their activities with tissues able to supply fuel molecules. In the case of intermittent parathyroid hormone (iPTH) treatment, a therapeutic strategy used clinically to reduce fracture risk, the increase in bone formation is preceded by a change in lipid homeostasis. The sequence of these events led us to hypothesize that fatty acid β-oxidation is required for the anabolic actions of this therapy. In vitro, osteoblasts treated with PTH exhibited increases in oxidation of oleate, genes involved in fatty acid β-oxidation (RNA sequencing) and in the rate of oxygen consumption. Etomoxir, an irreversible inhibitor of the rate limiting enzyme in β-oxidation, attenuated the effect of PTH on oxygen consumption, indicating that fatty acid catabolism is key to this response. In vivo, iPTH-induced (100 μg/kg/d for six weeks) increases in trabecular bone volume were reduced by approximately 50% in mice lacking Cpt2, an obligate enzyme in β-oxidation, in osteoblasts (Cpt2$^{flox/flox}$; Ocn-Cre) when compared to control littermates. We speculated that the fatty acids necessary to fuel iPTH-induced bone formation are released from adipose tissue since acute PTH administration increased serum free fatty acids, induced the phosphorylation of hormone sensitive lipase in white adipose depots, and stimulated a rapid decrease in the respiratory exchange ratio, indicative of an increase in fatty acid oxidation. To test this hypothesis, mice lacking the PTH receptor in adipocytes (Pth1r$^{flox/flox}$; AdipoQ-Cre), or mice with impaired lipolysis due to the ablation of Atgl in adipocytes (Atgl$^{flox/flox}$; AdipoQ-Cre) were treated with

iPTH for six weeks.   When compared to control littermates, iPTH-induced acquisition of bone volume was severely blunted in each mutant mouse line. Dynamic histomorphometric analysis of Pth1r$^{flox/flox}$; AdipoQ-Cre and Atgl$^{flox/flox}$; AdipoQ-Cre mice revealed an impaired ability of iPTH to enhance the mineral apposition rate and the bone formation rate. Collectively, these data suggest that PTH's anabolic effect requires signaling in bone as well as in fat, wherein a lipolytic response in adipose tissue liberates fatty acids that are oxidized by osteoblasts to fuel bone formation.

Advisor: Ryan C. Riddle, PhD   Reader: Thomas L. Clemens, PhD
Associate Professor   Professor

Preface

There are many people in my life who guided me through this journey as a graduate student. If it weren't for them, this work, and my success, wouldn't have been possible. First and foremost, I want to thank my mentor, Ryan Riddle. He welcomed me into his lab at the end of my third year. I had already begun my thesis in another lab in an entirely different field yet, he welcomed me, giving me a space to freely learn and grow as a scientist. Because of his mentorship and scientific expertise, I was able to master a broad range of laboratory techniques, develop a strong ability to analyze data and ask scientific questions, and most importantly, develop into an independent thinker confident in my own abilities. I thank him endlessly for creating a supportive environment where students can grow, be themselves, and not be fearful of stumbling and making mistakes. I will endlessly be grateful to him for giving me a chance to become a successful scientist. I want to thank all other members of the Riddle and Clemens labs both past and present including, Priyanka Kushwaha, Naomi Dirckx, Jean Garcia-Diaz, Soohyun Kim, Zhu Li, Robert Tower, and Qian Zhang for their endless support and kindness. Thank you to Arby Abood (University of Virginia) for his assistance in the analysis of the RNA sequencing data (Chapter 2), Elizabeth Rendina-Ruedy (Vanderbilt) for providing the data from Seahorse analysis (Chapter 2), and Susan Aja (Johns Hopkins) for her assistance with the CLAMS experiment (Chapter 3).

anything. Yet, he encouraged me to do what I love because he would always be proud of me. Thank you to my dad for the endless love and encouragement, I hope I made you proud. Big thanks to my older brother, Alex, for always guiding me when it came to major life and adult decisions. He always believes in me and encourages me to reach for the stars.

The person that deserves the most acknowledgement, is my husband, Bobby. Not only did he want to marry me in the middle of my graduate studies, but he was an endless source of encouragement, stability, and support. There were countless difficult moments, long days, late nights, working on weekends and holidays, during the last six years. There were countless times I had doubt in my path, purpose, and in my abilities. Despite it all, he never wavered in his strong belief in me. Thank you for always being the certainty in a world full of doubt, pushing me to be my best but also reminding me it's okay to be imperfect. Thank you for always being by my side and choosing me to go through life with. Thank you to my extended family who provided an endless source of support and encouragement especially my brother in-law, Dimitri, YiaYia Mary Kapos, my Theia Julia Kapos, Theios Kostas Valelis, and Theia Eva Anifantis.

Thank you to all my incredible friends for all your love and support during the last six years. Without your endless encouragement and belief in me, I wouldn't have made it. Thank you to everyone who contributed to my growth as a person and a scientist, I will be forever grateful for your endless love, support, encouragement, mentorship, and guidance.

THIS PAGE IS INTENTIONALLY

LEFT BLANK

Table of Contents

List of Figures

Chapter 1

Introduction: The Relationship Between Lipid Metabolism and Osteoblast Function

1.1 Introduction to the Skeleton

Development of the mammalian skeleton and maintenance of its structure for the life of the organism requires the coordinated actions of two specialized cells. Osteoclasts, large multinucleated cells that are derived from the monocyte/macrophage lineage of hematopoietic cells, are responsible for the resorption of bone. After attaching to an exposed bone surface, osteoclasts acidify a resorption lacuna to dissolve the mineral fraction of bone and then secrete proteolytic enzymes that degrade the organic matrix component [1]. During the resorption process, growth factors trapped within bone matrix are released and trigger the recruitment of osteoblasts responsible for new bone formation [2, 3]. Derived from mesenchymal stem cells present in the bone marrow stroma, these cells are characterized by their cuboidal shape and abundance of rough endoplasmic reticulum necessary for the production of the collagen-rich bone matrix [4]. After building a packet of bone most osteoblasts will die by apoptosis, but small fractions will either become encapsulated within the bone matrix and fulfill regulatory functions as osteocytes or dedifferentiate and line bone surfaces. Known as bone remodeling, this process prevents the accumulation of old or damaged bone that may lead to fracture. In humans, peak bone mass is reached during the second decade of life as a result of net bone accrual during childhood,

when bone formation exceeds resorption and osteoblasts and osteoclasts act on different bone surfaces to maintain the overall shape of bones during longitudinal growth (known as modeling). A balance between formation and resorption then occurs in early adulthood. However, with advancing age or as a result of numerous endocrine pathologies, an acceleration of osteoclastic activity leads to bone loss as osteoblastic activity is unable to keep pace. As bone mass decreases and structure integrity deteriorates, the risk of fracture increases [5, 6].

The tremendous economic impact of osteoporotic fractures [7-9] and development of comorbidities after fracture [10-12] highlight the need to understand the genetic, cellular, and endocrine mechanisms that influence bone mass. With the renewed interest in intermediary metabolism in cancer [13-15] and the recognition that bone is not merely a structural organ acting as a reserve of minerals but also an endocrine organ that can influence systemic metabolism [16-21], research in the field of skeletal biology has coalesced over the last few years on the contributions of cellular metabolism to osteoblast function and bone formation. The field reasoned that if bone contributes to the regulation of metabolic homeostasis through the release of osteocalcin and other hormones [16, 21], then the availability of nutrients must be critical to osteoblast function. Indeed, hierarchical analysis of energy requirements of cellular function [22] suggest that the bone remodeling process is energy intensive due to the synthesis of large extracellular matrix proteins and the necessity of concentrating mineral ions for hydroxyapatite crystal formation. Evidence from both the laboratory and clinic

supports this hypothesis as caloric restriction during gestation or during postnatal life strongly influences the trajectory of both the accrual and the maintenance of bone mass [23-25]. Additionally, an increase in oxidative phosphorylation and the abundance of mitochondria appears to be a requirement for the differentiation of osteoblasts from marrow stem cells [26-29].

Osteoblasts harvest energy from a number of fuel molecules. Studies performed more than 50 years ago first highlighted the avidity of osteoblasts for glucose. Isolated osteoblasts or bone tissue explants from mice, rats, rabbits, and humans all used glucose to produce lactate even under aerobic conditions [30-34]. More contemporary studies indicated that glucose acquisition is mediated by glucose transporter-1 [35] and that metabolic programming of glucose utilization is adjusted according to the stage of differentiation [28, 36]. Cells of the osteoblast lineage also consume a significant amount of glutamine which is required for skeletal stem cell specification, can be catabolized by the tricarboxylic acid cycle to generate ATP, and serves as a regulatory signal to maintain endoplasmic reticulum health during stages of heightened protein synthesis [37, 38].

While lipid metabolism yields significantly more ATP than glucose or glutamine catabolism, its role in osteoblast function remains more controversial. Recent studies have highlighted the importance of fatty acid catabolism for normal bone formation [39, 40], but detrimental effects of lipids on osteoblast performance are also well known [41, 42].

3

1.2 Overview of Lipid Metabolism

The lipid molecules that support cellular metabolism are primarily derived from three sources: ingested fat, lipoproteins produced by the liver, and non-esterified fatty acids released by white adipose tissue (Fig 1.1). Postprandial triglycerides and cholesterol esters are broken down in the intestinal lumen by cholesterol esterases, pancreatic lipases, and bile salts. These molecules are then taken up by the enterocyte of the small intestine, re-esterified, and packaged with lipid-soluble vitamins, and apolipoproteins into chylomicrons. Chylomicrons enable water-insoluble fats and cholesterol to move through the lymphatic system and into the circulatory system. Engagement of the chylomicron by lipoprotein lipase (LPL) on capillary endothelium results in the hydrolysis of triglycerides and the delivery of fatty acids to target tissues [43, 44]. The chylomicron remnants containing cholesterol and apolipoproteins are then cleared by the liver [45].

In healthy individuals, the liver exhibits a nearly constant lipid flux. Chylomicron remnants and free fatty acids are taken up by the liver, while a portion of the circulating glucose taken up by the organ is used for de novo lipogenesis. Lipid molecules from each of these sources can be used to generate ATP in the liver or they can be packaged along with apolipoprotein (Apo) B-100, ApoC, and ApoE into very low-density lipoproteins (VLDL) on the endoplasmic reticulum. VLDL are released into the circulation and metabolized by target tissues in a manner similar to that of chylomicrons, with LPL hydrolyzing triglycerides to fatty acids that can be imported by cells. In this case, the remaining lipoprotein particle is further

metabolized to low density lipoprotein (LDL), which can be taken up by many tissues via the LDL receptor [44].

White adipose tissue is the primary storage depot for excess calories. Non-esterified fatty acids are taken up by adipocytes, esterified and stored as triglycerides, while glucose is metabolized to acetyl-CoA and then used as a substrate for *de novo* fatty acid synthesis. When energy expenditure exceeds caloric intake or in response to a number of lipolytic hormones, the stored triglycerides can be hydrolyzed to glycerol and free fatty acids that are released into the circulation to be used for β-oxidation in other organs, including the skeleton. Lipolysis is mediated by the stepwise action of three lipases (illustrated in Fig 1.2). The rate limiting enzyme, adipose triglyceride lipase (ATGL), catalyzes the first reaction by hydrolyzing triacylglycerols at the sn-2 position to diacylglycerol and one fatty acid. Diacylglycerides are then preferentially hydrolyzed by hormone sensitive lipase (HSL) at the sn-3 position to yield a second free fatty acid [46]. Monoacyglycerol lipase (MGL) catalyzes the final reaction generating glycerol and a third fatty acid [47]. Most free fatty acids released into circulation are bound by albumin [48].

The intracellular metabolism of fatty acids taken up by cells depends on chain length. Short-chain (1-6 carbons) and medium-chain (7-12 carbons) fatty acids are produced by the bacterial fermentation of dietary fiber or the ingestion of dairy products. These lipids are primarily metabolized by enterocytes or by hepatocytes

[47]. Long-chain fatty acids (13-21 carbons) are transported into cells by specific transporters (discussed below) but have limited solubility in the cytosol. To increase solubility, trap fatty acids in the cell, and produce a high energy thioester necessary for the next steps of catabolism, long-chain fatty acyl-CoA ligases catalyze the formation of fatty acyl-CoA in a reaction that requires the hydrolysis of 1 ATP to AMP. Acyl-CoA must then be transferred to the mitochondria by a carnitine exchange system to undergo β-oxidation. Carnitine palmitoyltransferase 1 (CPT1), the first and rate-limiting step in this process, is located on the outer mitochondrial membrane and catalyzes the replacement of CoA with carnitine. Acyl-carnitines are recognized and transferred by carnitine-acylcarnitine translocase into the mitochondria matrix where carnitine palmitoyltransferase 2 (CPT2) reverses the reaction of CPT1 and regenerates Acyl-CoA. The four reaction β-oxidation process removes 2 carbons from the carboxy end of the acyl-CoA to generate acetyl-CoA, 1 NADH and 1 $FADH_2$ that are transferred to the TCA cycle and electron transport chain for the generation of ATP (Fig 1.2). Successive rounds of β-oxidation are necessary to fully metabolize long-chain fatty acids [49].

Very long chain fatty acids (more than 22 carbons) can also be used to generate ATP but must be chain-shortened in peroxisomes before they can enter the mitochondria [50]. Multi-functional peroxisomes encase more than 50 enzymes, with more than half involved in fat metabolism, in a single lipid bilayer. As in long chain fatty acid metabolism, very long chain fatty acids are first converted to acyl-CoAs in the cytosol. The fatty acyl-CoA is then transported into

the peroxisome by members of the ATP binding cassette transporter D subfamily. Peroxisomal oxidation also involves four reactions but utilizes a separate set of enzymes to shorten the fatty acid chain and is not as efficient at ATP generation as there is no respiratory chain. Indeed, while the $FADH_2$ produced by one round of mitochondrial β-oxidation yields 2 ATP, the electrons from $FADH_2$ produced by peroxisomal oxidation are donated to oxygen to form H_2O_2. For this reason, chain shortened fatty acids can be shuttled to the mitochondria for further metabolism via β-oxidation.
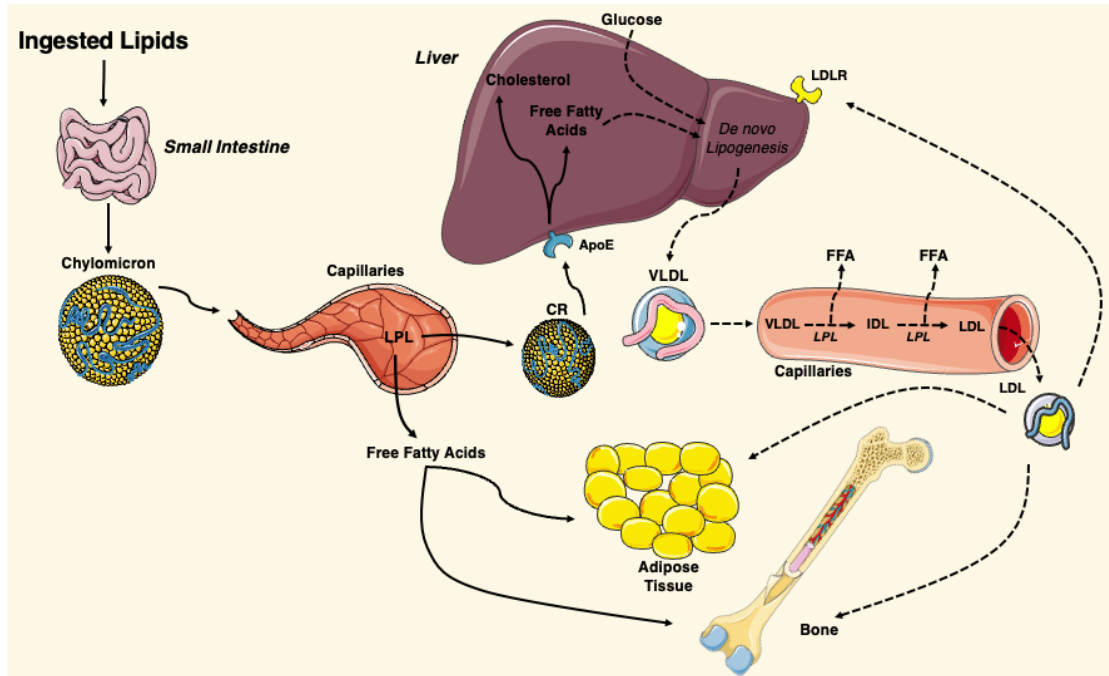
Figure 1.1 Overview of tissue-targeted lipid metabolism. Ingested lipids are broken down in the intestinal lumen and internalized by enterocytes of the small intestine. The water insoluble triglycerides and cholesterol are repackaged into chylomicrons and travel through the lymphatic system and into the circulatory system where they engage lipoprotein lipase (LPL) on the surface of capillary endothelial cells. The hydrolyzed triglycerides result in release of free fatty acids that are taken up by adipose tissue and the skeleton. The remaining chylomicron remnants (CR) are cleared by the liver via the apolipoprotein E (ApoE) receptor. CR-derived cholesterol and free fatty acids and circulating glucose are used for de novo lipogenesis, generating ATP for the liver, or repackaged into very low-density lipoproteins (VLDL). VLDL particles are released into the circulation where they engage LPL and release free fatty acids, which are also available for uptake. The remaining low-density lipoprotein (LDL) are internalized by cells expressing the low-density lipoprotein receptor (LDLR) including adipocytes and osteoblasts. This figure was created using Servier Medical Art image templates under a Creative Commons Attribution 3.0 Unported License.

1.3 Mechanisms of Lipid Uptake by Osteoblasts

Although they are smaller than those evident in adipocytes, most cells contain a lipid droplet that can presumably be used to generate ATP via β-oxidation. Histological studies indicate that both mature osteoblasts and differentiating osteoblast progenitors contain stored lipid [51, 52], but these stored lipids do not appear to be a major energy source for mature osteoblast function. Kim and colleagues [39] ablated the expression of ATGL in cultures of calvarial osteoblasts and mature osteoblasts and osteocytes in vivo (Atgl$^{flox/flox}$; Osteocalcin-Cre), which should eliminate intracellular lipolysis, but did not find a defect in either in vitro osteoblast performance or bone structure in vivo. Therefore, osteoblasts appear to require extracellular lipid sources.

A combination of in vivo and in vitro studies have examined the uptake of circulating lipoproteins and free fatty acids by the osteoblast and the skeleton. In perhaps the most comprehensive study, Neimeier and colleagues [53] modelled postprandial lipoprotein uptake by intravenously injecting fluorescent- or ^{125}I-labelled chylomicron remnants into mice. Skeletal uptake was 17% that of liver but was greater than other catabolic organs including muscle and heart. Importantly, chylomicron remnant uptake by the osteoblast-/osteocyte-enriched femoral diaphysis was greater than that of bone marrow, indicating the skeletal acquisition was not simply carried out by marrow adipocytes. Osteoblasts also appear to take up of LDL and VLDL and acquisition can be enhanced by co-

9

administration with ApoE, but these studies have primarily been performed in cultured osteoblasts [54-56]. Skeletal uptake of fatty acids was assessed in vivo by Bartelt et al [57] and Kim et al. [39] after delivering ^{3}H-linoleic acid and ^{14}C-palmitic acid or ^{3}H-bromo-palmitate, respectively, via oral gavage. Similar to the uptake of chylomicron remnants, these studies revealed that skeletal acquisition of fatty acids is comparable to tissues that are more classically associated with fatty acid metabolism. Together, these studies highlight a potential role of bone in fatty acid metabolism and postprandial clearance of fat from the circulation.

The identity and requirements for specific receptors and transporters that allow osteoblasts to take up fatty acids and lipoproteins (Fig 1.2) need additional study, but experimental data exists for a number of possible mechanisms. Consistent with osteoblastic uptake of chylomicron remnants and lipoproteins, osteoblasts express the low-density lipoprotein receptor (LDLR) and low-density lipoprotein receptor-related protein-1 (LRP1) [58, 59]. Interpretation of the skeletal phenotypes of mice engineered to be deficient for LDLR (LDLR^{-/-}) requires care as studies have reported both reduced [60] and elevated bone volume [61] relative to wildtype mice. Both in vivo [60] and in vitro [62] analyses indicate that the actions of the LDLR are important for osteoblast function as its ablation results in reductions in the expression of gene markers of osteoblastic differentiation. These data accord with the ability of LDL to stimulate cell growth and sustain responsivity to anabolic stimuli in osteoblasts cultured under serum-free conditions [63]. The

discrepancies in bone volume observed in vivo are likely be related to the requirement for LDLR during osteoclast differentiation [60, 61].

LRP1 can facilitate the endocytosis of triglyceride and cholesterol containing chylomicron remnants in cultures of osteoblastic cell models [58] and polymorphisms in the gene encoding this receptor are associated with bone mineral density [64]. However, analysis of an osteoblast-specific knockout mouse (Lrp1$^{flox/flox}$; Runx2-Cre) revealed an osteopenic phenotype but there was no effect on systemic lipoprotein clearance or osteoblasts' ability to sequester fatty acids [65]. While the bone phenotype has been attributed to marked increases in osteoclastogenesis [65], the sustained ability to take up lipoproteins could be due to the engagement of other LDLR family members. LRP5 and LRP6 are most typically associated with the propagation of signaling in response to Wnt ligands [66], but these receptors also have the capacity to bind and mediate the endocytosis of lipoproteins and chylomicron remnants [67, 68]. Cultured osteoblasts rendered deficient for LRP5 also retained the ability to take up LDL [56], indicating that combinatorial genetic studies wherein the expression of multiple LRP receptors are simultaneously ablated may be necessary to discern receptor function in lipid particle uptake.

Osteoblasts also take up high density lipoproteins (HDL) and express Scarb1 (also referred to as SR-B1) [55], the major receptor for high-density lipoproteins [69]. Some epidemiological studies suggest a positive correlation between BMD and HDL levels, but others have reported contradictory results (see [70] for a

11

comprehensive review). Interpretation of an association between HDL and bone mass in animal models has been equally challenging. Martineau and colleagues [71] reported that Scarb1 null mice display increases in HDL-associated cholesterol and increases in femoral bone volume and mineralization at 2 and 4 months in association with increases in osteoblast surface and bone formation rate, which suggests a detrimental effect of HDL on skeletal homeostasis. However, it remains possible that the high bone mass phenotype in these mice is due to an increase in serum adrenocorticotropin (ACTH), which has anabolic effects on osteoblasts [72, 73]. Furthermore, control and Scab1 deficient osteoblasts exhibited similar levels of HDL-cholesterol [71]. A follow-up study by this same group reported that Scarb1 deletion in MSCs increased osteoblastogenesis but decreased terminal osteocyte differentiation as vertebral osteocyte density was modestly decreased in the mutant mice [74]. However, a more recent study contradicted these findings and reported Scarb1 null animals to be osteopenic in the veterbrae at 16 weeks with decreases in resorption and formation markers, and diminished osteoblast differentiation markers both in vitro and in vivo [73]. Hereto, alterations in bone volume were attributed to dose dependent effects of ACTH on bone. Similarly, mice with impaired HDL synthesis displayed reduced bone mass and impaired differentiation [75] suggesting a necessity for HDL in osteoblast function. Further in vivo studies using genetic models with osteoblast specific deletions are required to further delineate Scarb1 function and a role for reverse cholesterol transport will need to be considered.

12

Osteoblasts also express the receptors necessary to take up and metabolize free fatty acids. CD36 is a two-transmembrane glycoprotein receptor that binds long-chain fatty acids as well as oxidized low-density lipoprotein (oxLDL) and facilitates their transport into the cell [55, 76]. While direct studies of its effect on fatty acid uptake have not yet been completed, CD36 null mice exhibit a low bone mass phenotype secondary to impaired bone formation [77] that implies fatty acid uptake is essential for osteoblast function. The SLC27 family of fatty acid transport proteins (also referred to as FATP1-6), may also contribute to osteoblasts acquisition of long-chain fatty acids for oxidation [76, 78], as multiple family members are expressed by primary osteoblasts [40].
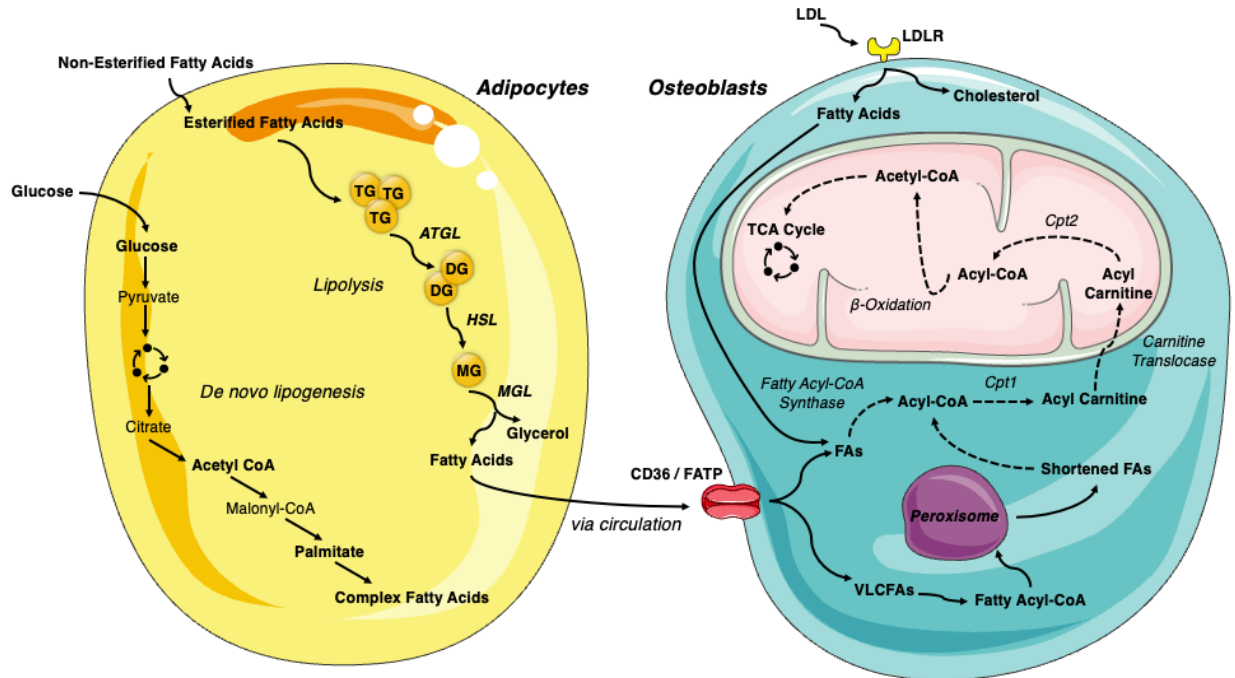
Figure 1.2 Lipid- flux between the adipocyte and osteoblast. White adipose tissue is the primary storage depot of lipids during excess consumption, which are subsequently released when energy expenditure exceeds caloric intake. Esterified fatty acids are stored in the adipocytes as triglycerides and are hydrolyzed by the rate limiting enzyme, adipose triglyceride lipase (ATGL), into diglycerides. Diglycerides are hydrolyzed into monoglycerides by hormone sensitive lipase (HSL) and further into fatty acids by monoacyglycerol lipase (MGL), which are then released into circulation. Adipocyte uptake of glucose is metabolized to acetyl-CoA and used for *de novo* fatty acid synthesis. These newly synthesized fatty acids are another lipid source for the osteoblast. LDL-derived fatty acids and uptake of circulating free fatty acids via CD36/FATPs are vital energy sources for the osteoblast. These internalized free fatty acids are converted into acyl-CoA by fatty acyl-CoA synthase. Very long chain fatty acids (VLCFAs) (more than 22 carbons) are first shortened by the peroxisome. Acyl-CoA is transported to the mitochondrial matrix by a carnitine exchange system in order to undergo β-oxidation. The product, acetyl-CoA is

14

transferred to the TCA cycle and electron transport chain for generation of ATP. This figure was created using Servier Medical Art image templates under a Creative Commons Attribution 3.0 Unported License.

1.4 Requirement for Fatty Acid Oxidation in Osteoblasts

Many studies have examined the essential and negative roles of various saturated and unsaturated fatty acids and their role in bone cells (reviewed in [79]). However, direct examination of the requirement for fatty acid oxidation during postnatal bone acquisition and bone repair has been examined in two studies. In the first, Kim and colleagues disrupted the expression of CPT2 in mature osteoblasts and osteocytes (Cpt2$^{flox/flox}$; Osteocalcin-Cre) [39]. As noted above, CPT2 catalyzes an obligate step in fatty acid β-oxidation and was selected for ablation in this model because it is encoded by a single gene (three isoforms of *CPT1* are present in mammalian genomes). The skeletal phenotype of the mutant mice was sexually dimorphic, with male mice fed a normal chow diet exhibiting only a transient decrease in trabecular bone volume in the distal femur and L5 vertebrae at 6 weeks of age. By contrast, female mutants exhibited defects in trabecular bone volume in the distal femur and L5 vertebrae and an expansion of cortical bone tissue area at both 6 and 12 weeks. This discrepancy between sexes appears to be related to a greater ability to adjust fuel utilization in males, as male mutants exhibited an increase in femoral glucose uptake that was not evident in

female mutants. The greater inhibition of osteoblast performance and inhibition of glucose uptake in CPT2 mutant osteoblasts treated with estrogen may explain the sex differences in metabolic flexibility. Interestingly, both male and female CPT2 mutants exhibited an increase in serum free fatty acid levels, which suggests that disrupting fatty acid utilization by osteoblasts and osteocytes is sufficient to alter lipid homeostasis [39].

In the second study, van Gastel et. al. [40] identified a role for fatty acid utilization during fracture healing and the specification of skeletal cell fate. During the bone healing process, endochondral ossification is initiated by periosteal progenitor cells that differentiate to chondrocytes and form an avascular, cartilaginous callus. The callus is subsequently invaded by the vasculature [80] and replaced by bone [81, 82]. Blood vessels are expected to deliver the oxygen, nutrients, and growth factors necessary to drive bone formation.   Through biochemical assays and the reanalysis of an existing single cell RNAseq study of skeletal progenitors [83], Van Gastel et. al. [40] reported that chondrocytes express low levels of CPT1a and high Glut1 levels as well as elevated lactate production, which suggests that glycolysis meets the chondrocyte's energy needs. On the other hand, osteoblasts expressed high levels of Glut1 and CPT1a, exhibited higher levels of oxygen consumption, and an increased ability to metabolize palmitate, indicating a reliance on fatty acid oxidation. Importantly, knocking down the expression of CPT1a prevented the differentiation of skeletal stem cells to osteoblasts while local injection of free fatty acids during fracture repair increased

the amount of bone formed in the callus and reduced the amount of cartilage. Mechanistic studies demonstrated that reduced fatty acid availability increased the activation of FOXO3, which in turn activated SOX9 and chondrogenic specification. Taken together, these studies highlight the requirement for fatty acid β-oxidation for bone-forming osteoblasts in bone repair and skeletal development.

Evidence for a role of peroxisomal lipid oxidation in bone is largely based on the phenotypes evident in patients affected by peroxisomal disorders and global knockout models. Human and mouse genetic studies have identified 14 peroxin genes (*PEX1- PEX26*) that encode proteins necessary for either the formation of peroxisomes or the transport of cargo into the organelle. Loss of function mutations in peroxin genes, which occur at a rate of approximately 1 in 50,000 births, result in autosomal recessive peroxisomal biogenesis disorders (PBD) that affect a number of organ systems. Individuals with more severe PBD subtypes often exhibit craniofacial anomalies, short stature, and limb length discrepancies. Less severe subtypes have been associated with reductions in bone mineral density and an increased susceptibility for non-traumatic fractures [84-86]. In the mouse, hypomorphic alleles for Pex7 leads to a reduction in longitudinal growth and impaired ossification of the digits [87], while a global knockout resulted in delayed ossification at multiple skeletal sites [88]. Additional mouse genetic studies will be necessary to fully delineate the role of peroxisomes in skeletal tissue maintenance and function.

1.5 Pathways Regulating Fatty Acid Oxidation

If fatty acid metabolism is used to generate the ATP necessary for osteoblast function, then metabolic flux in this pathway should be regulated by the signals that drive bone formation. Indeed, two of the most potently anabolic pathways, Wnt signaling and parathyroid hormone signaling, appear to drive fatty acid oxidation.

Wnt signaling

The anabolic effects of Wnt signaling on skeletal development, repair, and homeostasis have been well studied [89, 90], and a number of studies have now demonstrated that the pathway coordinates the intermediary metabolism of the osteoblast with the energetic demands of bone formation [38, 91-93]. LRP5 and LRP6 act as co-receptors for the Frizzled receptors that propagate Wnt signals and lead to the stabilization and activation of β-catenin [66]. While the osteoblast-specific ablation of either receptor (Lrp5$^{flox/flox}$; Osteocalcin-Cre and Lrp6$^{flox/flox}$; Osteocalcin-Cre) results in decreases in bone mineral density and vertebral trabecular bone volume [94], Frey and colleagues [56] found that the LRP5 mutants also exhibited increases in fat mass and serum triglycerides and free fatty acids, suggestive of a disruption in fatty acid utilization. Indeed, analysis of gene expression in cultured osteoblasts by microarray revealed that LRP5-deficient osteoblasts exhibited a downregulation of multiple genes involved in mitochondrial long-chain fatty acid β-oxidation. The effects of these changes in gene expression

on β-oxidation were confirmed by examining the oxidation of oleate, which was reduced in LRP5 deficient osteoblasts when compared to control. Expression of LRP5 with a gain of function mutation (Lrp5[G171V]) in osteoblasts produced the opposite phenotype, as the transgenic mice exhibited increases in bone volume and oxidative gene expression as well as decreases in fat mass, serum triglycerides, and fatty acids.

Subsequent genetic studies revealed that Wnt-mediated regulation of fatty acid oxidation proceeds via a β-catenin-dependent mechanism. Frey et al. [95] found that only Wnt ligands that increase the abundance of β-catenin in cultured osteoblasts, increase the capacity to fully oxidize oleate to carbon dioxide. Since constitutive ablation of β-catenin in osteoblasts results in early lethality [96] in vivo, the generation of an inducible β-catenin knockout mouse (Ctnnb[flox/flox]; Osteocalcin-CreER[T2]) was necessary to examine the transcription factor's effects on fatty acid oxidation. In this model, the temporal ablation of β-catenin resulted in high-turnover bone loss as well as increased fat mass and the development of insulin resistance. Additionally, the expression of genes involved in long-chain fatty acid oxidation and the ability to oxidize oleate were reduced in β-catenin deficient osteoblasts in vitro, while serum fatty acid levels were increased in the mutants in vivo. These studies have expanded the role of canonical Wnt-signaling to influencing fatty acid utilization and coordinating whole-body energy homeostasis

As indicated above, a number of contemporary studies suggest that Wnt signaling also regulates glucose and glutamine utilization by the osteoblast. Wnt signaling through LRP5 increased aerobic glycolysis in the ST2 bone marrow stromal cell line [93] and mice engineered to overexpress Wnt7b in osteoblasts exhibit dramatic increases in bone volume, but simultaneously ablating the expression of Glut1 completely inhibited the increase in bone accrual [92]. Similarly, Wnt signaling induced glutamine catabolism via the TCA cycle [38] which in turn stimulated the expression of genes involved in protein synthesis. Interestingly, these effects were mediated by the activation of mTOR and not β-catenin [92, 93, 97]. Thus, the metabolic actions of Wnt signaling appear to depend on the specific downstream pathways that are activated.

Parathyroid Hormone Signaling

In this thesis, we will be focusing on the anabolic effects of parathyroid hormone (PTH) and the requirement for fatty acid oxidation. PTH is a master regulator of serum calcium that signals in the bone, kidney and intestine to increase calcium levels. Intermittent administration of human recombinant PTH (1-34) is now used to reduce the occurrence of vertebral and non-vertebral fractures and to increase bone mineral density in postmenopausal osteoporotic women [98]. This therapeutic effect is mediated by PTH's ability to decrease apoptosis of mature osteoblasts [99], activate preexisting bone lines cells [100, 101], and stimulate osteoprogenitor recruitment [102].

The first indication that PTH might influence fatty acid oxidation were completed by Adamek and colleagues [103]. In this study, PTH increased palmitate oxidation in specific cell populations isolated from bone by enzymatic digestion, while 1,25-Dihydroxycholecalciferol administration produced a more dramatic effect in multiple cell fractions. Catherwood et al. [63] demonstrated that the inclusion of LDL or VLDL in a basic medium was sufficient to support the proliferative response of rat ROS17/2.8 to PTH. In a more recent work, Esen and colleagues [104] used Seahorse technology, radiolabeled metabolites, and MC3T3-E1 cells to examine the effect of PTH on osteoblast metabolism. These studies demonstrated that PTH stimulates glucose uptake and increases lactate production but reduces the shuttling of glucose-derived carbon to the TCA cycle. These findings suggest that the increased rate of oxygen consumption after PTH administration is due to the oxidation of another fuel source, perhaps fatty acids imported from serum. While additional studies will be necessary, this paradigm is congruent with findings from Maridas et. al [105] that tracked the transfer of fatty acids from adipocytes to bone marrow stromal cells as well as the established ability of PTH to induce lipolysis in adipocytes [106]. Likewise, the reduction in marrow adipose tissue volume after intermittent PTH treatment suggests that marrow adipocytes represent an energy reserve that provides fatty acids to fuel the anabolic activity of osteoblasts [105, 107]. The finding that PTH can increase bone mass even under conditions of caloric restriction suggests that the relationship between PTH activity and metabolism is more complex and worthy of further study [105].

1.6 Summary and Conclusions

The skeleton is a dynamic and metabolically active organ with the capacity to influence whole body metabolism. This newly recognized function has propagated interest in the connection between bone health and metabolic dysfunction. Osteoblasts, the specialized mesenchymal cells responsible for the production of bone matrix and mineralization, rely on multiple fuel sources. The utilization of glucose by osteoblasts has long been a focus of research, however, lipids and their derivatives, are increasingly recognized as a vital energy source. Osteoblasts possess the necessary receptors and catabolic enzymes for internalization and utilization of circulating lipids. Disruption of these processes can impair osteoblast function, resulting in skeletal deficits while simultaneously altering whole body lipid homeostasis. Mitochondrial long chain fatty acid oxidation is of sufficient importance for osteoblast function that 1) genetic impairments in this metabolic pathway led to alterations in whole body lipid homeostasis and 2) signaling pathways essential to bone mass accrual influence fatty acid metabolism. Future studies should be directed towards more fully delineating the mechanisms of fatty acquisition by osteoblasts. These studies will require the development of new genetic mouse models in which transporters are disrupted specifically in the osteoblasts as global knockout models exhibit disturbances in metabolism that may indirectly influence bone remodeling. Determining the mechanisms by which osteoblasts convey their need for sufficient fatty acid supply to other tissues is equally vital. In this regard, the emergence of bone as a hormone-producing tissue

is likely to provide key insights into the responsible endocrine networks. The increased recognition of bone as a lipid-utilizing tissue is likely to lead to a renewed interest in this area.   Together these studies will provide a deeper understanding of the intimate interaction between the skeleton and metabolism and hopefully lead to treatment strategies that simultaneously reduce the burden of obesity and metabolic disease and preserve skeletal homeostasis

Chapter 2

PTH-induced alterations in fatty acid oxidation in osteoblasts is essential for its anabolic response

2.1 Introduction, rationale, and results

Osteoblasts, derived from mesenchymal progenitors in the bone marrow and periosteum, are responsible for the synthesis, secretion and deposition of the collagen-rich, mineralized matrix composing the skeleton. This synthesis of large matrix proteins and concentration of mineral ions for hydroxyapatite crystal formation by osteoblasts is an energetically demanding process during growth but also in the lifelong maintenance of skeletal integrity. These cells possess an abundant of well-defined rough endoplasmic reticulum and increases in mitochondria and oxidative phosphorylation are required for differentiation of osteoblasts from marrow stem cells [4, 26-29, 108]. To sustain these high energetic costs, osteoblasts utilize various fuel sources to satisfy this demand.

The first studies on the energy metabolism of osteoblasts were completed over 50 years ago and were primarily focused on glucose utilization. These studies showed that metaphyseal bone slices take up significant amounts of glucose, even greater than liver explants however with a much lower level of oxygen consumption suggesting glycolysis is dominant to oxidation of glucose [32, 33, 109, 110]. More recent studies using better defined genetic models and primary cells cultures have demonstrated the conversion of glucose to lactate by immature osteoblasts [28,

36, 93, 111, 112]. Additional genetic studies have demonstrated that glucose uptake by the Glut1 transporter is necessary for early osteoblast commitment and regulates the expression of Runx2 [35]. Osteoblasts also rely on amino acids. A recent study suggested that glutamine metabolism, the most prevalent amino acid, is necessary for osteoprogenitor function and bone formation but, whose function is mainly for establishing redox homeostasis [113]. The requirement and utilization of fatty acids has only been recently receiving more attention despite a study completed over 30 years ago revealing that osteoblasts can metabolize fatty acids, accounting for nearly 40 to 80% of energy they derive from glucose [103]. In fact, oxidation of a complete molecule of palmitate (C16:0) yields over two times the ATP generated by one molecule of glucose, demonstrating its efficiency. The requirement for fatty acid oxidation has been discussed in Chapter 1 and studies have examined substrate requirement in osteoblast function. Previous work in our lab identified considerable uptake of fatty acids in the skeleton [39]. Additionally, mitochondrial long chain fatty acid β-oxidation increases dramatically during osteoblast differentiation [56]. However, no studies have examined the requirement of fatty acids in vivo during states of heightened anabolism.

The intermittent administration of teriparatide (recombinant human PTH_{1-34}), is a well-established therapeutic agent for treatment of osteoporosis as it reduces fracture risk and increases bone mineral density in post-menopausal osteoporotic women [98, 114]. Many studies using rodent models have investigated the physiological basis of PTH's anabolic effect on bone. Intermittent

PTH treatment increases osteoblast numbers [115], reduces bone cell apoptosis [99], stimulates osteoprogenitor recruitments [102], and reactivates quiescent bone lining cells [100], actions leading to an anabolic effect on bone. This anabolic response is due to PTH directly acting on osteoblasts via the PTH receptor (Pth1r) [116]. Pth1r is a G-protein coupled receptor that leads to the activation of primarily $G_s\alpha$, activating adenylyl cyclase which generates 3',5'-cyclic adenosine 5'-monophosphate (cAMP). This second messenger activates PKA which translocates to the nucleus and phosphorylated CREB regulates the transcription of genes containing a cAMP-responsive element (CRE) [116]. PTH can also activate PKC but is not required for its osteoanabolic actions [117]. It is important to note that in addition to its anabolic effects by its actions on osteoblasts, PTH triggers osteoclastogenesis by stimulating osteoblast expression of receptor activator of nuclear factor-κB ligand (RANKL) and decreasing osteoprotegerin (OPG), a soluble RANKL decoy [118-120]. RANKL binds to RANK on the surface of hemopoietic precursors, promoting osteoclasts differentiation and survival. PTH's regulation leads to an increase in the RANKL/OPG ratio increasing bone resorption by osteoclasts, leading to its catabolic effects [121]. Although intermittent treatment of PTH has an anabolic effect on bone, chronic exposure to PTH, as in hyperparathyroidism, has a catabolic affect [122] and increases in RANKL in this disease are positively correlated with bone resorption markers and bone loss [123].

In addition to PTH's stimulatory effects, it's control of intermediary metabolism in the osteoblast has been demonstrated. As discussed in Chapter 1, Esen and colleagues [111] reported PTH is a strong inducer of lactate production in primary osteoblasts and MC3t3-E1 cells and also demonstrated that dichloroacetate, a PDK1 inhibitor that stimulates glucose oxidation while decreasing glycolysis, inhibited PTH induced bone formation in vivo. However, interpreting these results requires care as dichloroacetate also inhibits the oxidation of fatty acid [124-126] and because it was delivered systemically in this study, an indirect effect cannot be ruled out. Additionally, this study reported a paradoxical increase in oxygen consumption in PTH treated osteoblasts while there was a reduction in glucose oxidation [111]. These alterations in metabolic activity suggest that the utilization of other metabolites is also influenced by PTH and may be necessary for PTH's anabolic effects.

To comprehensively examine the effects of PTH on osteoblast metabolism, we performed a non-biased screen of PTH-induced changes in gene expression. Calvarial osteoblasts were isolated from newborn mice, differentiated for seven days, and then treated with 100 nM PTH$_{1-34}$ overnight. RNA isolated from these cultures was then analyzed by RNA sequencing. Sequencing analysis revealed the differential expression of over 7,000 genes. Pathway analysis revealed that genes involved in expected pathways including Wnt, TGF-beta, and HIF-1 were increased with PTH treatment. With regards to metabolism, three gene families were upregulated. Specifically, there were 32 upregulated genes in oxidative

phosphorylation involved in the electron transport chain. The upregulation of 27 genes involved in insulin signaling were primarily related to the utilization of glucose. Of note, 17 genes were upregulated involved in adipocytokine signaling which were involved in fatty acid utilization. PTH's metabolic effects on osteoblasts proved extensive as there was a total of 149 upregulated genes involved in metabolic pathways (Fig 2.1).
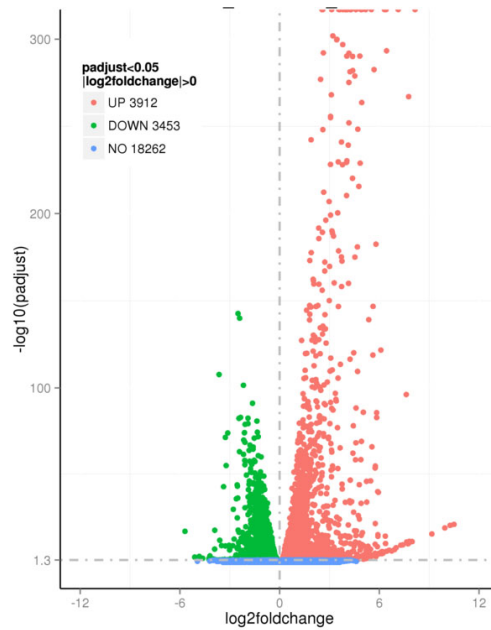
Pathway		Gene Ct	p value
Oxidative Phosphorylation	mmu00190	32	3.70E-05
Insulin Signaling	mmu04910	27	2.80E-03
Adipocytokine Signaling	mmu04920	17	2.90E-03
HIF-1 Signaling	mmu04066	21	4.40E-03
Wnt Signaling	mmu04310	26	6.20E-03
TGF-beta Signaling	mmu04350	18	6.73E-03
Metabolic Pathways	mmu01100	149	8.80E-02

Figure 2.1 Pathway analysis of RNA sequencing from PTH- treated primary osteoblast cultures. Overnight 100 nM PTH$_{1-34}$ treatment resulted in the differential expression of over 7,000 genes including 149 increased genes involved in metabolic pathways including glucose and fatty acid utilization.

Heat map analysis highlights the genes altered in fatty acid and glucose metabolism. Genes involved in the fatty oxidation pathway were already highly expressed in osteoblasts but increased further with PTH treatment including Acsl 1, Acsl 3, Acsl 4, long chain acyl-CoA synthetases which are essential enzymes that activate fatty acids essential for synthesis and degradation via β-oxidation. There are a few genes upregulated in glucose metabolism including Hk2 and Slc2a1 (Glut1) (Fig 2.2). Overall, these data revealed that intermediary metabolism is strongly affected by PTH and provided a basis for investigation into the effects of PTH on fatty acid metabolism. Having established that PTH alters the metabolic profile of osteoblasts in vitro, we next sought to directly examine PTH's effect on the oxidation of fatty acids and glucose. Primary osteoblasts were differentiated for seven days and then treated with vehicle control or 100 nM PTH$_{1-34}$ treatment overnight followed by labelling of cells with either ^{14}C-oleate or ^{14}C-glucose for three hours. PTH induced a 20% increase in oxidation of ^{14}C-oleate but did not significantly alter oxidation of ^{14}C-glucose (Fig 2.3), which is in line with previous findings [111] and reveals the specificity of PTH's induced utilization of substrates. These data accord with RNA sequencing data that shows more genes involved in fatty acid metabolism were preferentially increased compared to glucose metabolism.
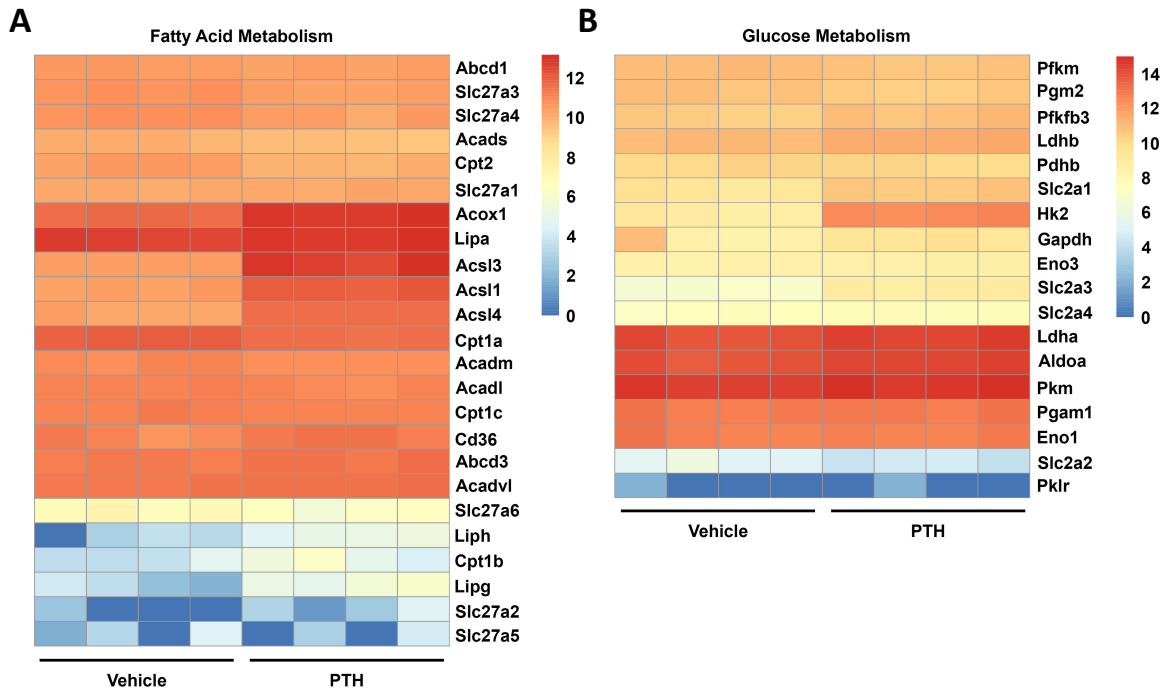
Figure 2.2 PTH treatment increased genes involved in fatty acid and glucose metabolism in vitro. (A) RNA sequencing from primary osteoblasts revealed that overnight 100 nM PTH$_{1-34}$ treatment further increased some highly expressed genes involved in fatty acid metabolism while also increasing, to a lesser extent, a number of genes involved in glucose metabolism (B).
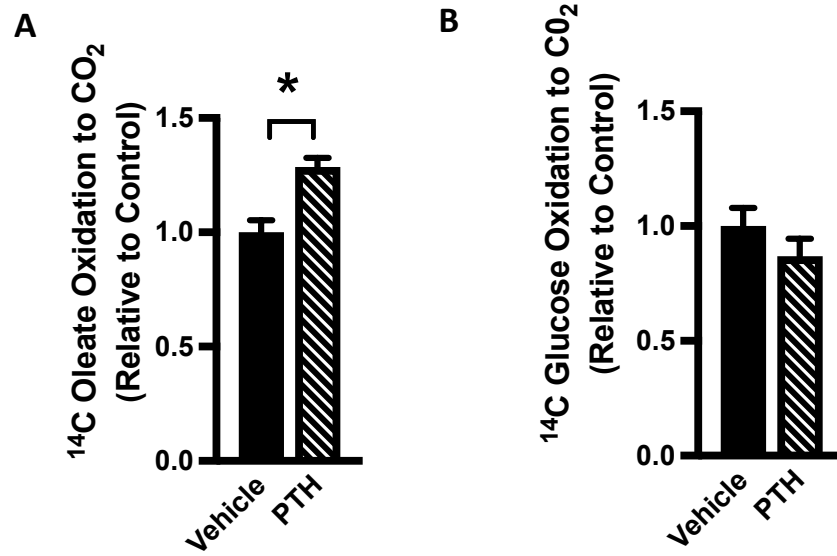
Figure 2.3 PTH increased fatty acid oxidation but not glucose oxidation in osteoblasts. Osteoblast primary cultures were treated with vehicle control or 100 nM PTH$_{1-34}$ overnight and labelled with ^{14}C-oleate or ^{14}C-glucose for three hours. PTH increased release of $^{14}CO_2$ in cells treated with ^{14}C-oleate but not ^{14}C-glucose. All data are represented as mean ± SEM. *$p < .05$

To further examine PTH's effect on intermediary metabolism, we assessed the oxygen consumption rate (OCR) and the extracellular acidification rate with a Seahorse XF96 extracellular flux analyzer. Cells were isolated from bone marrow stromal cells from adult murine long bones and adherent cells were differentiated into osteoblasts for seven days. Metabolic flux analysis demonstrated that 2-hour treatment with 100 nM PTH_{1-34} increased mitochondrial oxidative phosphorylation in mature osteoblasts. Treatment with 10 μM etomoxir (Eto) which inhibits fatty acid entry into the mitochondria via CPT1/2, abolishes the PTH-induced increase in the OCR (Fig 2.4). These results confirm that fatty acids are the substrates that are responsible for the increase in mitochondrial respiration.

These in vitro experiments demonstrated that PTH increases fatty acid oxidation in osteoblasts and that fatty acid mitochondrial oxidation is necessary for the PTH-induced increase in the oxygen consumption rate. We next wanted to understand the requirement for fatty acid oxidation in PTH's effect on matrix deposition in vitro. Previous work from our lab found that ablating the expression of carnitine palmitytranferase-2 (Cpt2), an obligate enzyme in β-oxidation, in mature osteoblasts and osteocytes, inhibited fatty acid oxidation and impaired the bone mass accrual in vivo [39]. Cells were isolated from neonatal calvaria from Cpt2[flox/flox] mice and were infected with adenovirus encoding Cre recombinase to disrupt the floxed allele or GFP as a control and differentiated for seven days. Maturing osteoblasts were then treated with vehicle control or 100 nM PTH_{1-34} every other day until Day 14 (total of 4 treatments). Osteoblasts were stained with

Sirius Red (SR) to assess collagen deposition and alkaline phosphatase (ALP), an early marker for osteoblast differentiation. Consistent with the previous results from our laboratory [39], ablation of Cpt2 resulted in decreased collagen deposition and alkaline phosphatase activity. In control osteoblasts, PTH treatment increased both markers compared to vehicle. However, PTH was unable to increase the osteoblastic markers in osteoblasts deficient for Cpt2 (Fig 2.5). These results were evidence that fatty acid oxidation in vitro is required for PTH-induced increases in matrix deposition.

By performing a series of in vitro experiments using primary osteoblasts, we characterized the metabolic profile of PTH-induced changes. Prior data from our lab, showed that osteoblasts rely on fatty acids as energy substrates during differentiation and that fatty acid oxidation is necessary for proper bone mass accrual. This reliance laid the groundwork for further studies on how PTH alters the metabolism of osteoblasts to initiate the agent's anabolic effects. Treatment of differentiated osteoblasts revealed transcriptional changes in genes related to fatty acid metabolism and glucose metabolism. However, PTH increased oxidation of oleate but not glucose. We also showed that PTH's increases in mitochondrial respiration is due to oxidation of fatty acids. Lastly, we established that fatty acid β-oxidation in osteoblasts is essential for PTH-induced increases in matrix deposition. These studies prove that PTH alters fatty acid metabolism in osteoblasts and may be essential for PTH's anabolic effect.
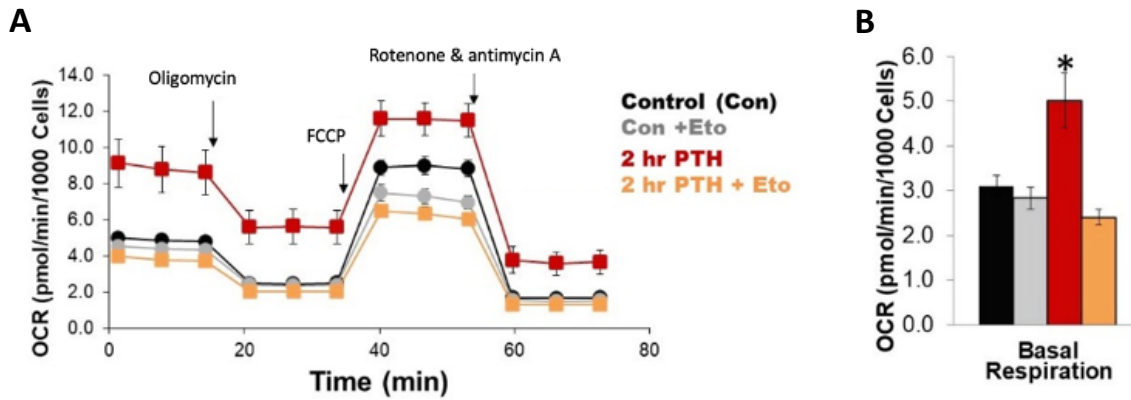
Figure 2.4 PTH increases mitochondrial fatty acid oxidation in osteoblasts. (A) Oxygen consumption rate of osteoblasts treated with vehicle control or 100 nM PTH_{1-34} for 2 hours with and without treatment of 10 μM etomoxir (Eto). (B) Basal mitochondrial respiration was calculated by subtracting non-mitochondrial respiration (measurement after rotenone and antimycin A injection) from measurements before oligomycin injection. Treatment with PTH for 2 hours increased oxygen consumption rate which was attenuated by Eto, an irreversible inhibitor of the rate limiting enzyme in β-oxidation. All data are represented as mean $\pm$ SEM. *$p < .05$.
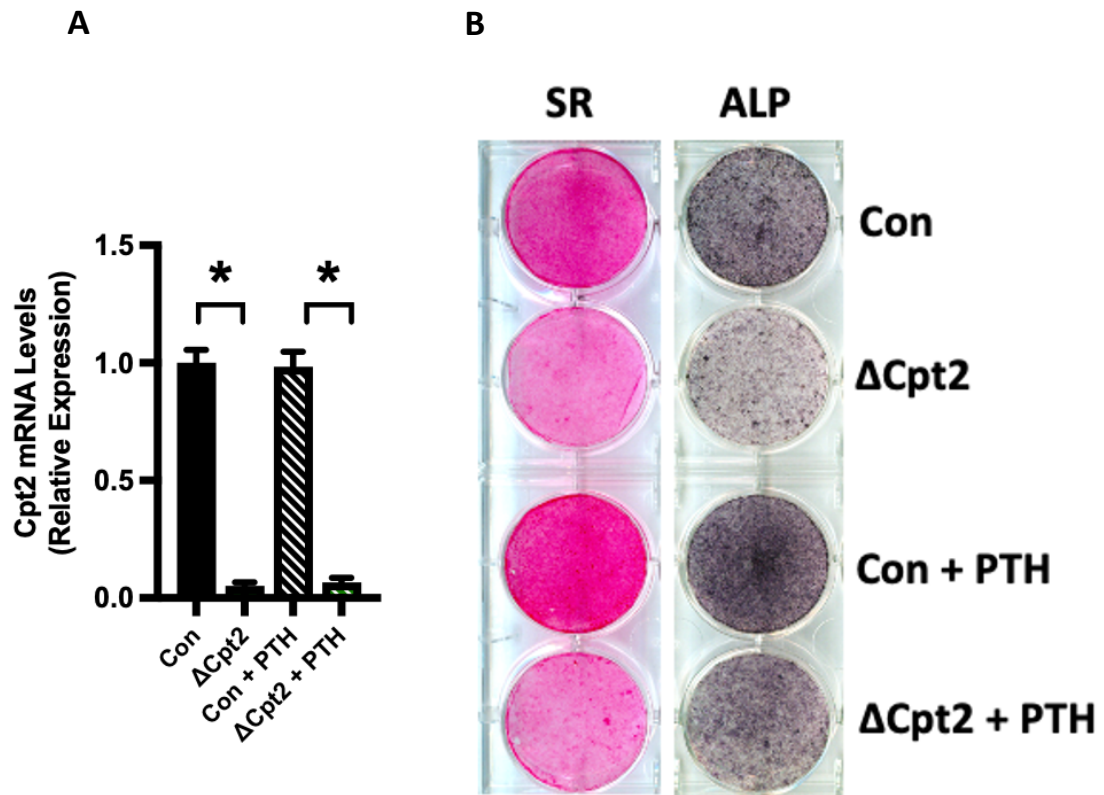
Figure 2.5 Fatty acid oxidation is necessary for PTH-induced increases in collagen deposition and alkaline phosphatase in vitro. (A) qPCR analysis of Cpt2 mRNA levels in primary osteoblasts after infection with adenoviral constructs encoding GFP (control) or Cre-recombinase (ΔCpt2). (B) Staining of collagen deposition by Sirus Red (SR) and alkaline phosphatase (ALP) activity on Day 14 after 4 treatments of 100 nM PTH_{1-34} (Days 7, 9, 11, 13) of control and ΔCpt2 osteoblasts. All data are represented as mean ± SEM. *$p < .05$.

To confirm these findings in vivo, we crossed Cpt2$^{flox/flox}$ mice to Osteocalcin-Cre (Oc-Cre$^{TG/+}$) mice to generate animals in which Cpt2, and obligate enzyme in β-oxidation, was deleted in mature osteoblasts and osteocytes. Beginning at 8 weeks of age, male Cpt2$^{flox/flox}$; Oc-Cre$^{TG/+}$ (OcnΔCpt2) and littermate controls, Cpt2$^{flox/flox}$; Oc-Cre$^{+/+}$ (Con) were treated with Saline or PTH$_{1-34}$ (100ug/kg) 5 days a week for 6 weeks. Male mice were used because previous research showed only transient deficits in skeletal architecture in OcnΔCpt2 compared to females [39]. Microarchitecture analysis using micro-CT revealed intermittent treatment increased bone volume fraction (BV/TV) in control animals which is the ratio of the segmented bone volume to the total volume of the region of interest. PTH did not significantly increase trabecular number (Tb.N) but did increase trabecular thickness (Tb.Th) in control littermates. PTH-induced increases in trabecular parameters that were expected and evident in control mice were abolished or greatly diminished in Cpt2 mutant mice (Fig 2.6). As expected, there were no changes between saline treated control and knockouts. These data demonstrated in vivo that long chain fatty acid β-oxidation in osteoblasts is essential for PTH-induced anabolic response of trabecular parameters in distal femurs of mice. The abolished response in trabecular parameters in PTH- treated OcnΔCpt2 mice was accompanied by changes to some parameters in the mid-diaphysis cortical bone, although to a lesser extent. PTH-induced increases in total cross-sectional area (T.Ar.) in the periosteal envelope, cortical bone area (B.Ar.), and mean moment of inertia (pMOI) were diminished in Cpt2 mutants.

37

However PTH treatment still significant increased the ratio between B.Ar and T.Ar and cortical thickness (Cs.Th) in both mutant and control littermates (Fig 2.7). The discrepancy between trabecular and cortical parameters may be attributed to the characteristics of cortical bone, which is less susceptible to microarchitectural changes. Perhaps, if animals were injected for a longer time courses, changes may become evident. The diminished anabolic response to PTH in Cpt2 mutants as exhibited by trabecular and some cortical parameters, is consistent with in vitro data in which PTH failed to increase matrix deposition in differentiated osteoblasts.
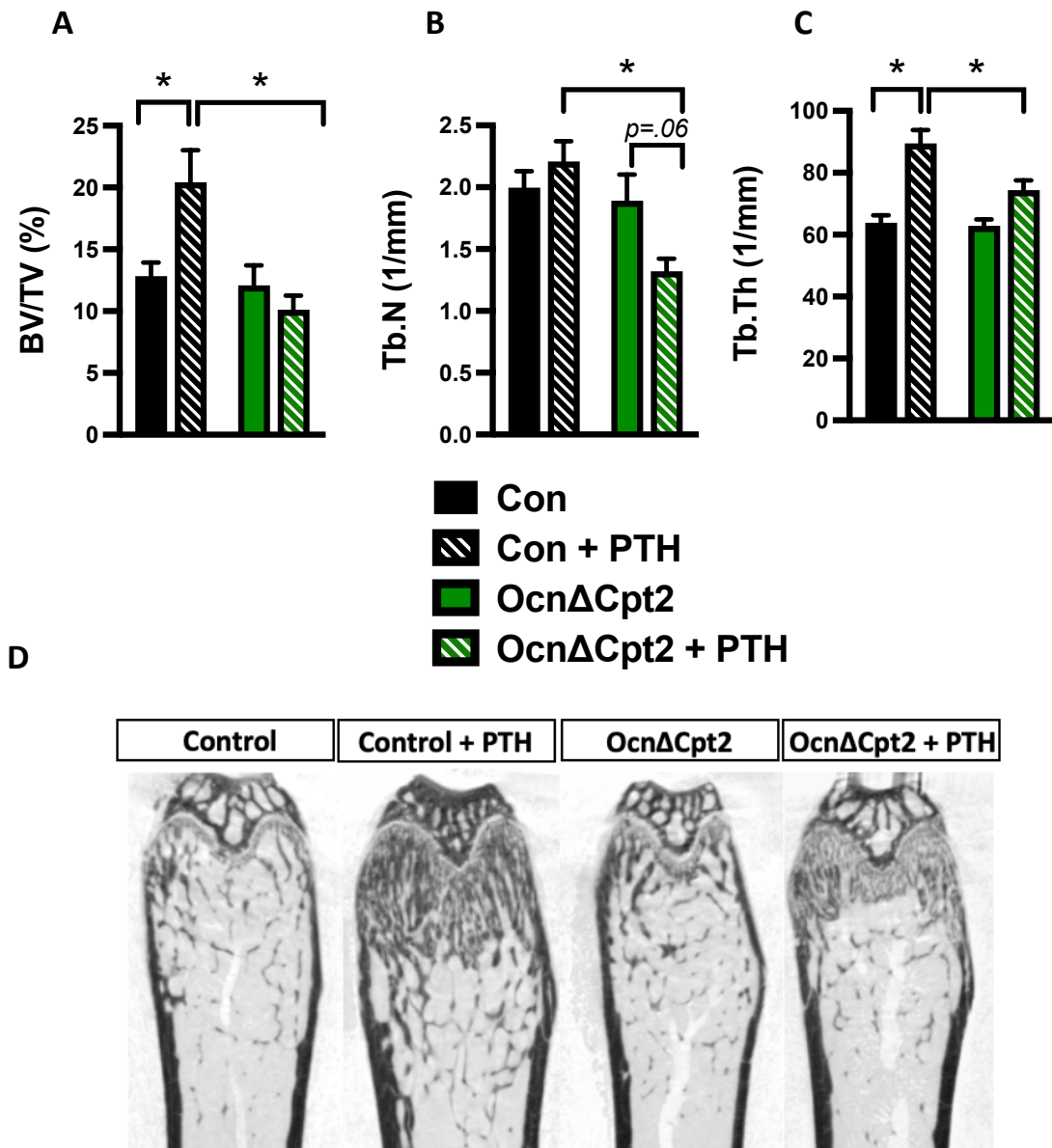
Figure 2.6 Trabecular analysis reveals long chain fatty acid β-oxidation in osteoblasts is essential for PTH-induced anabolism. Male mice were treated with PTH$_{1-34}$ (100ug/kg) 5 days a week for 6 weeks. PTH-induced increases in trabecular (A) bone volume per tissue volume (BV/TV (%)), (B) trabecular number (Tb.N (1/mm)), and (C) trabecular thickness (Tb.Th (μm)) evident in control mice were abolished or greatly diminished in Cpt2 mutants. (D) Representative 2D images from distal femurs used in the analysis of trabecular parameters. All data are represented as mean ± SEM. *$p < .05$.
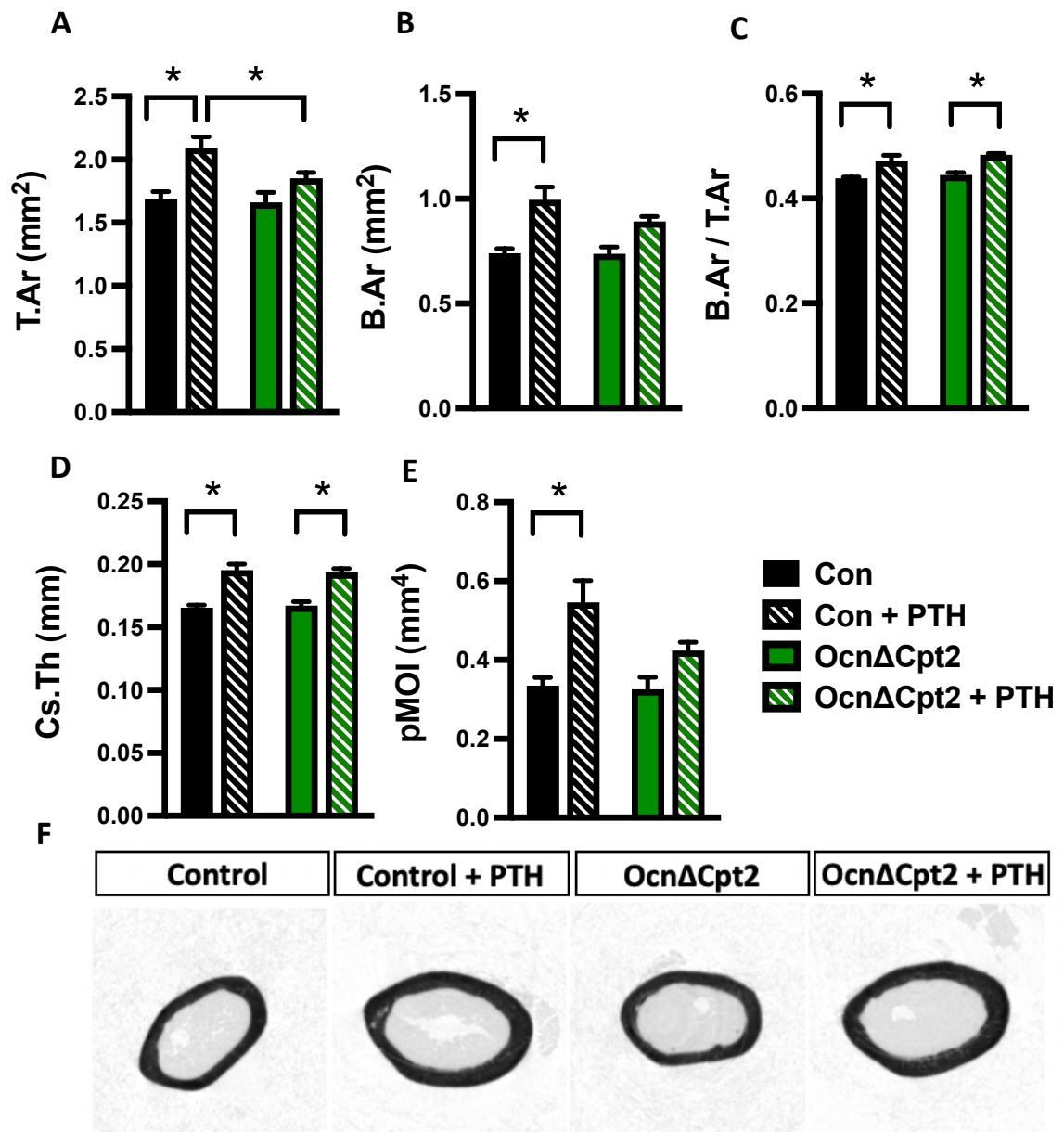
Figure 2.7 PTH-induced changes in cortical parameters were evident in control and OcnΔCpt2 mice. Male mice were treated PTH$_{1-34}$ (100ug/kg) or saline 5 days a week for 6 weeks. Intermittent PTH increased (A) total cross sectional area (T.Ar (mm^2)), (B) cortical bone area (B.Ar (mm^2)), (C) the ratio between B.Ar and T.Ar, (D) the cortical thickness (Cs.Th (mm)), (E) mean moment of inertia (pMOI (mm^4)) in control and to a lesser extent in knockout littermates. (F) Representative images from the mid-diaphysis of femurs. All data are represented as mean ± SEM. *$p < .05$.

Microarchitecture trabecular analysis from femurs of control and Ocn∆Cpt2 animals revealed that long chain fatty acid β-oxidation in necessary for the anabolic response in bone to intermittent PTH treatment. To begin to understand the mechanism for the abolished response, dynamic histomorphometry was performed. Analyses performed in the distal femur indicated that the inhibition of fatty acid oxidation impaired osteoblast function after PTH administration. In control mice, PTH induced a marked increase in mineral apposition rate (MAR), leading to an overall increase in bone formation rate (BFR/BS). Intermittent treatment increased mineralizing surface over bone surface (MS/BS) in controls but was not statistically significant (p=0.08). However, PTH had little effect on all three parameters in mutants. There were no changes between saline treated control and knockout littermates (Fig 2.8). These results are consistent with the idea that fatty acid oxidation in osteoblasts in necessary for the anabolic response to PTH and abolishing this function in osteoblasts, impairs their ability to appropriately respond to this anabolic hormone by forming mineralized bone. As expected, PTH increased osteoclast number relative to bone surface (Oc.N/BS) but also increased numbers in Ocn∆Cpt2 mice (Fig 2.9). These data suggest that the impaired mineralization of PTH-treated Cpt2 mutants is related to osteoblasts and not osteoclasts.
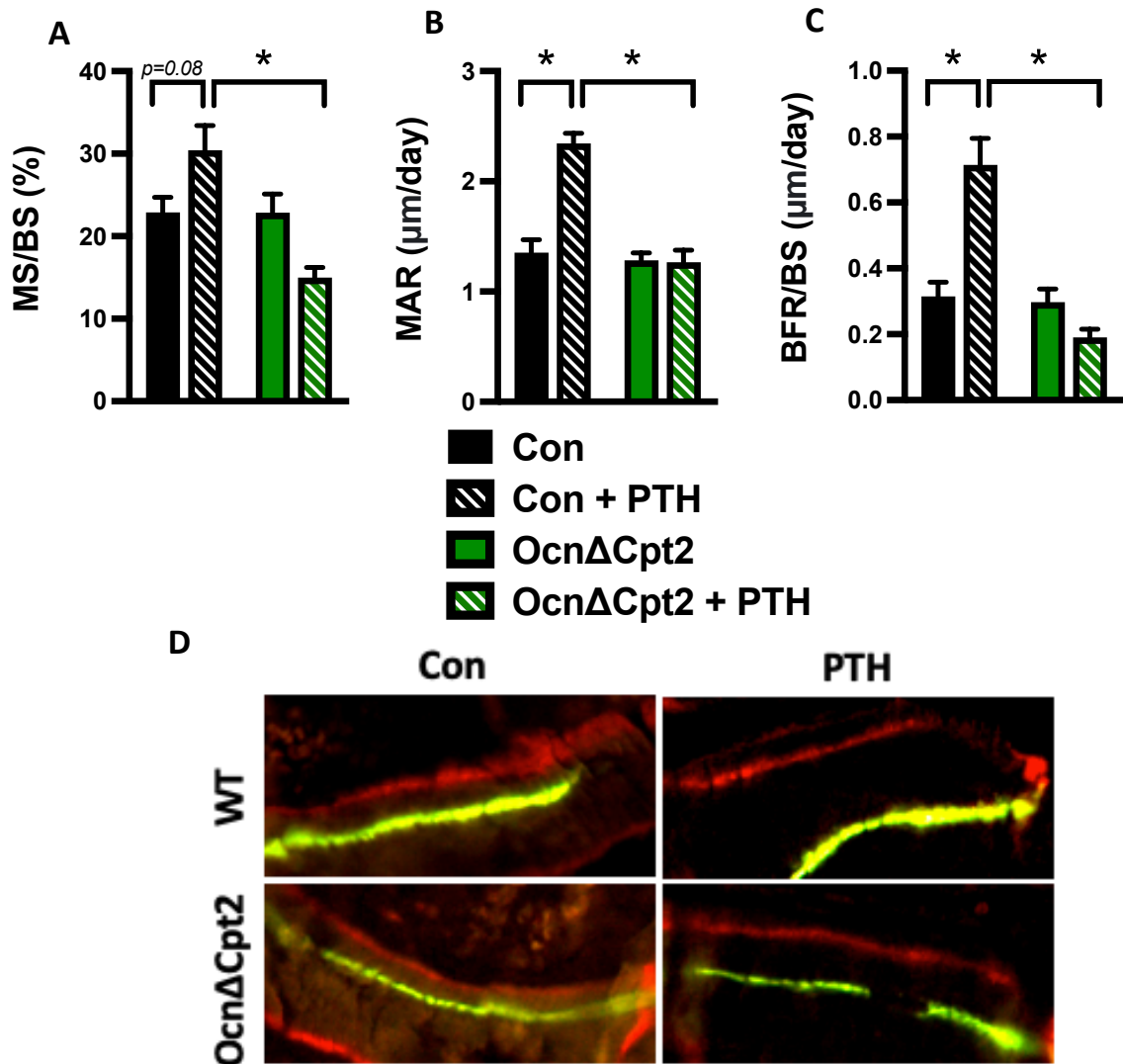
Figure 2.8 Dynamic histomorphometry analysis reveals Cpt2 deletion abolishes PTH-induced increases in mineralization. Control (Con) male mice treated PTH_{1-34} (100ug/kg) 5 days a week for 6 weeks have increased (A) mineralizing surface per bone surface (MS/BS (%)) (no significance p=0.08), (B) mineral apposition rate (MAR μm/day), (C) bone formation rate over bone surface (BFR/BS (μm/day) with abolished effects on mutants. (D) Representative images represent the abolished mineralizing response of trabecular bone to PTH when fatty acid oxidation is abolished in osteoblasts. All data are represented as mean ± SEM. *$p < .05$.
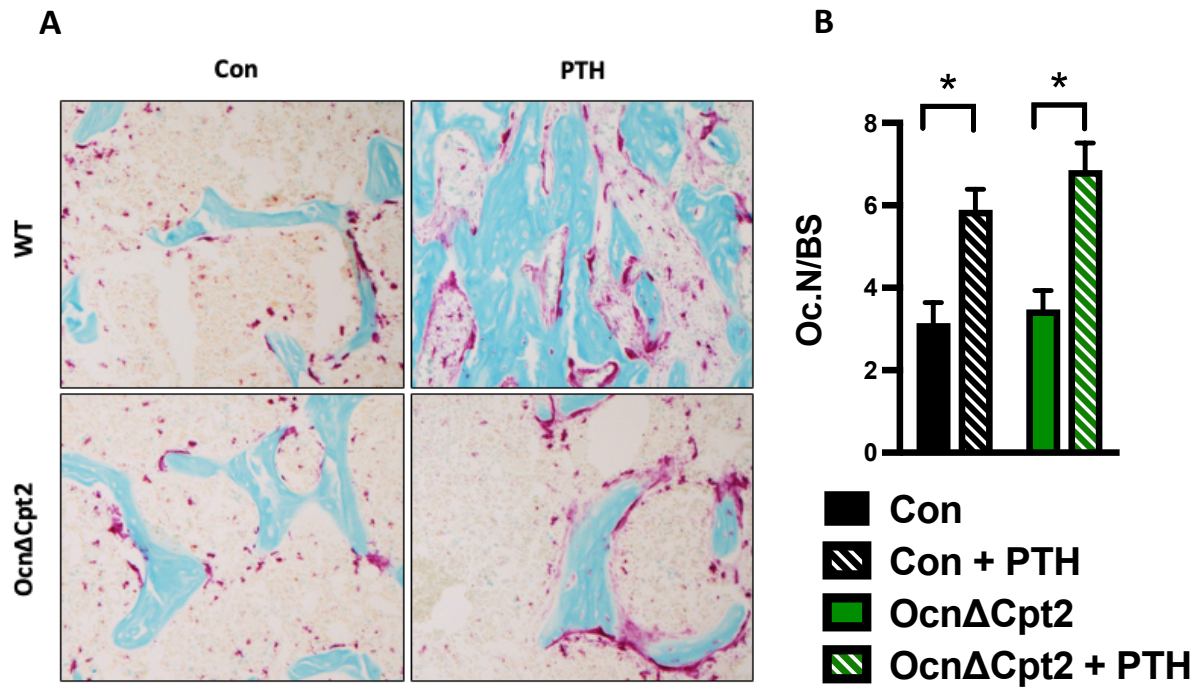
Figure 2.9 Impairing long chain fatty acid β-oxidation in osteoblasts does not affect osteoclast number. (A) TRAP staining of distal femurs from control (Con) and OcnΔCpt2 male mice treated with PTH$_{1\text{-}34}$ (100ug/kg) 5 days a week for 6 weeks. (B) Analysis revealed PTH increased osteoclast number per bone surface (Oc.N/BS) in both control and knockout littermates suggesting there is not a disruption in osteoclast function but impaired osteoblastic bone formation. All data are represented as mean ± SEM. *$p < .05$.

2.2 Materials and Methods

Culture of primary osteoblasts

Mouse osteoblasts were isolated from calvaria of 1- to 3-day old neonates by serial digestion in 1.8 mg/ml collagenase (Worthington Biochemical). For in vitro deletion of Cpt2, osteoblasts isolated from Cpt2$^{flox/flox}$ mice were infected with adenovirus encoding Cre recombinase or GFP (Vector Biolabs). A multiplicity of infection of 100 was used in all experiments and gene deletion was confirmed by quantitative PCR (qPCR). Osteoblast differentiation was induced by supplementing αMEM containing 10% serum with 10 mM β-glycerol phosphate and 50 μg/ul ascorbic acid. Differentiation was confirmed by Alizarin S staining for mineralization according to standard techniques. For matrix deposition studies, cells were treated with 100 mM PTH$_{1-34}$ human acetate (BACHEM, H-4835) resuspended in culture grade PBS (Corning) or PBS (vehicle) beginning on the Day 7 differentiation, alternating osteogenic media change and treatment every day until the completion of the study on Day 14. Cells were stained with Picro Sirius Red Stain Kit (abcam ab150681) and alkaline phosphatase.

RNA Sequencing

Mouse osteoblasts were isolated and differentiated as previously described. Cultures were serum starved (0.1% FBS) for 6 hours on Day 7 of differentiation. Osteoblasts were treated with 100 mM PTH$_{1-34}$ human acetate (BACHEM, H-4835) resuspended in culture grade PBS (Corning) or PBS (vehicle)

overnight. Total RNA was isolated with QIAGEN RNeasy Kit. Preparation of RNA library and transcriptome sequencing was conducted by Novogene Corporation Inc (Sacramento, CA). The mRNA library was prepared using poly A enrichment. Sequencing was performed using NovaSeq 6000 PE150. RNA was of sufficient quality for all samples (RIN > 9). Raw reads were aligned to the reference Mus musculus (GRCM38) using Hisat2 [127]. Binary read files (BAM) were generated and sorted using SAMtools. Transcript assembly was conducted using StringTie2 [128]. Differential Gene Expression analysis was completed using DESeq2. Following that, a raw read matrix was generated using StringTie2 companion python script. Differential Gene Expression analysis was completed using DESeq2 using default read filtration settings. Genes with adjusted p-value (FDR) < 0.05 and log2 fold change deviating from 0 (log2FC > 0 or log2FC < 0) were considered differentially expressed. A GitHub page has been created for additional information on analysis (https://github.com/aa9gj/Riddle_2022_analysis).

In vitro metabolic studies

Osteoblasts were cultured and differentiated in T25 cells culture flasks (Corning). Cultures were serum starved (0.1% FBS) for 6 hours on Day 7 of differentiation. Osteoblasts were treated with 100 mM PTH$_{1-34}$ human acetate (BACHEM, H-4835) resuspended in culture grade PBS (Corning) or PBS (vehicle) overnight. Fatty acid oxidation by osteoblast cultures were measured in flasks with rubber stoppers equipped with center wells as previously described [129].

Reactions were incubated at 37°C in media containing 0.5mM L-carnitine, 0.2%BSA, and ^{14}C-oleate or ^{14}C-D-glucose. Released CO_2 was captured and counted by the addition of 1N perchloric acid to the reaction mixture and 1M NaOH to the center well containing Whatman filter paper. The reaction was incubated overnight at 37°C and the filter paper was placed in scintillation fluid and counted.

Seahorse analysis

Bone marrow stromal cells (BMSCs) were isolated from femur and tibia from 8-week-old C57BL/6 mice. Adherent cells were trypsinized and seeded in a 96-well cell Seahorse culture microplate at 2.5 x 10^4 cells per well density. Cells were differentiated for 7 days in αMEM containing 10% serum with 5 mM b-glycerol phosphate and 50 mg/ mL ascorbic acid. Osteoblasts were treated with 100 nM PTH_{1-34} or vehicle for 2 hours. Metabolic flux analyses were performed with media containing 1 mM sodium pyruvate, 2 mM glutamine, 10 mM glucose, 200 nM insulin, and 200 μM oleic acid BSA. Analysis was performed using Agilent Seahorse XF Analyzer. Mito Stress test was performed using 1 μM oligomycin, 1 μM FCCP, 1 μM rotenone/antimycin, including 10 μM etomoxir (Eto). The oxygen consumption rate (OCR) was normalized to seeded cell number.

Gene expression studies

Total RNA was extracted from cell cultures using TRIzol (Life Technologies). Reverse transcriptase reaction was completed using 1μg of RNA

and iScript cDNA Synthesis system (Bio-Rad). qPCR was carried out using iQ Sybr Green Supermix (Bio-Rad) using primer sequences obtained from PrimerBank (https://pga-mgh-harvard-   edu.proxy1.library.jhu.edu/primerbank/index.html). Cpt2 primers for qPCR were 5'-CCT GCT CGC TCA GGA TAA ACA-3' (forward) and 5'-GTG TCT TCA GAA ACC GCA CTG-3' (reverse). Reactions were normalized to endogenous 18S reference transcripts. 18S primers were 5'-CTT AGA GGG ACA AGT GGC G-3' (forward) and 5'-ACG CTG AGC CAG TCA GTG TA-3' (reverse).

Animal models

All mice were cared for under strict compliance with the Animal Care and Use Committee of the Johns Hopkins University School of Medicine. Mice were housed on ventilated racks on a 14-hour light/10-hour dark cycle and fed ad libitum with a standard chow diet (Extruded Global Rodent Diet, Harlan Laboratories). Mice in which exon 4 of the mouse *Cpt2 gene* is flanked by *loxP* sequences were generated as described in [129, 130]. To generate an osteoblast and osteocyte-specific knockout, Cpt2$^{flox/flox}$ mice were crossed to Osteocalcin-Cre (Oc-Cre$^{TG/+}$) mice [131]. The resulting Cpt2$^{flox/+}$; Cre$^{TG/+}$ progeny were then backcrossed to Cpt2$^{flox/flox}$ mice to generate the tissue-specific knockouts. Breeding pairs of Cpt2$^{flox/flox}$; Cre$^{TG/+}$ and Cpt2$^{flox/flox}$ were used to generate control mice (Cpt2$^{flox/flox}$) and knockout littermates (Cpt2$^{flox/flox}$; Cre$^{TG/+}$) PCR analysis from DNA extracted from tail clippings were used to confirm genotypes. Genotyping primers for Oc-

Cre$^{TG/+}$ mice were 5'- GAA CCT GAT GGA CAT GTT CAGG-3' (forward) and 5'-AGT GCG TTC GAA CGC TAG AGC CTG T-3' (reverse). Genotyping primers for Cpt2$^{flox/flox}$ mice were 5'-GCT GGC TTA GGA GAT TCT TAA CTT CC-3' (forward) and 5'-AGC TCA GGT GGC AGA AAT GAT ACC-3' (reverse). All mice were maintained on a C57Bl/6 background. For intermittent PTH injections, male mice were injected subcutaneously with PTH$_{1-34}$ (BACHEM, H-4835) was resuspended in culture grade PBS (Corning) and injected at 100µg/kg, 5 days a week for 6 weeks. PBS was used as the control.

Skeletal phenotyping

High resolution images of the mouse femur were acquired using a desktop microtomographic imaging system (Skyscan 1172, Bruker). In accordance with the recommendation of the American Society for Bone and Mineral Research (ASBMR) [132]. Bones were scanned with an isotropic voxel size of 10 µm at 65 keV and 153 µA using a 1.0-mm aluminum filter. Trabecular bone parameters in the distal femur were assessed in a region of interest 500-µm proximal to the growth plate and extending for 2-mm (200 CT slices). Femoral cortical bone structure was assessed in a 500-µm region of interest centered on the mid-diaphysis. Dynamic bone formation was assessed at 14 weeks of age by one injection of calcein followed by 1 injection of alizarin separated by 7 days. After embedding femoral samples in methylmethacrylate, 5µm sections were cut with a Leica microtome (RM2265). Dynamic histomorphometry indices were measured at standardized sites under the growth plate using a semiautomatic method

48

(BIOQUANT OSTEO) in compliance with the guidelines established by the nomenclature committee from the ASBMR [133].

Histology

Mouse adipose tissue and femur samples were fixed in 4% paraformaldehyde for 24 hours at 4°C and washed with PBS. Adipose tissue samples were paraffin-embedded and stained with H&E using standard methods. Femurs were decalcified using 14% EDTA and paraffin embedded. After embedding, 5μm sections were cut and stained with hematoxylin and eosin (H&E) using standard methods for bone marrow adipose tissue analysis or stained for TRAP activity and analyzed using BIOQUANT OSTEO. Bone marrow adipocytes and inguinal and gonadal analysis was completed using ImageJ software.

Statistical analysis

Quantitative data are shown as bar graphs produced using Prism Graphpad software. All results are expressed as mean ± SEM. Statistical analyses were performed using unpaired, two-tailed Student's t-test or ANOVA tests followed by Tukey post-hoc tests using Prism Graphpad software. A p-value <0.05 was considered significant.

Chapter 3
An adipose tissue-specific response is essential for PTH-induced anabolism

3.1 Introduction, rationale, and results

Having established that PTH's alters fatty acid metabolism, and that this lipid is required for bone accrual in response to an anabolic stimulus, we questioned the primary source of fatty acids. A study conducted over 30 years ago found that PTH_{1-34} stimulates lipolysis of human adipose tissue by binding to receptors distinct from beta-adrenergic receptors of fat cells [134]. A more recent study confirmed the lipolytic actions of PTH on adipose tissue. PTH_{1-84} stimulated lipolysis in primary mouse adipocytes while PTH_{1-37} induced phosphorylation of known PKA targets including phosphorylation of HSL at serine 660 [106]. These studies were evidence that PTH treatment initiates a lipolytic response in humans and primary mouse cells, altering fat metabolism and a potential source of fatty acids. The first indication that PTH alters fat metabolism in mice was from the analysis of adipocyte morphology in Control and Cpt2 mutants in peripheral fat pads and bone marrow fat (bone phenotype discussed in Chapter 2). There were no changes in body weight at the completion of this study between the 4 groups (Fig 3.1A). Intermittent PTH treatment decreased fat pad weight in both knockout and control littermates, but only significantly decreased gonadal white adipose tissue (gWAT). No significant changes were reported in organ weights between Saline treated control and Ocn△Cpt2 mice with and without PTH treatment (Fig

50

3.1C). Intermittent PTH treatment decreased adipocyte area (Ad.Ar) in iWAT and gWAT fat pads regardless of genotype (Fig 3.2 and Fig 3.3). PTH also altered another adipose tissue niche, bone marrow adipose tissue (BMAT), although no significance was reached between groups. Adipocyte area relative to total area (Ad.Ar/T.Ar) trended downward with treatment in controls of the distal region of femurs. Saline treated Cpt2 mutants exhibited a decrease in BMAT area relative to saline controls which could be a result to alterations in metabolism. Potentially due to disruptions in metabolism, PTH treatment increased adipocyte area in mutants compared to saline treated mutants (Fig 3.4). The alteration in adipocyte morphology of iWAT and gWAT fat pads indicates Cpt2 deletion in osteoblasts does not affect PTH- induced metabolic changes in these tissues. However, alterations in metabolic profile were sufficient to alter bone marrow adipocytes.
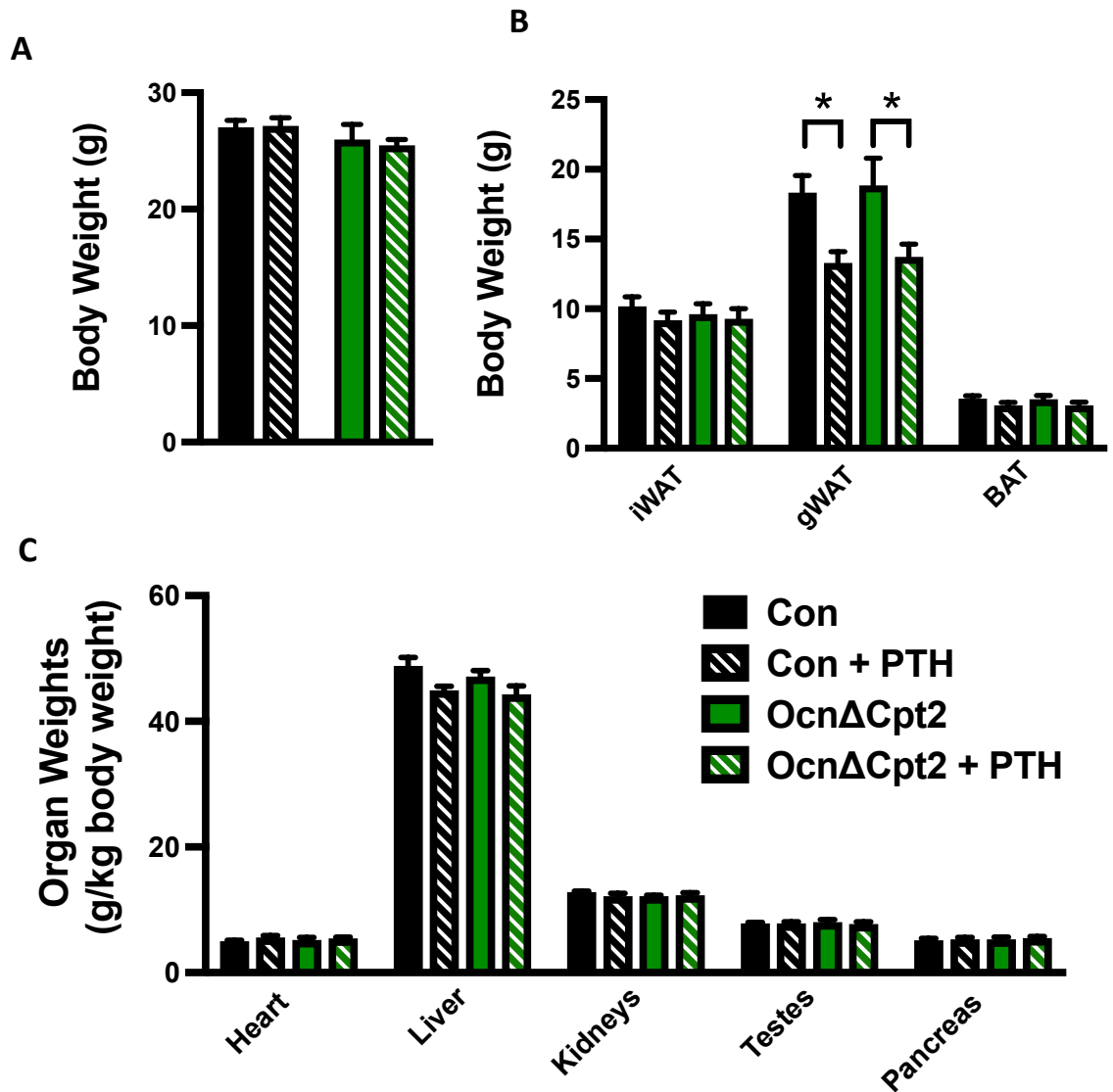
Figure 3.1. Body composition for OcnΔCpt2 and control littermates after 6 weeks of intermittent PTH treatment. Male Cpt2$^{flox/flox}$; Oc-Cre$^{TG/+}$ (OcnΔCpt2) and littermate controls, Cpt2$^{flox/flox}$; Oc-Cre$^{+/+}$ (Con) were treated with Saline or PTH$_{1-34}$ (100ug/kg) 5 days a week for 6 weeks. (A) There were no significant changes in body weights, (B) inguinal white adipose tissue (iWAT), or brown adipose tissue (BAT). PTH treatment did decrease gonadal fat pads (gWAT) in Controls and OcnΔCpt2 mice. (C) PTH did not alter any organ weights. All data are represented as mean ± SEM. *$p < .05$.
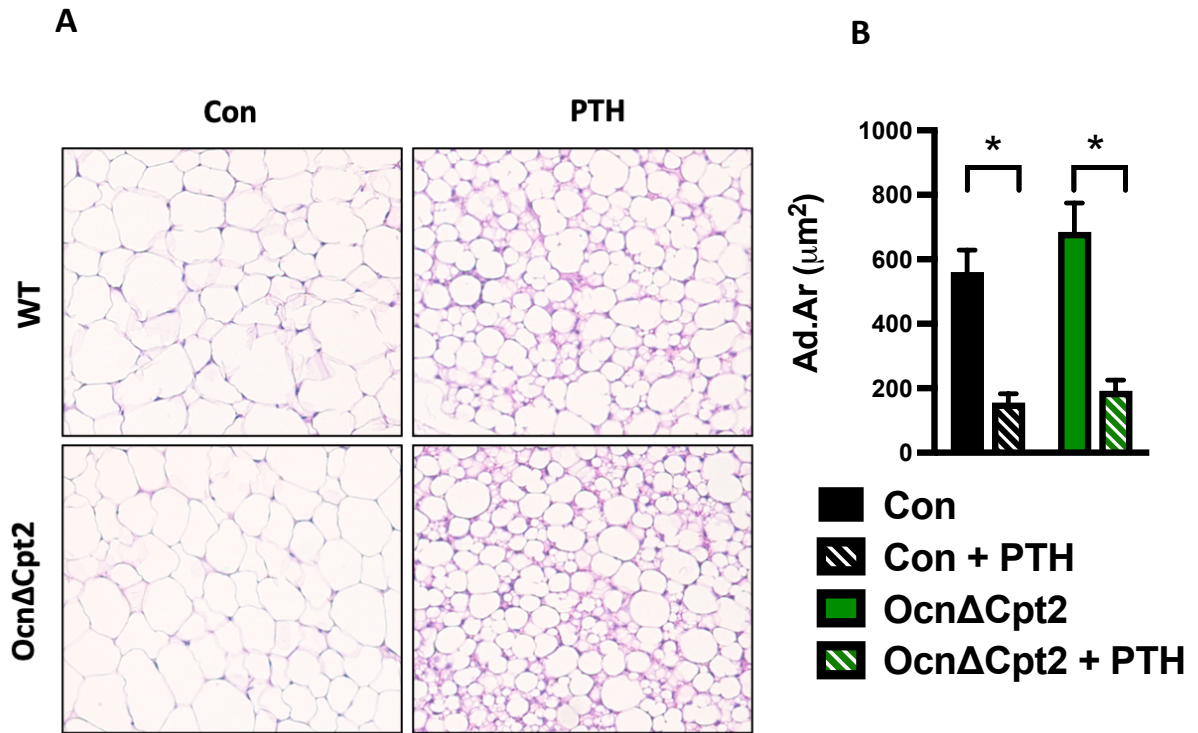
Figure 3.2 Intermittent PTH treatment alters inguinal white adipose tissue (iWAT) morphology. (A) Hematoxylin and Eosin (H&E) staining of iWAT from control (Con) and OcnΔCpt2 male mice treated with PTH_{1-34} (100ug/kg) or saline 5 days a week for 6 weeks. (B) PTH treatment decreased adipocyte area (Ad.Ar (μm^2)) in both controls and Cpt2 mutants. All data are represented as mean ± SEM. *$p < .05$.
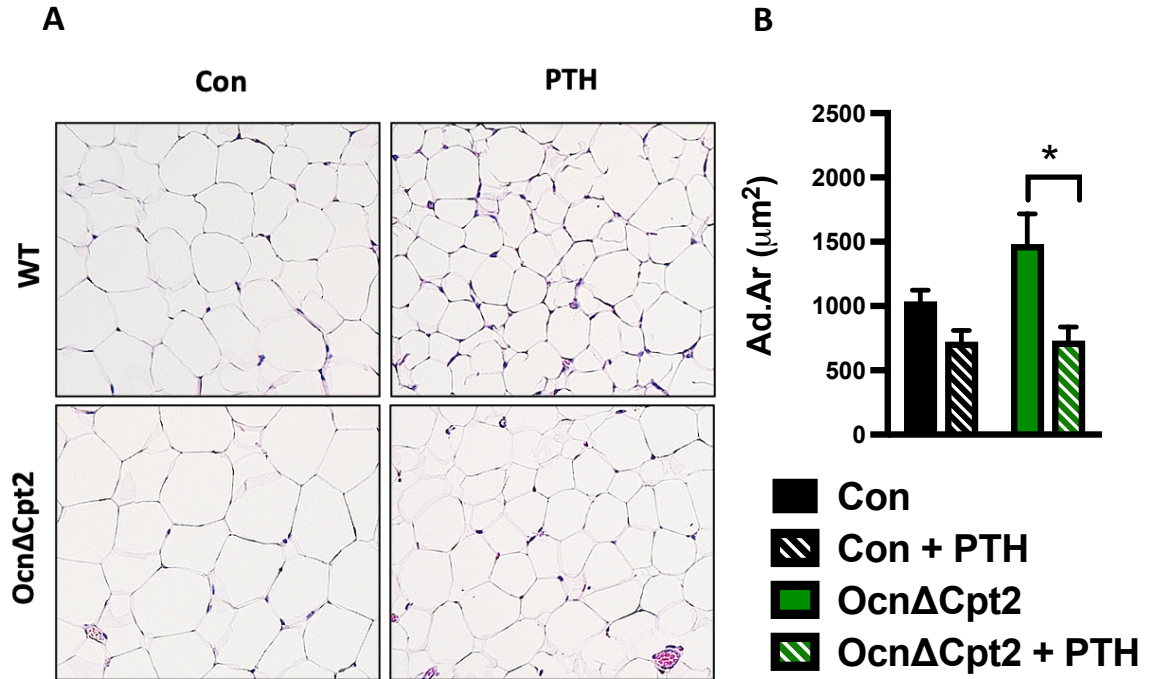
Figure 3.3 Intermittent PTH treatment alters gWAT white adipose tissue (gWAT) morphology. (A) Hematoxylin and Eosin (H&E) staining of gWAT from control (Con) and OcnΔCpt2 male mice treated with PTH$_{1-34}$ (100ug/kg) or saline 5 days a week for 6 weeks. (B) PTH treatment decreased adipocyte area (Ad.Ar (μm^2)) in controls (no significance) and Cpt2 mutants. All data are represented as mean ± SEM. *$p < .05$.
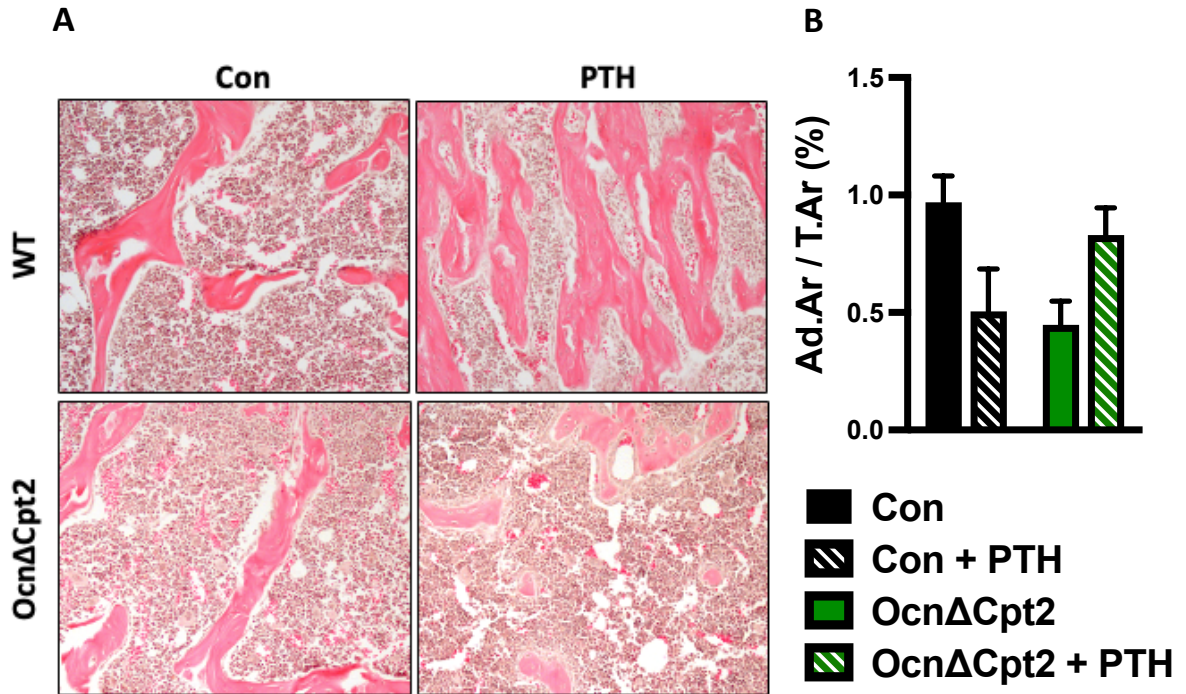
Figure 3.4 Intermittent PTH treatment alters bone marrow adipose tissue (BMAT) morphology. (A) Hematoxylin and Eosin (H&E) staining of femurs from control (Con) and OcnΔCpt2 male mice treated with PTH_{1-34} (100ug/kg) or saline 5 days a week for 6 weeks. (B) PTH treatment decreased adipocyte area relative to total area (Ad.Ar/T.Ar (%)) in controls. OcnΔCpt2 displayed a decreased Ad.Ar/T.Ar (%) relative to control. PTH increased OcnΔCpt2 BMAT area compared to saline treated mutants. All data are represented as mean ± SEM. *$p < .05$.

To confirm findings from previous studies and to further understand PTH's role in whole body fat metabolism, we asked if a lipolytic response evident in humans was also evident in mice. C57BL/6 male 8-week-old-mice were treated with PTH_{1-34} (100μg/kg) or saline subcutaneously for 30 minutes and serum and adipose tissue were collected for analysis. Relative to the control, PTH_{1-34} increased levels of serum free fatty acids and triggered the phosphorylation of HSL (Ser660) (Fig 3.5). In addition to PTH's activation of lipolytic enzymes in adipose tissue, an indirect calorimetric study revealed PTH alters whole-body fat metabolism. C57BL/6 8-week-old mice were individually housed in a Comprehensive Laboratory Monitoring System (CLAMS) which allows for the measurement of food intake, activity, oxygen consumption (VO_2) and carbon dioxide production (VCO_2). From these measurements, the respiratory exchange ratio ($RER = VCO_2/ VO_2$) and energy expenditure [$EE= VO_2$ x (3.815 + (1.232 x RER)] are calculated. Results were normalized to lean body mass determined by qNMR analysis. Mice were house in the CLAMS for 2 days and then treated with PTH on 2 consecutive days. Whole body energy expenditure did not change but acute PTH treatment did induce a rapid decrease in RER, indicative of an increase in the utilization of lipid relative to glucose (Fig 3.6).
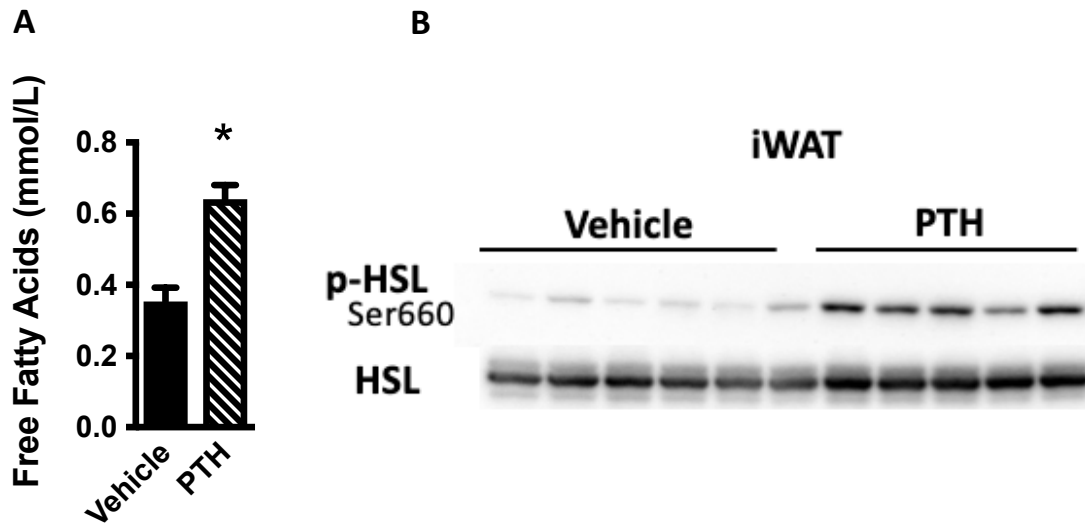
Figure 3.5 Acute PTH₁₋₃₄ activates lipolytic enzymes in adipose tissue. (A) Serum

analysis revealed an increase in free fatty acids of 8-week-old male C57BL/6 mice treated

with PTH$_{1-34}$ (100μg/kg) collected 30 minutes post injections. (B) Western Blot analysis of

inguinal white adipose tissue (iWAT) shows the phosphorylation of HSL (Ser660), an

enzyme involved in adipose tissue lipolysis. All data are represented as mean ± SEM.

*$p < .05$.
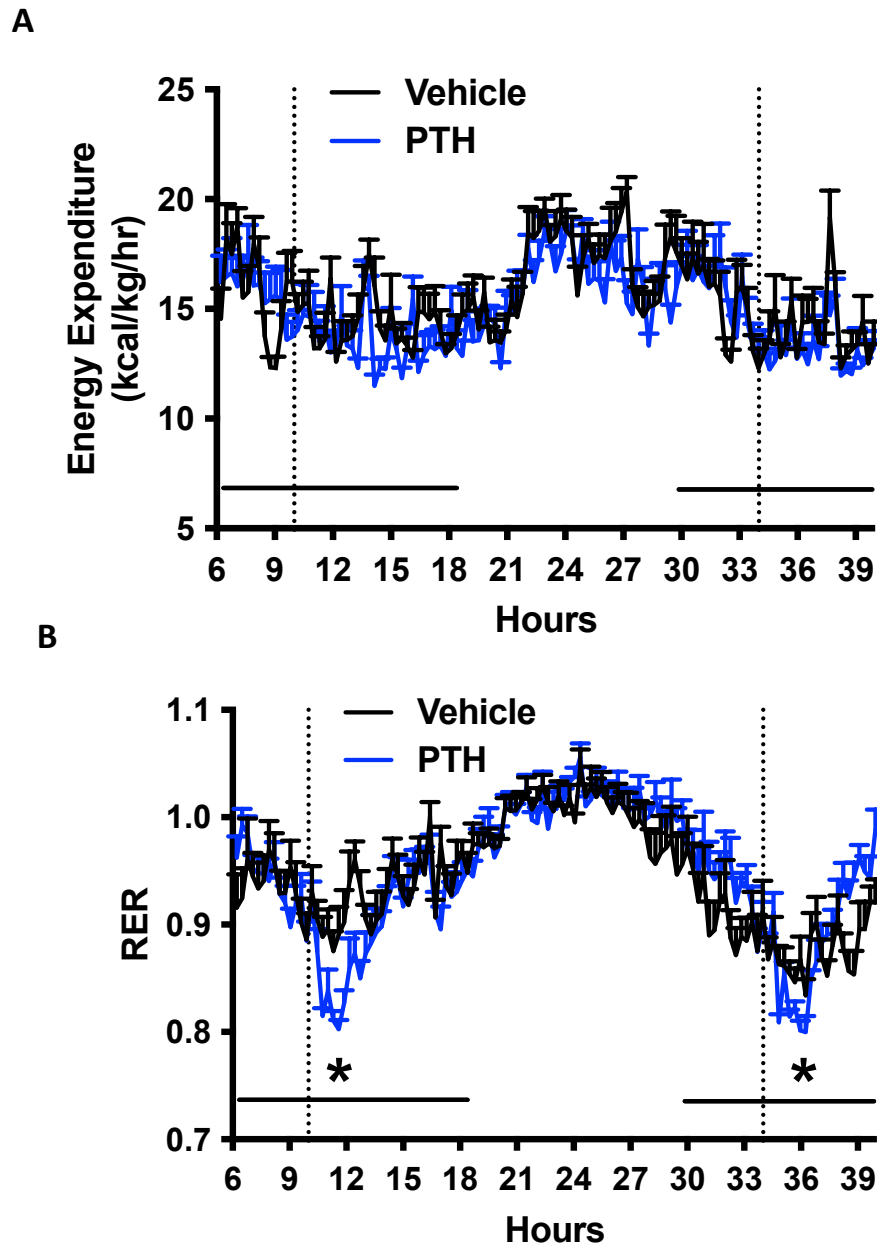
Figure 3.6 PTH alters whole body metabolism. C57BL/6 8-week-old mice were injected with PTH_{1-34} (100µg/kg) at the dotted lines. (A) PTH did not change energy expenditure ([EE= VO_2 x (3.815 + (1.232 x RER)] but, (B) did induce a rapid decrease in the respiration exchange ratio (RER = VCO_2/ VO_2), indicative of an increase in the utilization of lipid relative to glucose. All data are represented as mean ± SEM. *$p < .05$.

PTH's alters metabolism of mice by triggering lipolysis and release of free fatty acids and increases lipid utilization suggesting fat pads may function as a source of free fatty acids for osteoblasts. To further address the possible role of fat as a fuel source for bone, we wanted to determine if PTH signaling in adipose tissue and the activation of a lipolytic response is required for the full anabolic response of bone to PTH. Mice in which the PTH receptor was deleted specifically in adipocytes were generated by crossing the Pth1r$^{flox/flox}$ mice to AdipoQ-Cre mice. It is well established that both osteoblasts and adipocytes originate from a common progenitor, mesenchymal stem cells. Based on a recent study using single sequencing transcriptome analysis, a novel Adiponectin positive, non-lipid laden subpopulation of bone marrow mesenchymal lineage cells were identified [135]. The discovery of this population brings into question whether these adipogenic-like cells can differentiate into bone forming osteoblasts or lipid laden adipocytes. Due to this concern, we must firm confirm specificity of deletion of the Pth1r in adiponectin expressing cells. Pthr expression was assessed using qPCR in iWAT and femurs of Pth1r$^{flox/flox}$; AdipoQ-Cre$^{TG/-}$ (AdΔPth1r) and littermate controls (Pth1r$^{flox/flox}$; AdipoQ-Cre$^{+/-}$). The mutants exhibited a 60% decrease in Pth1r expression in adipose tissue but had normal expression levels in the femur tissue that was washed free of bone marrow (Fig 3.7). Additionally, immunofluorescence staining demonstrated the presence of the PTHR along the trabecular surface of femurs in both control and knockout mice. However, expression of PTHR is absent in bone marrow adipocytes of mutants (i.e., no colocalization between PTHR and

PLIN1, a common marker for lipid-laden adipocytes) unlike littermate controls which show the colocalization between PTHR and PLIN1. These expression patterns suggest that the Pth1r is disrupted in adipocytes but not in osteoblast lineage cells (Fig 3.8).

The specificity of deletion confirmed by gene expression analysis and protein expression validated our genetic model and allowed us to move forward in examining the requirement for the PTH1R in adipose tissue for an osteoanabolic response to PTH. It was first necessary to examine the lipolytic response in these mice to the hormone. Similar to Fig. 4-1, PTH_{1-34} (100μg/kg) or saline was injected subcutaneously in 8-week-old AdΔPth1r mice and littermate controls. Serum and adipose tissue were collected 30-minutes post administration. Acute PTH_{1-34} treatment induced a significant increase in serum free fatty acids, but the effect was abolished in mutants. Treatment also induced the phosphorylation of HSL (Ser660) in control animals but was diminished in AdΔPth1r mice (Fig. 3.9). These results establish that disrupting Pth1r expression in adipocytes, decreases the lipolytic response in fat to PTH.
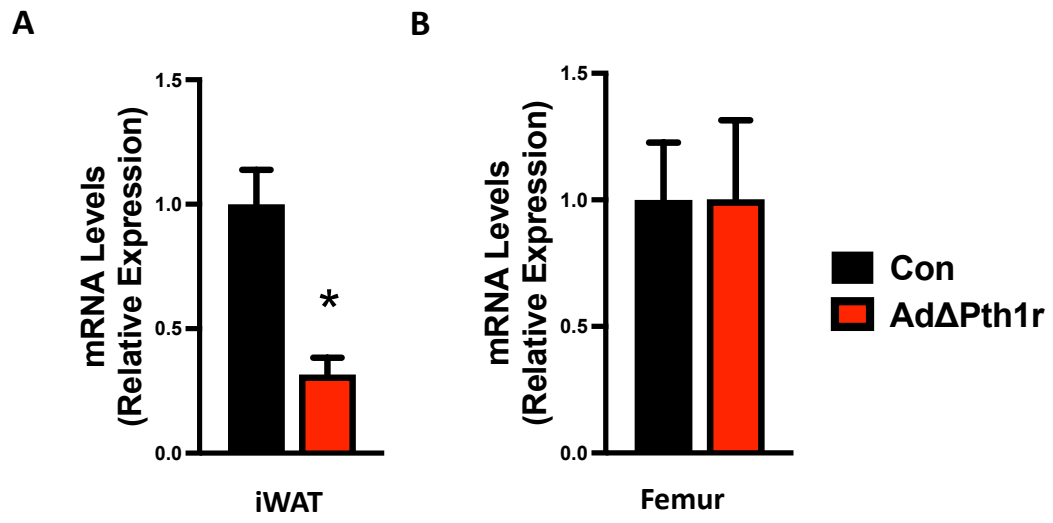
Figure 3.7 Gene expression analysis to confirm specificity of Pth1r deletion in Adiponectin positive cells. Pthr gene expression using qPCR showed that AdΔPth1r animals had a 60% reduction in expression in (A) iWAT but not in (B) femurs devoid of bone marrow. All data are represented as mean ± SEM. *$p < .05$.
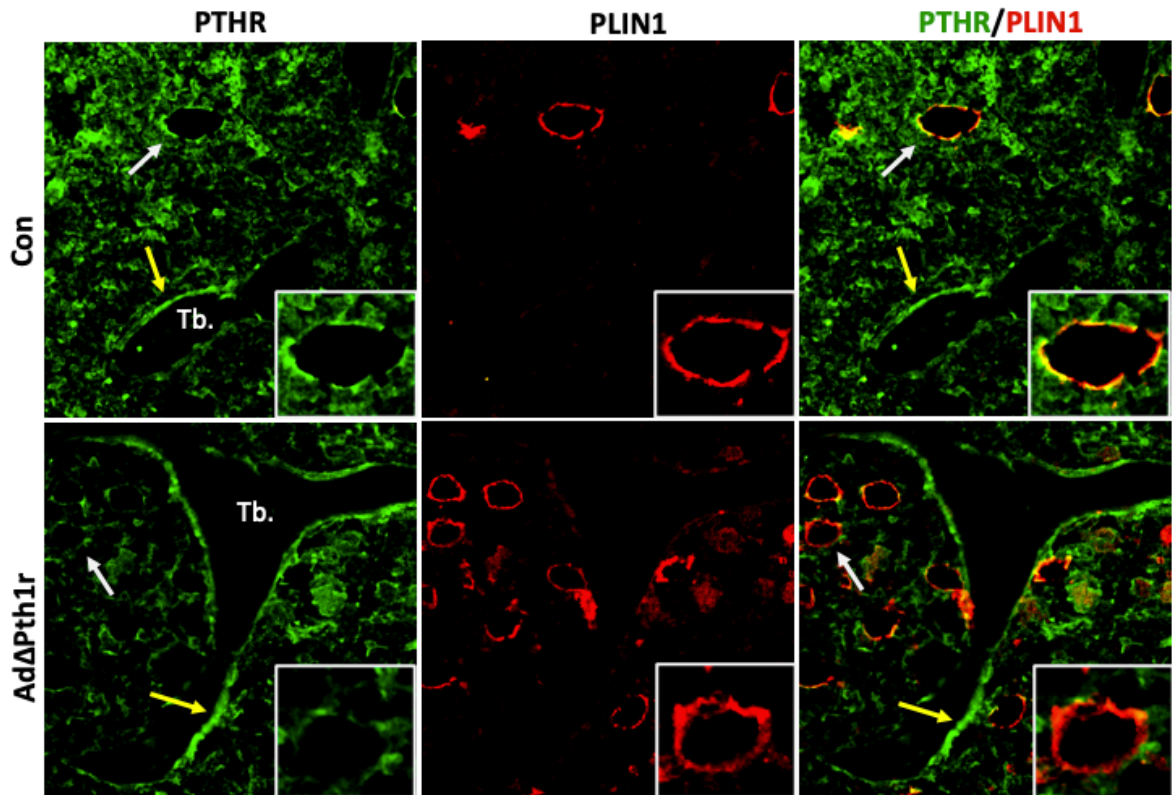
Figure 3.8 Immunofluorescence confirms specificity of the Pthr receptor deletion in Pth1r$^{flox/flox}$; AdipoQ-Cre$^{TG/-}$ mice. PTHR expression is present along the trabecular regions of mutants and littermate controls (yellow arrows) while expression is absent in PLIN1-expressing adipocytes in mutants but not controls (white arrows). This expression pattern confirms the disruption in adipocytes but not in osteoblast lineage cells.
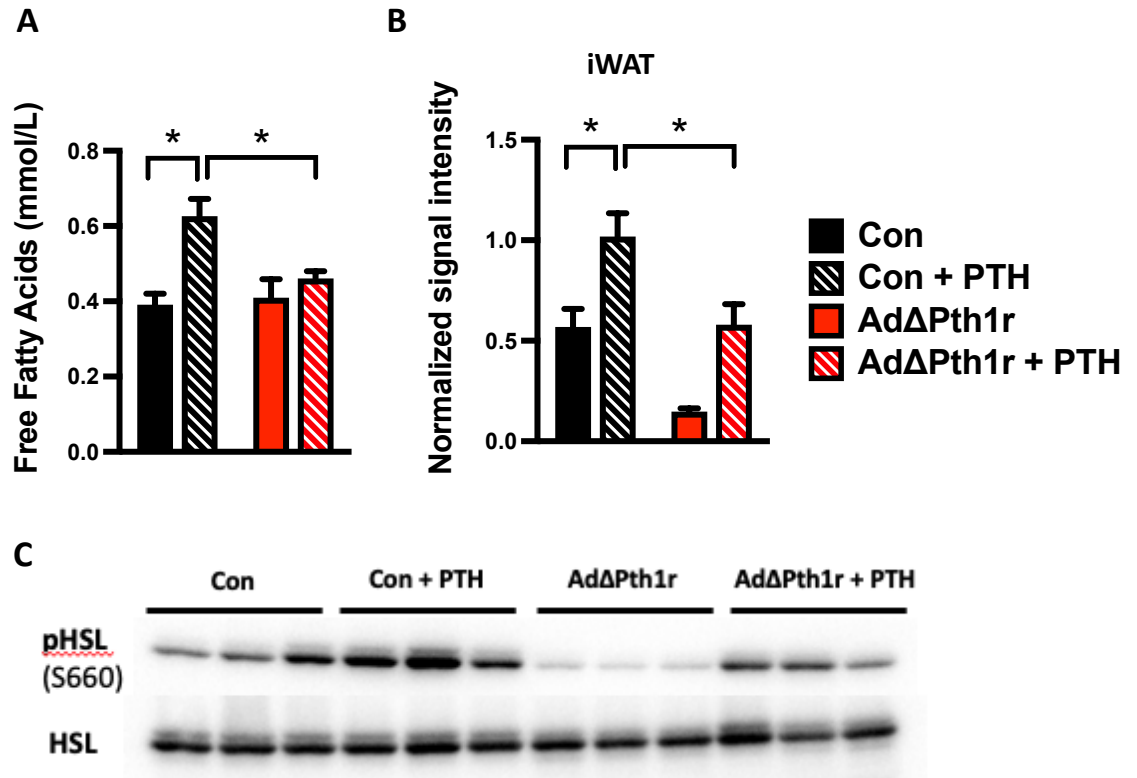
Figure 3.9 Pth1r expression by adipocytes is required for PTH-induced lipolysis.

PTH$_{1-34}$ (100µg/kg) or saline was injected subcutaneously in 8-week-old AdΔPth1r mice and littermate controls. (A) After 30 minutes, PTH increased serum free fatty acids in control but not in AdΔPth1r mice. (B,C) Western blot analysis revealed the phosphorylation of HSL (Ser660) in controls but AdΔPth1r littermates exhibited a diminished response. All data are represented as mean ± SEM. *$p < .05$.

The lipolytic response was impaired after acute administration of PTH therefore, adipocyte changes after prolonged PTH treatment were assessed. PTH$_{1-34}$ (100μg/kg) or saline was injected in 8-week-old male AdΔPth1r mice and littermate controls 5 consecutive days a week for 6 weeks. With extended treatment, PTH induced morphological changes in peripheral adipose depots (iWAT and gWAT) and in BMAT. In iWAT fat pads, intermittent PTH treatment reduced the size of adipocytes, but this was abolished in AdΔPth1r mice (Fig 3.10). Adipocyte size of gWAT trended downward with PTH treatment in controls but only a slight change was revealed in mutants (Fig 3.11). PTH administration in control mice decreased adipocyte area relative to total area (Ad.Ar/T.Ar) but affected bone marrow adiposity to a lesser extent in AdΔPth1r littermates (Fig 3.12). There were no differences between saline treated controls and mutants. Together these data demonstrate that PTH signaling in adipocytes induces acute and long-term effects on lipid homeostasis. When the Pthr is deleted in adipocytes, these effects on lipid homeostasis are abolished suggesting that peripheral adipocyte depots like iWAT and gWAT fat pads and proximal fat depots like BMAT may serve as a fatty acid source to osteoblasts.

Serum levels of free fatty acids, cholesterol, and triglycerides were measured to obtain and more thorough metabolic profile. In line with PTH-induced changes in lipid homeostasis, 6 weeks of PTH treatment induced a significant increase in serum free fatty acids but this increase was abolished in Pth1r knockouts. Mutants displayed decreased total serum triglycerides (no significance)

64

in saline and PTH treatment groups compared to wildtype counterparts. Cholesterol levels were not significantly different between groups (Fig 3.13). Body composition of control and AdΔPth1r mice treated with saline or PTH for 6 weeks revealed some alterations. PTH induced a significant increase in body weight in control littermates, but no increase was noticed in PTH treated AdΔPth1r mice compared to saline treated knockouts. Although there were trends observed with fat pad weights, there were no significant changes between groups. Pancreas weight significantly decreased between PTH treated controls and PTH treated mutants, no other differences were observed in organ weights (Fig 3.14).
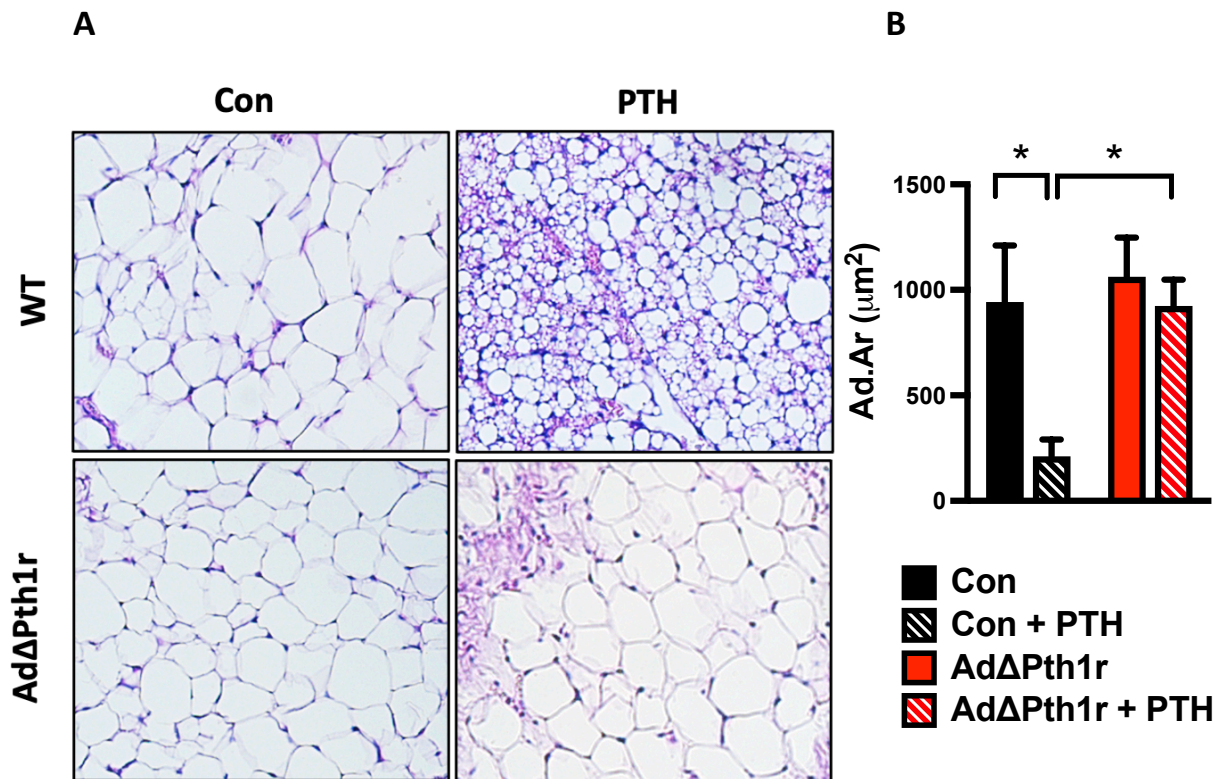
Figure 3.10 Pth1r deletion in adipocytes alters PTH-induced changes in inguinal white adipose tissue (iWAT). A) Hematoxylin and Eosin (H&E) staining of iWAT from control (Con) and AdΔPth1r male mice treated with PTH$_{1-34}$ (100ug/kg) or saline 5 days a week for 6 weeks. (B) PTH treatment decreased adipocyte area (Ad.Ar (μm^2)) in controls but not in knockouts. All data are represented as mean ± SEM. *$p < .05$.
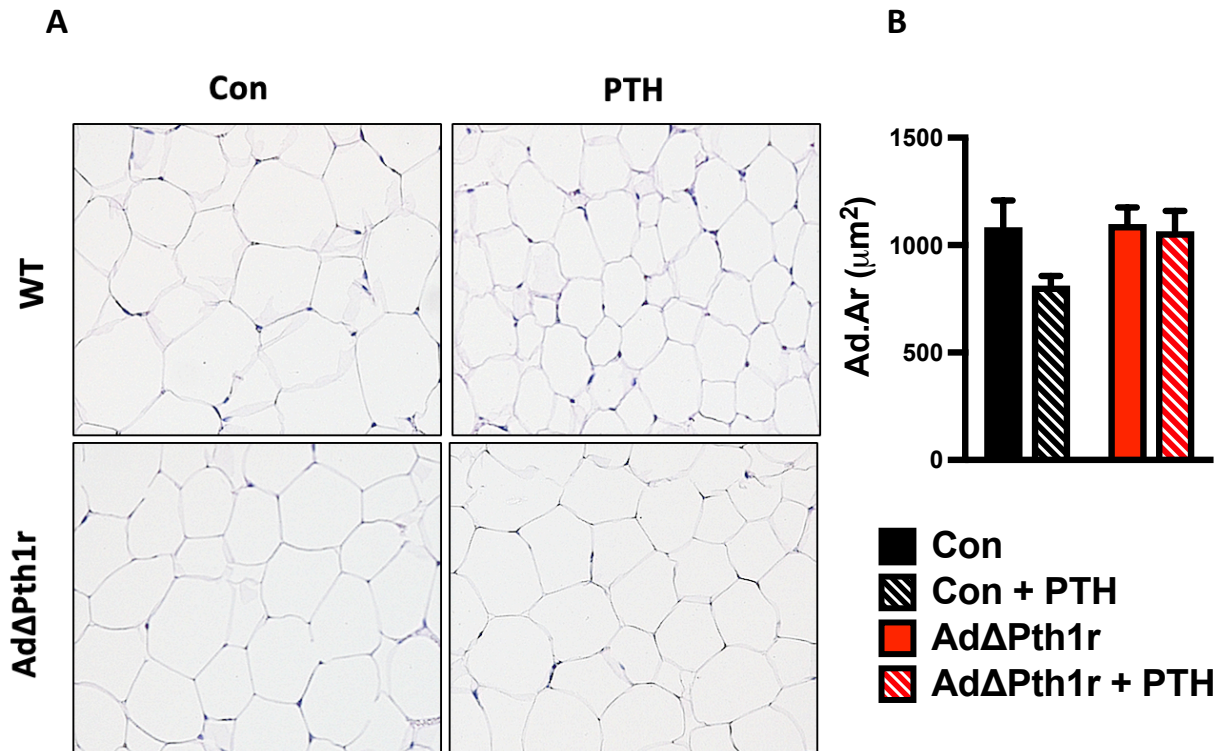
Figure 3.11 Pth1r deletion in adipocytes alters PTH-induced changes in gonadal white adipose tissue (gWAT). (A) Hematoxylin and Eosin (H&E) staining of gWAT from control (Con) and AdΔPth1r male mice treated with PTH_{1-34} (100ug/kg) or saline 5 days a week for 6 weeks. (B) PTH treatment decreased adipocyte area (Ad.Ar (μm^2)) in controls but not in knockouts. All data are represented as mean ± SEM. *$p < .05$.
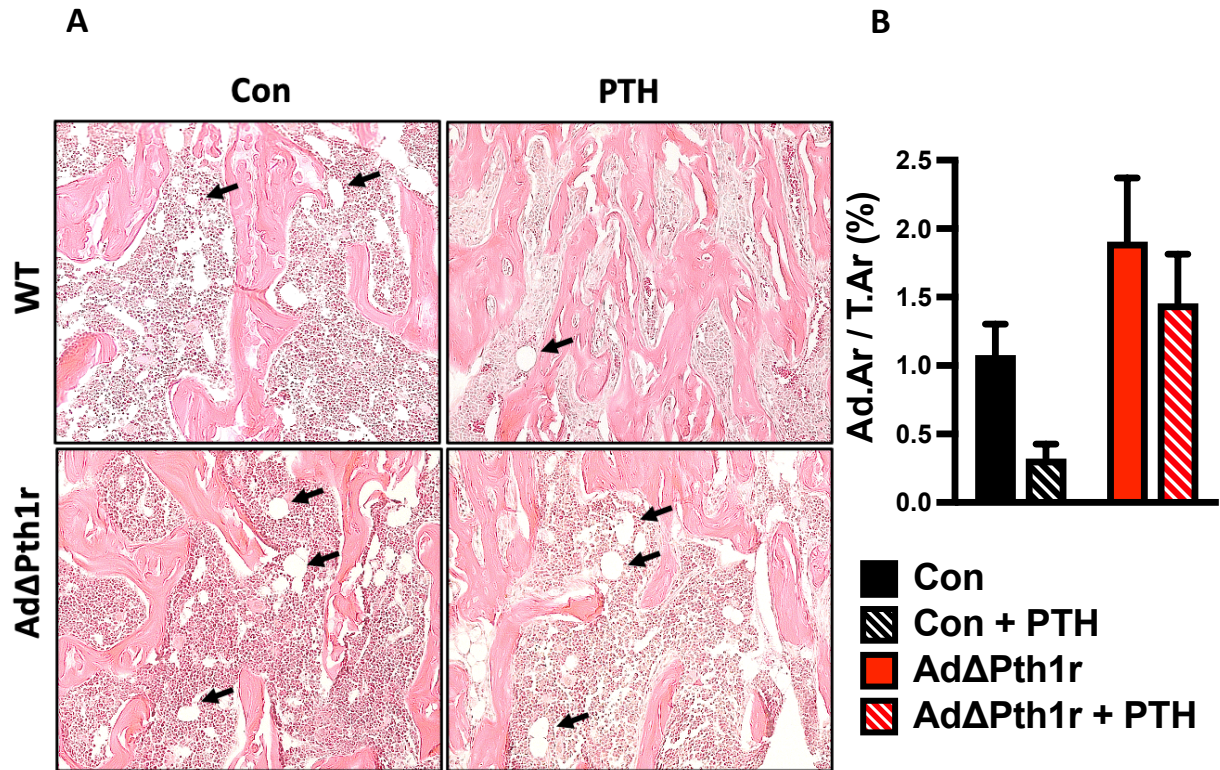
Figure 3.12 Pth1r deletion in adipocytes alters PTH-induced changes in bone marrow adipose tissue (BMAT). (A) Hematoxylin and Eosin (H&E) staining of femurs from control (Con) and AdΔPth1r male mice treated with PTH_{1-34} (100ug/kg) or saline 5 days a week for 6 weeks. (B) PTH treatment decreased adipocyte area relative to total area (Ad.Ar/T.Ar (%)) in controls but this response was diminished in AdΔPth1r mice. All data are represented as mean ± SEM. *$p < .05$.
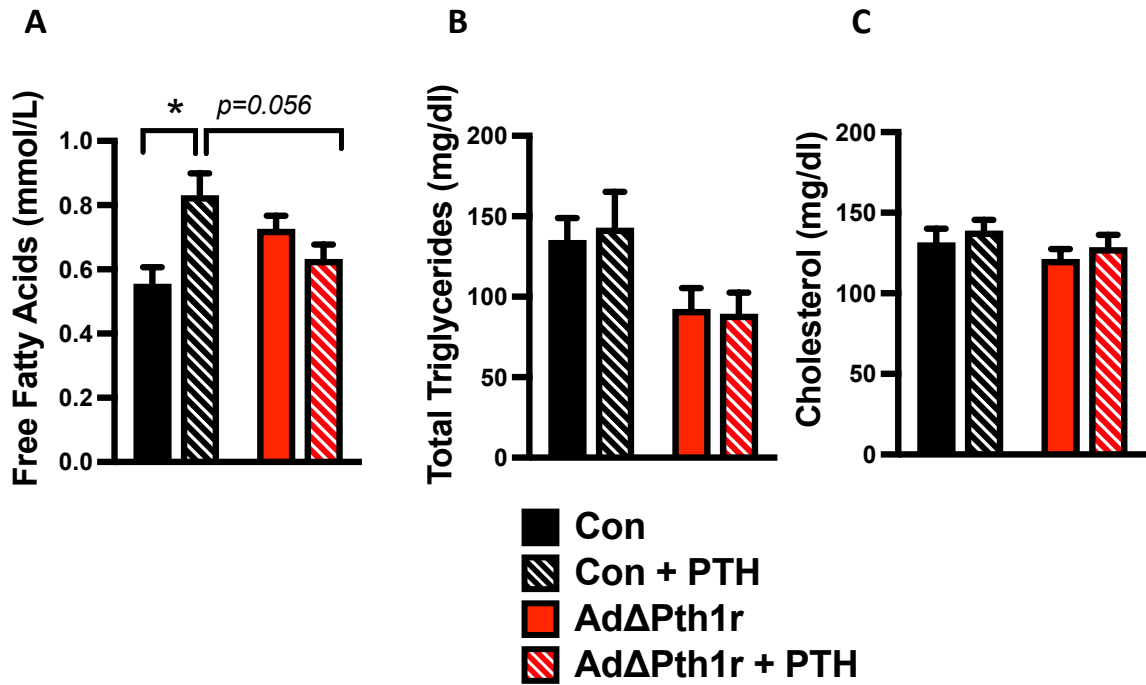
Figure 3.13 Free fatty acids, triglyceride, and cholesterol serum levels after intermittent PTH treatment. 8-week -old control (Con) and AdΔPth1r male mice were treated PTH_{1-34} (100ug/kg) or saline 5 days a week for 6 weeks. (A) Free fatty acids (mmol/L) (B) total triglycerides (mg/dl), and (C) cholesterol (mg/dl) serum levels. All data are represented as mean ± SEM. *$p < .05$.
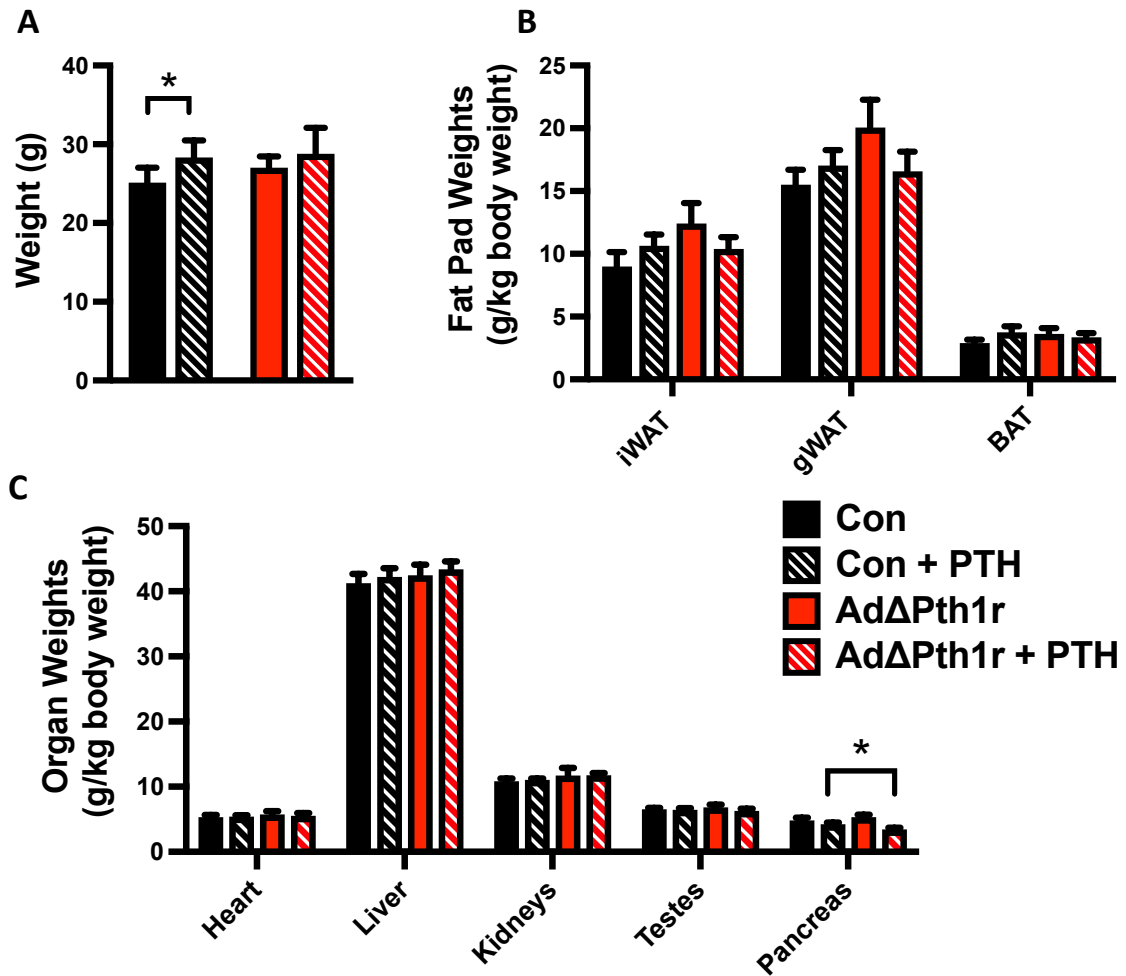
Figure 3.14 Body composition for AdΔPth1r and control littermates after 6 weeks of intermittent PTH treatment. 8-week -old control (Con) and AdΔPth1r male mice were treated PTH$_{1-34}$ (100ug/kg) or saline 5 days a week for 6 weeks. (A) There were changes in body weights observed, (B) but no changes in fat pads. (C) PTH did not alter any organ weights only a decrease in pancreatic weight between PTH treated controls and AdΔPth1r mice. All data are represented as mean ± SEM. *$p < .05$.

Thus far, the data has revealed intermittent PTH treatment induces changes in lipid homeostasis including alterations in adipocyte morphology. These changes are diminished or abolished in mice lacking the Pth1r in adipocytes suggesting PTH signaling through adipocytes is responsible for these changes. To understand the effects of deleting the Pth1r in adipose tissue on the anabolic response of bone to PTH, AdΔPth1r mutants and control littermates were treated with saline or PTH$_{1-34}$ (100ug/kg) 5 days a week for 6 weeks. Microarchitecture analysis by micro-CT revealed that PTH induced marked increases in bone volume fraction (BV/TV), trabecular number (Tb.N), and trabecular thickness (Tb.Th) in controls indicating a robust anabolic response. However, this anabolic response was abolished in knockouts (Fig 3.14) suggesting that PTH signaling through adipocytes is necessary for bone's anabolic response. Classically, PTH was thought to act directly on skeleton to stimulate bone accrual however, these data support that the hormone's signaling through another organ, adipose tissue in this case, is necessary to induce the anabolic response in bone. Another study reported skeletal muscle atrophy and adipose tissue browning, a result of kidney failure (modeled by 5/6 nephrectomy) and in cancer (modeled by Lewis lung carcinoma), was caused by PTH signaling through adipose tissue. Deletion of the Pth1r in adipose tissue resulted in atrophy-resistant skeletal muscle and adipose tissue resistant to browning [136]. This study, along with our data, suggests the importance of PTH signaling in adipose tissue to the function and processes of other organs in anabolism or disease. Although PTH-induced increases in femoral

trabeculae was abolished in Pth1r knockouts, mutants were mostly responsive to PTH in the cortical region of the mid diaphysis of femurs (Fig 3.15). The ratio between B.Ar and T.Ar and cortical thickness (Cs.Th) did not significantly increase in PTH treated knockouts, suggesting minor cortical impairment. The cortex is a dense, compact area of the bone imperative to structure and mechanical loading with high resistance to stress such as bending and torsion. Due to its importance, more compensatory mechanisms in preserving its structure and function may be in place which could explain why there was still a significant response to PTH in Pth1r mutants.
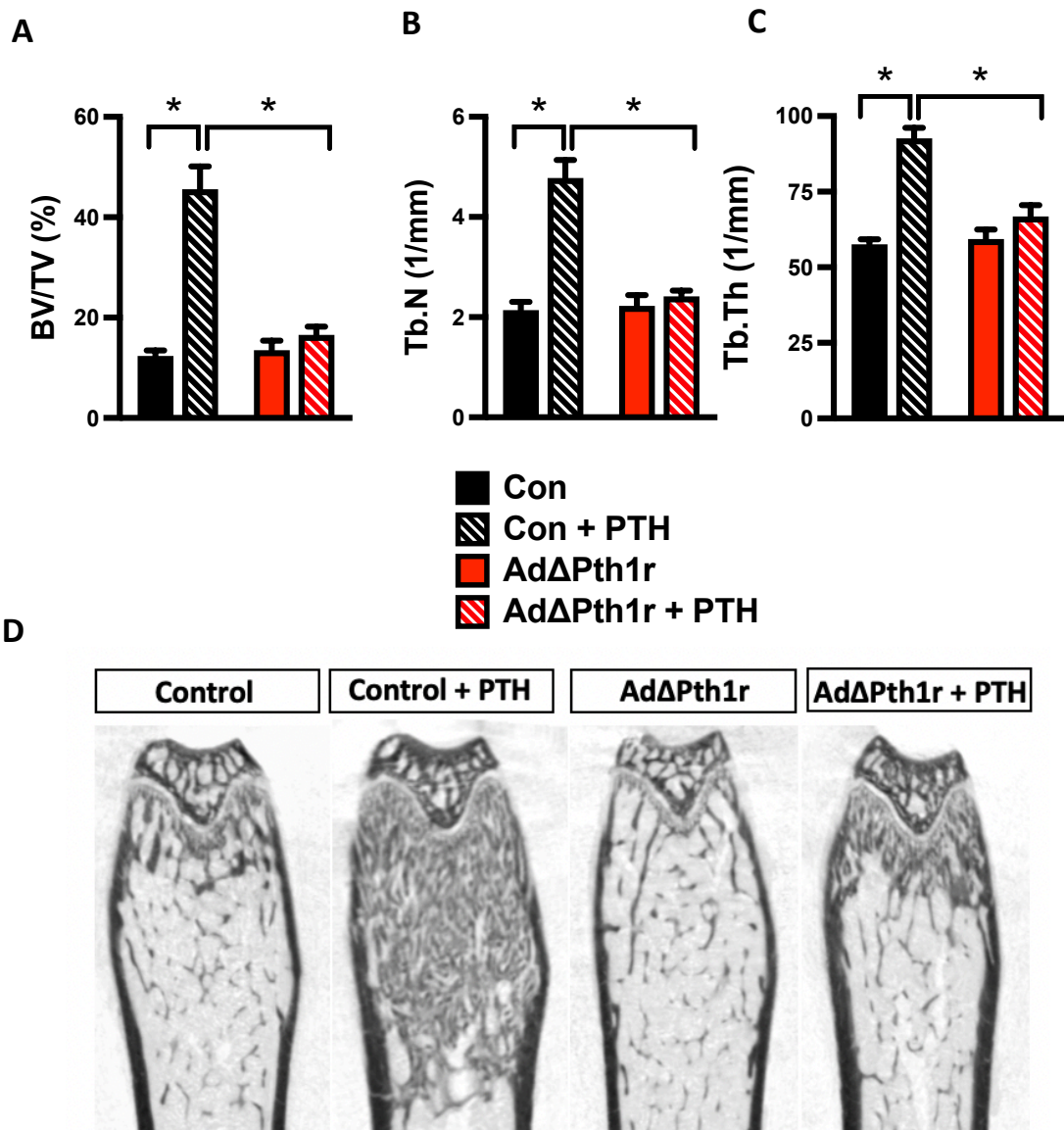
Figure 3.15 Trabecular analysis reveals Pth1r expression by adipocytes is required for PTH-induced anabolism. 8-week -old control (Con) and AdΔPth1r male mice were treated PTH_{1-34} (100ug/kg) or saline 5 days a week for 6 weeks. PTH-induced increases in trabecular (A) bone volume per tissue volume (BV/TV (%)), (B) trabecular number (Tb.N (1/mm)), and (C) trabecular thickness (Tb.Th (μm)) evident in control mice were abolished or greatly diminished in Pth1r mutants. (D) Representative 2D images from distal femurs used in the analysis of trabecular parameters. All data are represented as mean ± SEM. $^*p < .05$.
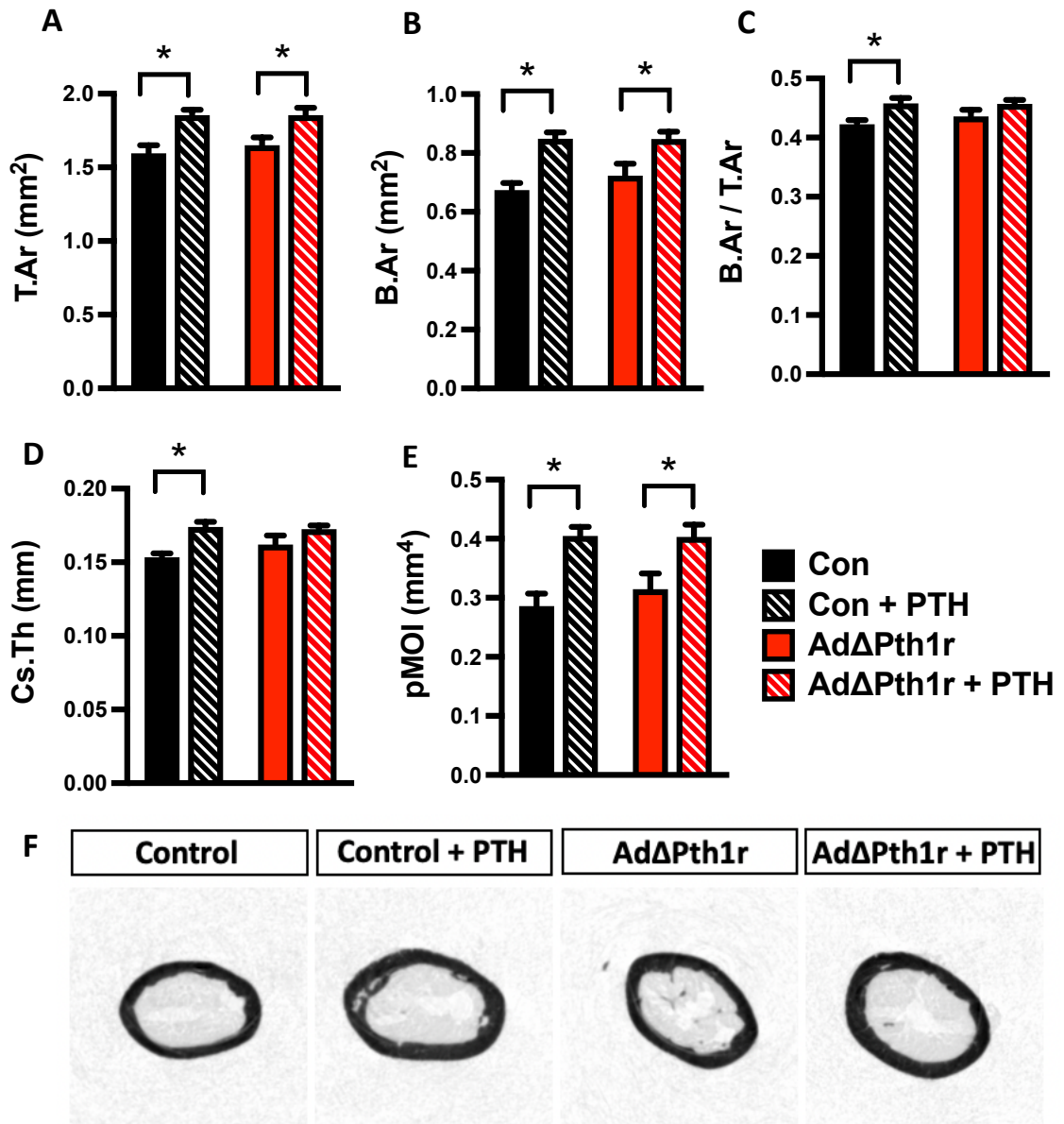
Figure 3.16 PTH-induced increases in cortical parameters were evident in control and AdΔPth1r mice. 8-week -old control (Con) and AdΔPth1r male mice were treated PTH$_{1-34}$ (100ug/kg) or saline 5 days a week for 6 weeks. Intermittent PTH effects in (A) total cross sectional area (T.Ar (mm^2)), (B) cortical bone area (B.Ar (mm^2)), (C) the ratio between B.Ar and T.Ar, (D) the cortical thickness (Cs.Th (mm)), (E) mean moment of inertia (pMOI (mm^4)) in control and knockout littermates. (F) Representative images from the mid-diaphysis of femurs. All data are represented as mean ± SEM. *$p < .05$.

Microarchitecture analysis of trabecular regions of the distal femurs of mice revealed that ablation of the Pth1r in adipocytes abolished the anabolic response of bone to intermittent PTH treatment. To understand the mechanism of the diminished response, dynamic histomorphometry was performed using the same femurs analyzed in the micro-CT analysis. As the experiment in Chapter 3, calcein and alizarin were injected 7 days apart and analyses was performed in the distal femur. Results indicated that deleting Pth1r in adipocytes impaired osteoblast function after PTH administration. In control mice, PTH induced a marked increases mineralizing surface per bone surface (MS/BS), and mineral apposition rate (MAR) which led to an overall increase in bone formation rate (BFR/BS). These parameters were only slightly altered in Pth1r knockouts (Fig 3.16). In addition to the Cpt2 mutant data suggesting that fatty acid oxidation is necessary for an anabolic response, this additional data highlights the importance of an adipose tissue specific response in the anabolic actions of PTH on bone. The significant absence of an anabolic response, as indicated by micro-CT and dynamic histomorphometric analysis, indicates a novel understanding of PTH signaling; PTH must signal through adipose tissue for increased bone accrual. It was also important to determine if osteoclast dysfunction plays a role in this model. TRAP staining and analysis of distal femurs of control and AdΔPth1r mice revealed that intermittent PTH similarly increased osteoclast number in controls and mutants (Fig 3.17). These data indicate that the impairment in bone acquisition in

adipocyte specific Pth1r knockout mice is due to an impairment in osteoblastic bone formation, independent of osteoclasts.
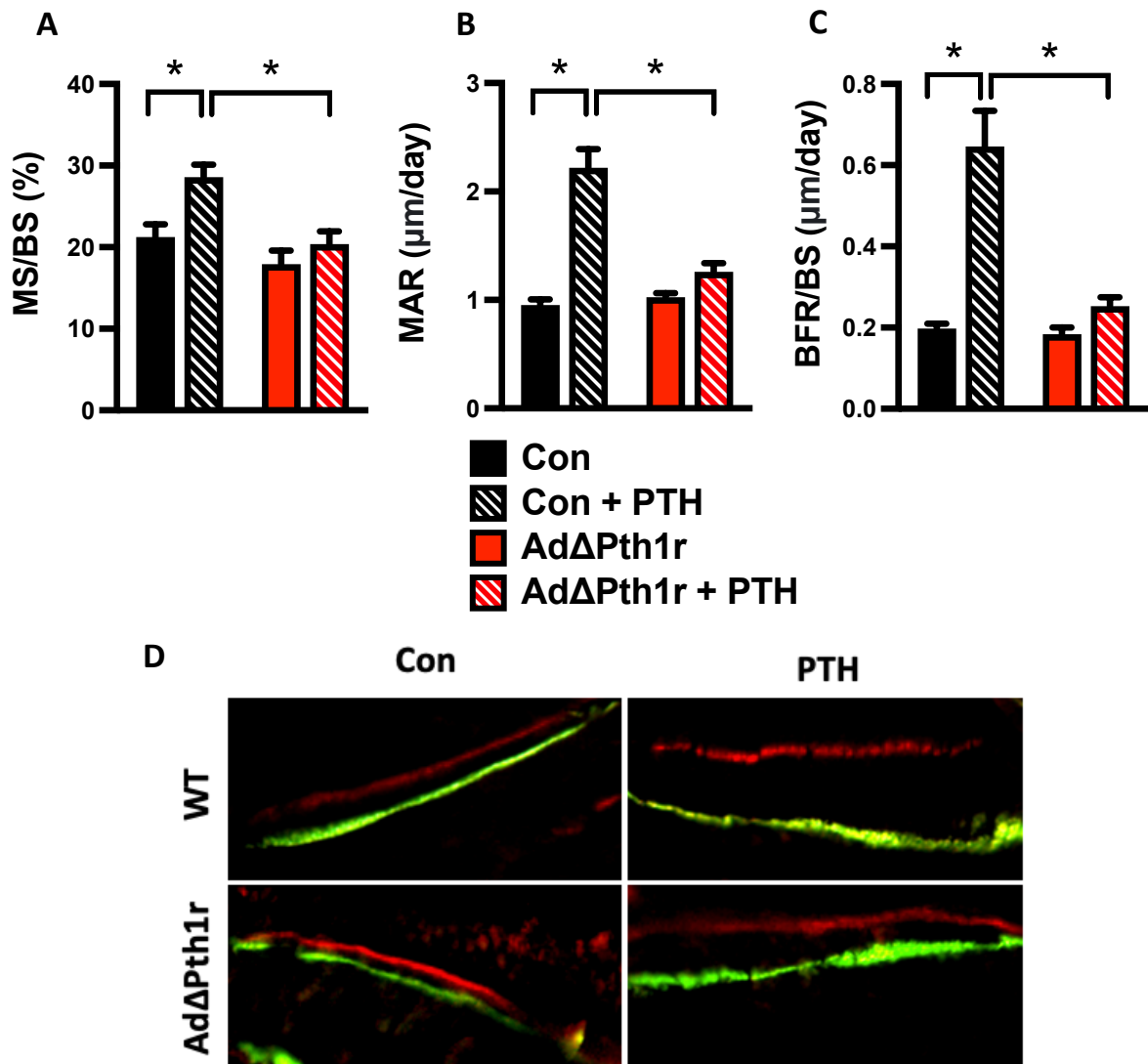
Figure 3.17 Dynamic histomorphometry analysis reveals Pth1r deletion in adipose tissue abolishes PTH-induced increases in mineralization. Control (Con) and AdΔPth1r male mice treated PTH$_{1\text{-}34}$ (100ug/kg) 5 days a week for 6 weeks have increased (A) mineralizing surface per bone surface (MS/BS (%)) (no significance p=0.052), (B) mineral apposition rate (MAR μm/day), (C) bone formation rate over bone surface (BFR/BS (μm/day). (D) Representative images indicate the abolished mineralizing response of trabecular bone to PTH when Pth1r is abolished in adipocytes. All data are represented as mean ± SEM. *$p < .05$.
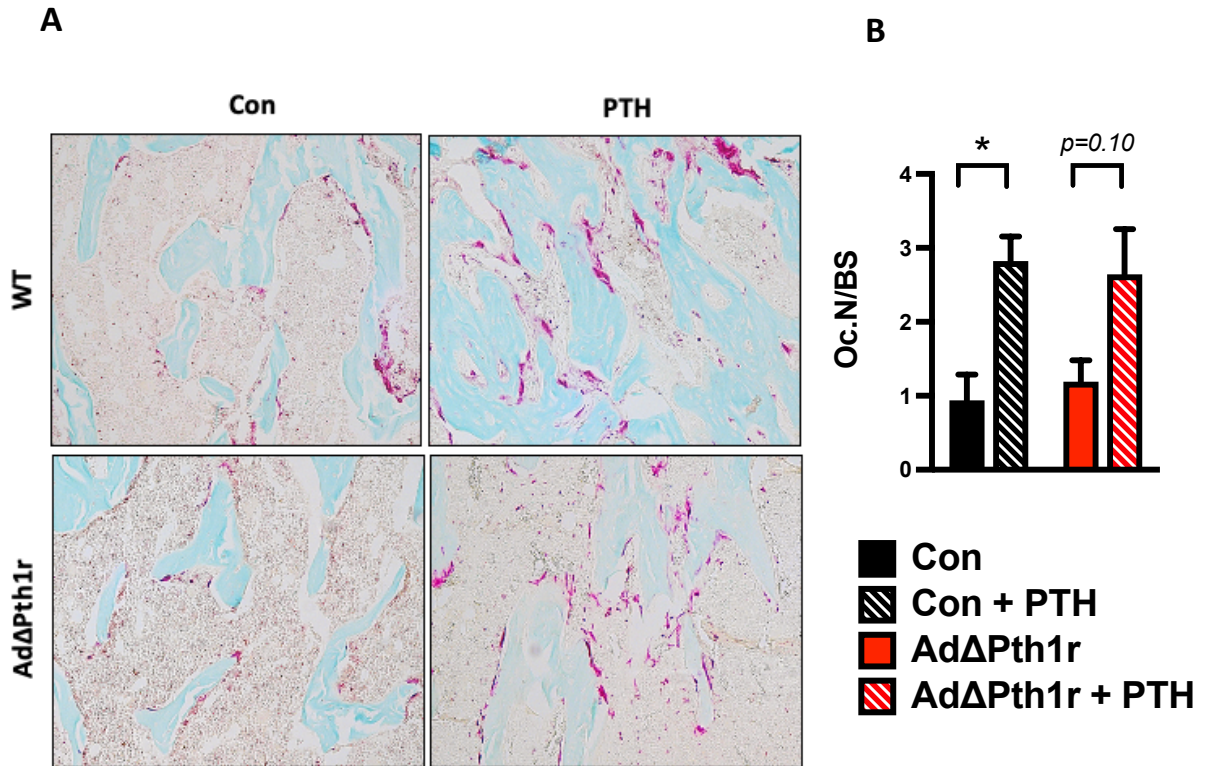
Figure 3.18 Impairing PTH signaling in adipocytes does not affect osteoclast number. (A) TRAP staining of distal femurs from control (Con) and AdΔPth1r male mice treated with PTH_{1-34} (100ug/kg) or saline 5 days a week for 6 weeks. (B) Analysis revealed PTH increased osteoclast number per bone surface (Oc.N/BS) in both control and knockout littermates (p=0.10) suggesting there is not a disruption in osteoclast function but impaired osteoblastic bone formation. All data are represented as mean ± SEM. *$p < .05$.

Thus far, the data presented indicates a new understanding of PTH's anabolic effects on the skeleton. PTH's ability to alter fatty acid metabolism in osteoblasts by stimulating catabolism and utilization of fatty acids in vitro is echoed in in vivo studies that show the necessity of this process. Long chain fatty acid β-oxidation in osteoblasts is necessary for PTH-induced bone accrual in femurs. Additional data shows the alterations in lipid metabolism by acute and prolonged PTH treatment. An acute treatment of PTH is sufficient to trigger lipolytic enzymes in peripheral adipose tissue and increase the release of free fatty acids in the serum. Prolonged treatment with PTH increased bone density but also causes morphological changes in fat depots including inguinal and gonadal white adipose tissue and in bone marrow adipocytes. These metabolic changes are dependent on PTH signaling through adipocytes. When the Pth1r in adipocytes is ablated, there is a diminished lipolytic response, resulting in decreased serum free fatty acids, and diminished changes in adipocyte morphology to PTH treatment. This necessity for PTH signaling through adipose tissue is reflected in the significantly diminished response in bone to PTH-induced anabolism. These data highlight the important role that adipose tissue plays in contributing to bone's anabolic response, specifically to osteoblastic bone formation. To further understand this critical role, we investigated how adipocyte lipolysis directly impacts the anabolic and metabolic response to PTH.

Adipose triglyceride lipase (ATGL) is the rate limiting enzyme in lipolysis and is encoded by the PNPLA2 gene (patatin like phospholipase domain

containing 2). ATGL is expressed highly in white and brown adipose tissue and hydrolyzes triglycerides to produce diacylglycerol and one fatty acid. Diacylglycerol is preferentially hydrolyzed by hormone sensitive lipase (HSL), generating a second free fatty acid. Lastly, monoacylglycerol lipase (MGL) catalyzes the last reaction releasing glycerol and a third fatty acid. Post transcriptionally, ATGL is activated by phosphorylation by AMPK [137, 138] or PKA [139]. PTH promotes adipocyte lipolysis through cAMP-dependent activation of PKA [106] indicating a pathway for which PTH releases free fatty acids. To understand how adipocyte lipolysis is important for PTH's metabolic and anabolic affects in vivo, we targeted the lipolytic step by crossing the AdipoQ-Cre line to Atgl[flox/flox] mice which exons 2 though 7 are flanked by loxP sites [140]. Western blot analysis of Atgl protein expression in inguinal white adipose tissue (iWAT) of Atgl[flox/flox]; AdipoQ-Cre^{+/+} (Controls) and Atgl[flox/flox]; AdipoQ-Cre[TG/+] (AdΔAtgl) animals indicates deletion (Fig 3.18). Using this Cre line will target both peripheral adipose depots and bone marrow adipocytes which may serve as external and local sources of fatty acids respectively for osteoblasts [105]. We targeted adipocyte lipolysis because previous work from our laboratory showed that the loss of Atgl function in osteoblasts did not affect oxidation of fatty acids and matrix mineralization [39]. These findings indicate that the acquired fatty acids by the osteoblast rely primarily on exogenous supplies rather than utilization of intracellular stores.

To confirm that adipocytes were the source of the increase of serum free fatty in response to PTH, AdΔAtgl and control littermates were injected

subcutaneously with PTH or saline and serum was collected 30 minutes post administration. Ablating the expression of Atgl resulted in an abolished increase in serum free fatty acid levels (Fig. 3.19).
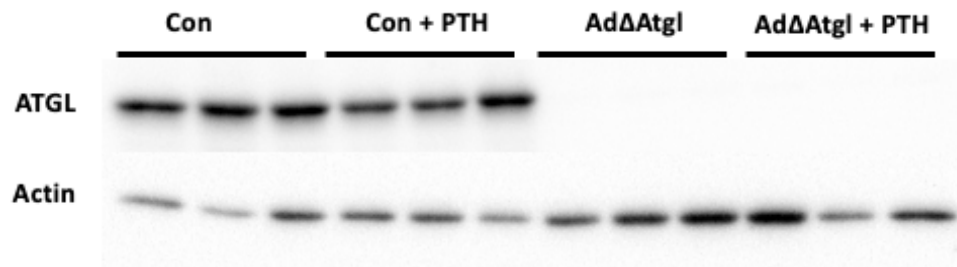
Figure 3.19 Protein expression of ATGL in AdΔAtgl and littermate control. Western blot analysis of ATGL protein levels reveals the successful deletion of Atgl in inguinal white adipose tissue. Acute PTH administration had no effect on expression in AdΔAtgl.
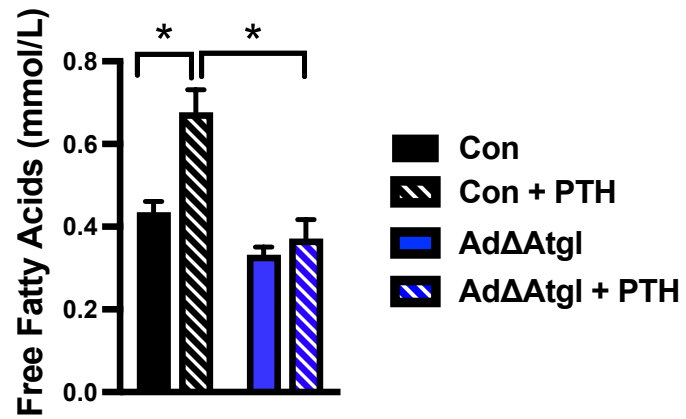
Figure 3.20 Atgl is required for PTH-induced lipolysis. 8-week-old AdΔAtgl and control littermates were injected subcutaneously with PTH$_{1-34}$ (100μg/kg) or saline. After 30 minutes, PTH increased serum free fatty acids in control but not in AdΔAtgl mice. All data are represented as mean ± SEM. *$p < .05$.

Adipocyte-specific deletion of Atgl resulted in a decreased lipolytic response to PTH as indicated by the lack of increase in serum free fatty acids. Next, we sought to understand the metabolic changes after prolonged PTH treatment. 8-week-old AdΔAtgl and control littermates were injected subcutaneously with PTH$_{1-34}$ (100μg/kg) or saline 5 days week for 6 weeks. Intermittent PTH treatment resulted in decreased adipocyte size in inguinal white adipose tissue (iWAT), but PTH failed to decrease adipocyte area with Atgl ablation (Fig 3.20). PTH did not significantly alter adipocyte area in gonadal white adipose tissue (gWAT) in knockout or control littermates (Fig 3.21). The inability for PTH to significantly alter gWAT area in controls could be a mouse line-dependent response. However, saline treated Atgl mutants did trend toward larger adipocyte area compared to saline controls in both iWAT and gWAT fat depots (Fig 3.20 and 3.21).

Serum was collected from these animals 30 minutes after the final administration of PTH. PTH treatment slightly elevated free fatty acids in both control and Atgl mutants (no significance). Atgl knockouts did have significantly lower serum free fatty acids which has been previously reported in fasted mice [141]. Total triglycerides and cholesterol levels were not significantly altered between any of the four groups (Fig 3.22).
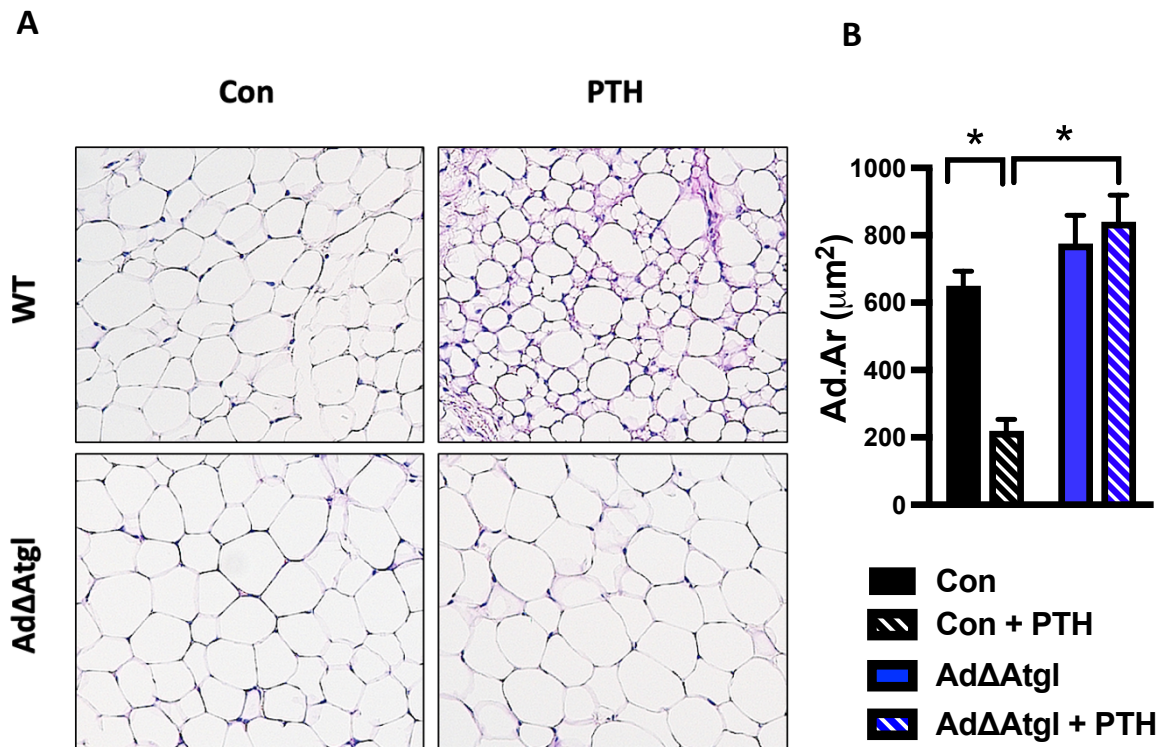
Figure 3.21 Atgl deletion in adipocytes alters PTH-induced changes in inguinal white adipose tissue (iWAT). (A) Hematoxylin and Eosin (H&E) staining of iWAT from control (Con) and AdΔAtgl male mice treated with PTH_{1-34} (100ug/kg) or saline 5 days a week for 6 weeks. (B) PTH treatment decreased adipocyte area (Ad.Ar (μm^2)) in controls but not in knockouts. All data are represented as mean ± SEM. *$p < .05$.
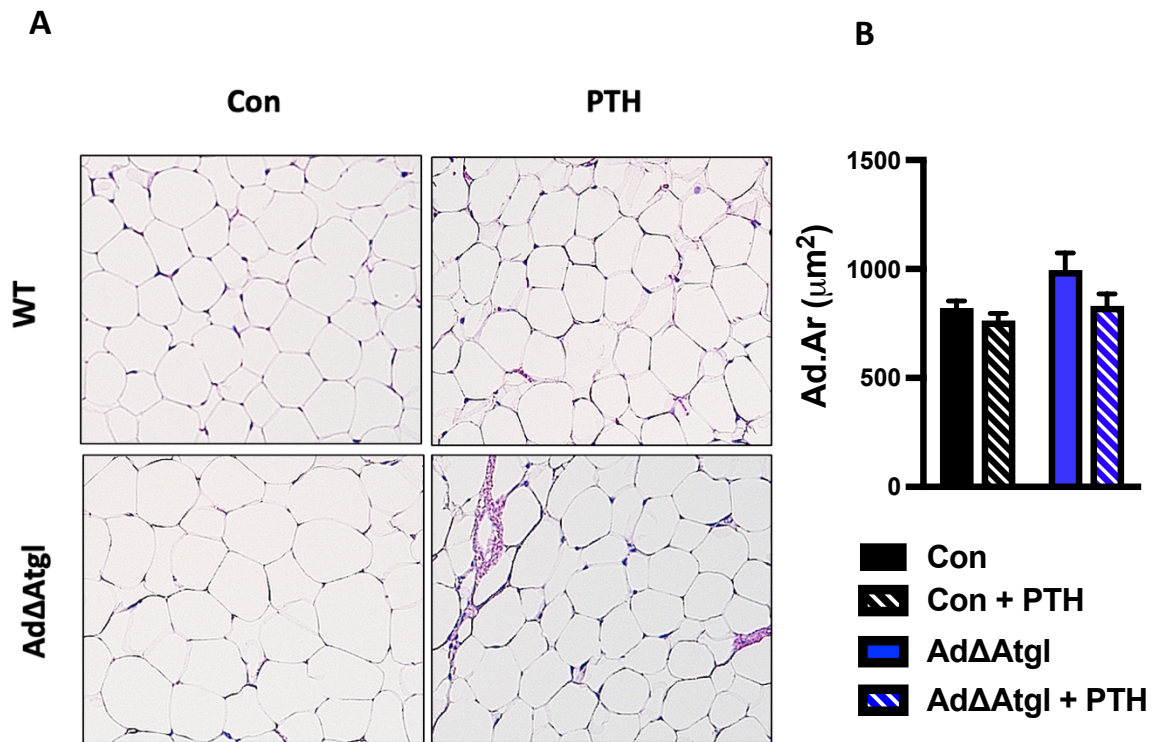
Figure 3.22 Atgl deletion in adipocytes alters changes in gonadal white adipose tissue (gWAT). (A) Hematoxylin and Eosin (H&E) staining of gWAT from control (Con) and AdΔAtgl male mice treated with PTH$_{1-34}$ (100ug/kg) or saline 5 days a week for 6 weeks. (B) PTH did not significantly alter Adipocyte area (Ad.Ar (μm^2)) in control or Atgl mutants. All data are represented as mean ± SEM. *$p < .05$.
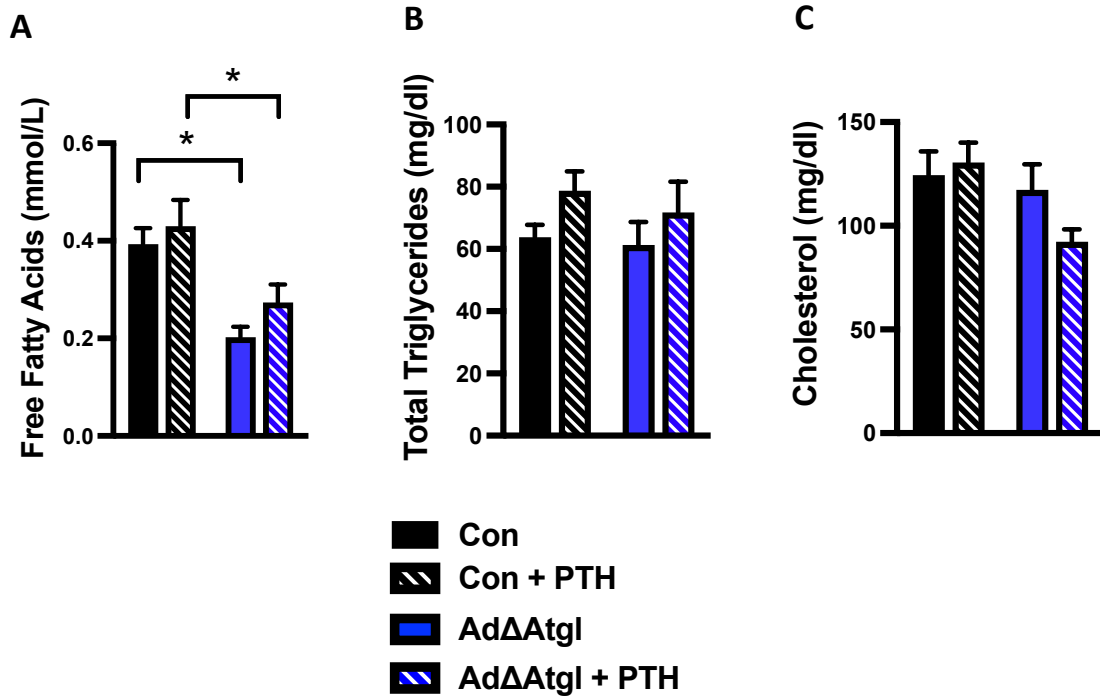
Figure 3.23 Free fatty acids, triglyceride, and cholesterol serum levels after intermittent PTH treatment. 8-week -old control (Con) and AdΔAtgl male mice were treated PTH$_{1-34}$ (100ug/kg) or saline 5 days a week for 6 weeks. (A) Free fatty acids (mmol/L) (B) total triglycerides (mg/dl), and (C) cholesterol (mg/dl) serum levels. All data are represented as mean ± SEM. *$p < .05$.

In addition to changes in adipocyte morphology, changes in body composition proceeded 6 weeks of PTH treatment despite no marked alterations in final body weight. Significant increases in iWAT and brown adipose tissue (BAT) were seen in AdΔAtgl mutants compared to littermate controls, findings that have been reported in previous studies [141, 142]. Intermittent treatment had no significant effect on fat pad weights although values were trending downward for control mice while there was an upward trend for AdΔAtgl littermates (iWAT and BAT). PTH treatment and/or Atgl ablation had effects on the weights of liver and the testes. PTH significantly decreased liver size in Atgl mutants compared to control PTH or saline treated mutants. A previous study reported that liver weight decreased at 24 weeks for AdΔAtgl mice and that the weight decreased when animals were given a high fat diet [141].Atgl deletion did not significantly cause a decrease in liver weight for our study, but values were trending downward. This study also reported that hepatic lipid synthesis and gluconeogenesis decreased with adipocyte-specific deletion of Atgl and previous studies that indicate PTH affects glucose metabolism [143] together could explain our findings. The weight of the testes decreased with PTH treatment, an effect not seen in seen in data reported in Chapter 3 or 4. Atgl deletion also caused a decrease in testes weight (Fig 3.23).

Impairing the lipolytic response in fat did not have any impact on overall bone mass. After 6 weeks of treatment, microarchitecture analysis using micro-CT revealed PTH induced marked increases in bone volume fraction (BV/TV),

trabecular number (Tb.N), and trabecular thickness (Tb.Th) while Atgl ablation in adipocytes led to a diminished response to PTH in the trabecular region of distal femurs (Fig 3.24). Cortical parameters of the mid diaphysis of femurs increased with intermittent PTH treatment including cross sectional area (T.Ar.) in the periosteal envelope, cortical bone area (B.Ar.), the ratio between B.Ar and T.Ar, cortical thickness (Cs.Th), and mean moment of inertia (pMOI). However, PTH had little effect on these parameters in Atgl mutants (Fig 3.25). These data indicate a necessity for adipose-derived fatty acids in PTH-induced bone formation in the trabecular and cortical parameters of femurs. Unlike the Pth1r mutants that exhibited only slightly altered cortical responses to PTH, Atgl mutants had impaired cortical bone accrual. This may indicate an inability for compensation highlighting the importance of adipose derived fatty acid in PTH induced anabolism in the cortex.

To further understand the mechanism behind this diminished trabecular response, dynamic histomorphometric analysis was performed in the distal femur using calcein and alizarin, injected 7 days apart. Analysis revealed a marked increase in mineral apposition rate (MAR) and bone formation rate (BFR/BS) with PTH treatment. However, PTH failed to increase these parameters in Atgl mutants suggesting an impairment in mineralization (Fig 3.26). PTH did not significantly increase mineralizing surface relative to bone surface (MS/BS) but there was an upwards trend. In contrast, PTH failed to increase MS/BS with Atgl deletion, which trended downward relative to saline treated mutant littermates. Saline treated Atgl

knockouts exhibited a lower MAR compared to wildtype controls suggesting that even without an anabolic stimulus there are still cellular alterations induced by impaired adipose lipolysis despite no changes in overall bone accrual. Together, the microarchitecture and the histomorphometric analyses demonstrate the necessity for adipose derived fatty acids in fueling PTH-induced bone formation. In addition to our data that β-oxidation in osteoblasts (Chapter 2) and PTH signaling through adipocytes is necessary for PTH anabolism, we now provide evidence that adipose lipolysis and liberated free fatty acids are necessary for bone accrual in response to an anabolic stimulus.
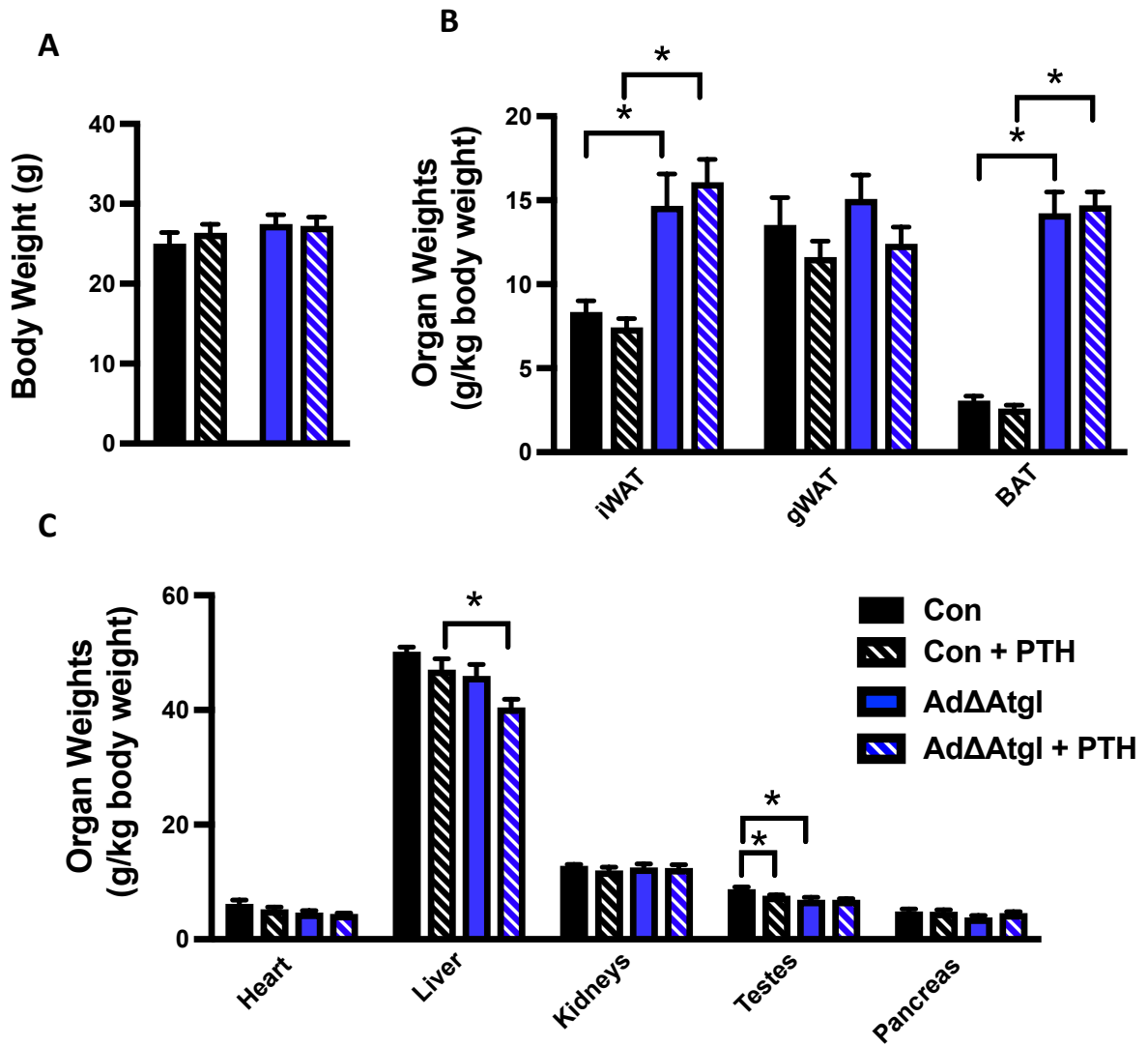
Figure 3.24 Body composition for AdΔAtgl and control littermates after 6 weeks of intermittent PTH treatment. 8-week-old control (Con) and AdΔAtgl male mice were treated with PTH_{1-34} (100ug/kg) or saline 5 days a week for 6 weeks. (A) There were no changes in body weights observed, but there were alterations in inguinal white adipose tissue (iWAT) and brown adipose tissue (BAT) (B). (C) There were also changes seen in liver and testes weights. All data are represented as mean ± SEM. *$p < .05$.
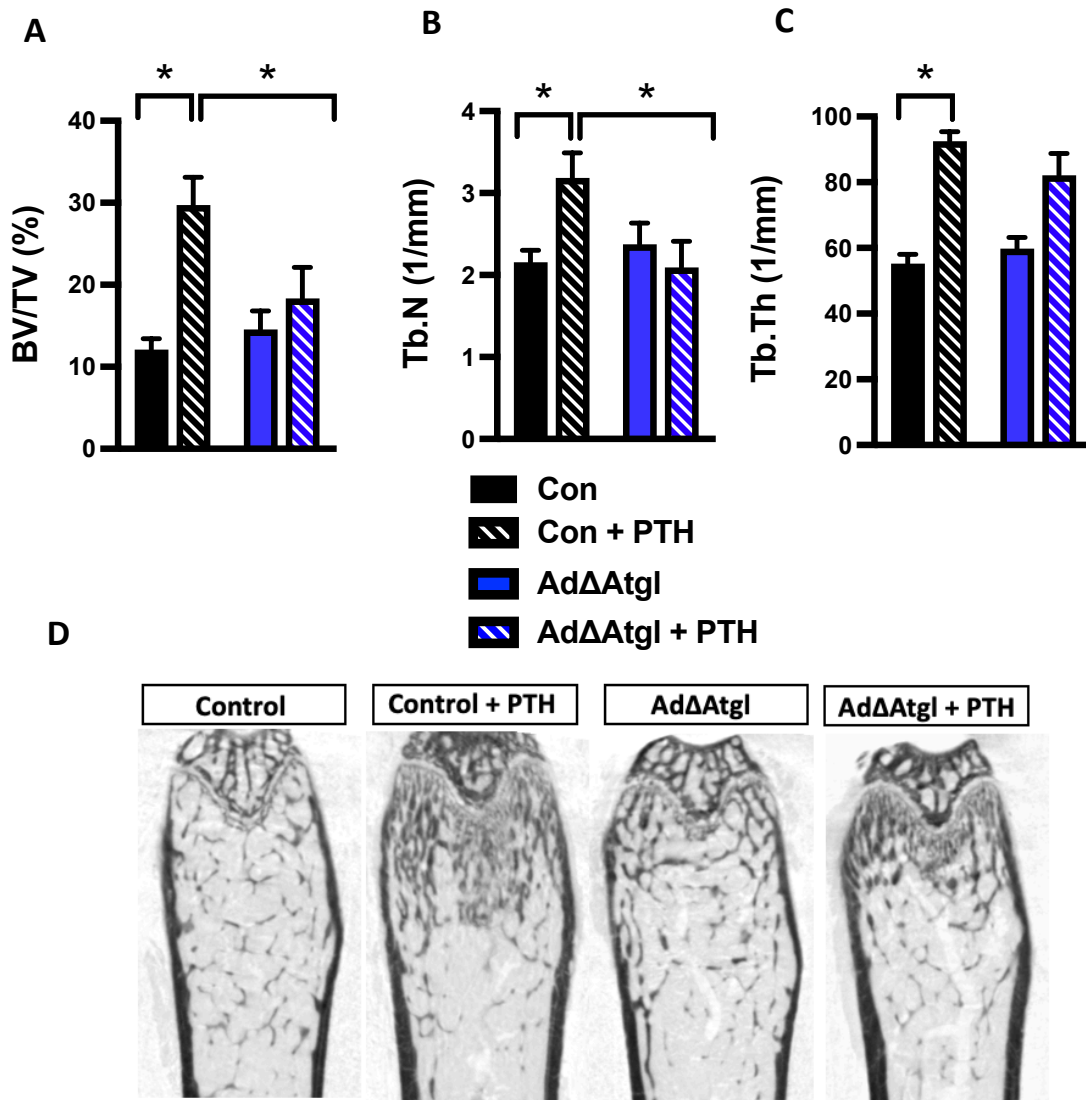
Figure 3.25 Trabecular analysis reveals Atgl expression by adipocytes is required for PTH-induced anabolism. 8-week-old control (Con) and AdΔAtgl male mice were treated with PTH_{1-34} (100ug/kg) or saline 5 days a week for 6 weeks. PTH-induced increases in trabecular (A) bone volume per tissue volume (BV/TV (%)), (B) trabecular number (Tb.N (1/mm)), and (C) trabecular thickness (Tb.Th (µm)) evident in control mice were abolished or greatly diminished in Pth1r mutants. (D) Representative 2D images from distal femurs used in the analysis of trabecular parameters. All data are represented as mean ± SEM. *$p < .05$.
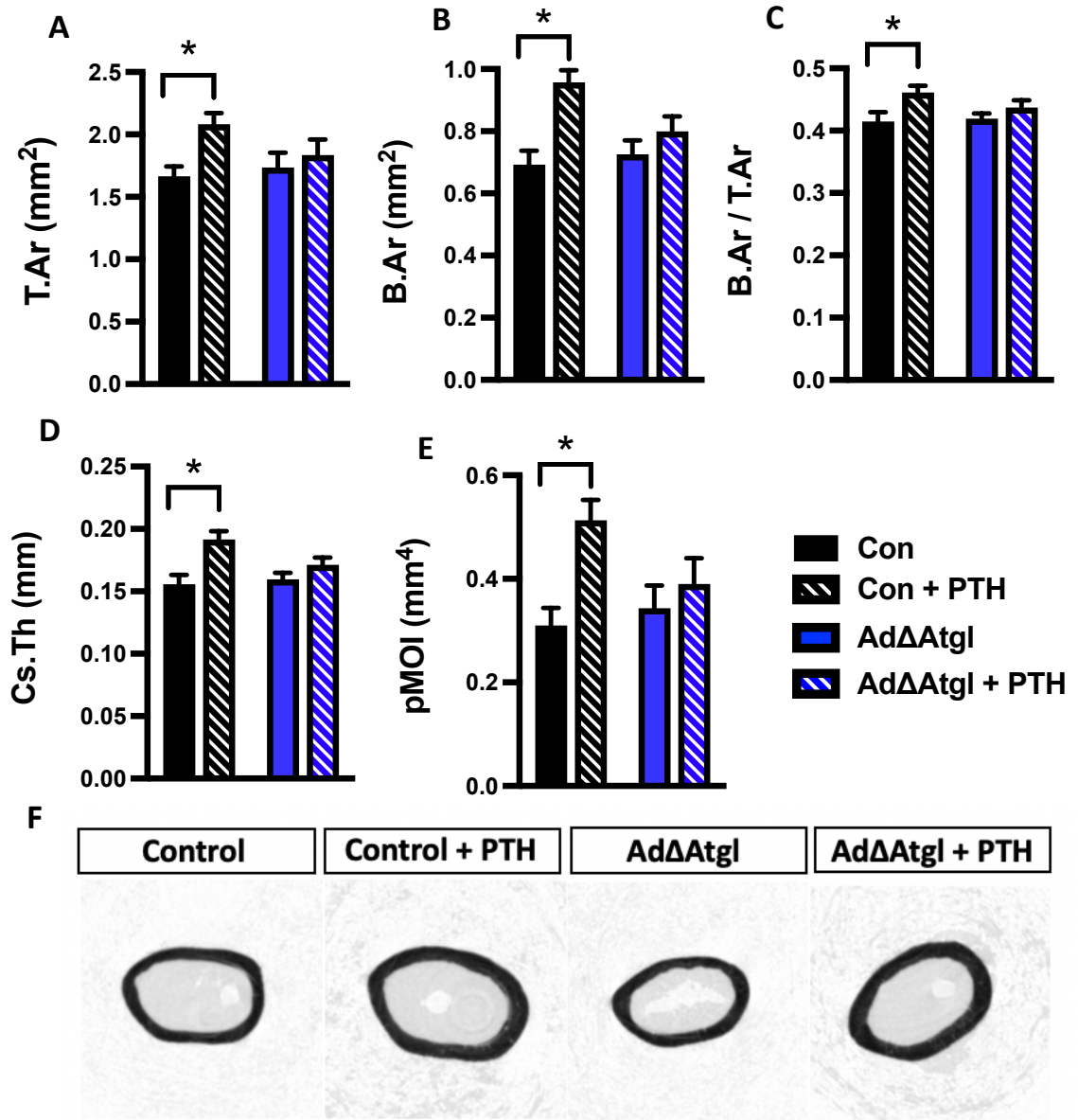
Figure 3.26 Atgl is necessary for PTH-induced increases in cortical bone. 8-week-old control (Con) and AdΔAtgl male mice were treated with PTH_{1-34} (100ug/kg) or saline 5 days a week for 6 weeks. Intermittent PTH increased (A) total cross sectional area (T.Ar (mm^2)), (B) cortical bone area (B.Ar (mm^2)), (C) the ratio between B.Ar and T.Ar, (D) the cortical thickness (Cs.Th (mm)), and (E) mean moment of inertia (pMOI (mm^4)) in controls but this response was diminished in Atgl mutants. (F) Representative images from the mid-diaphysis of femurs. All data are represented as mean ± SEM. *$p <$
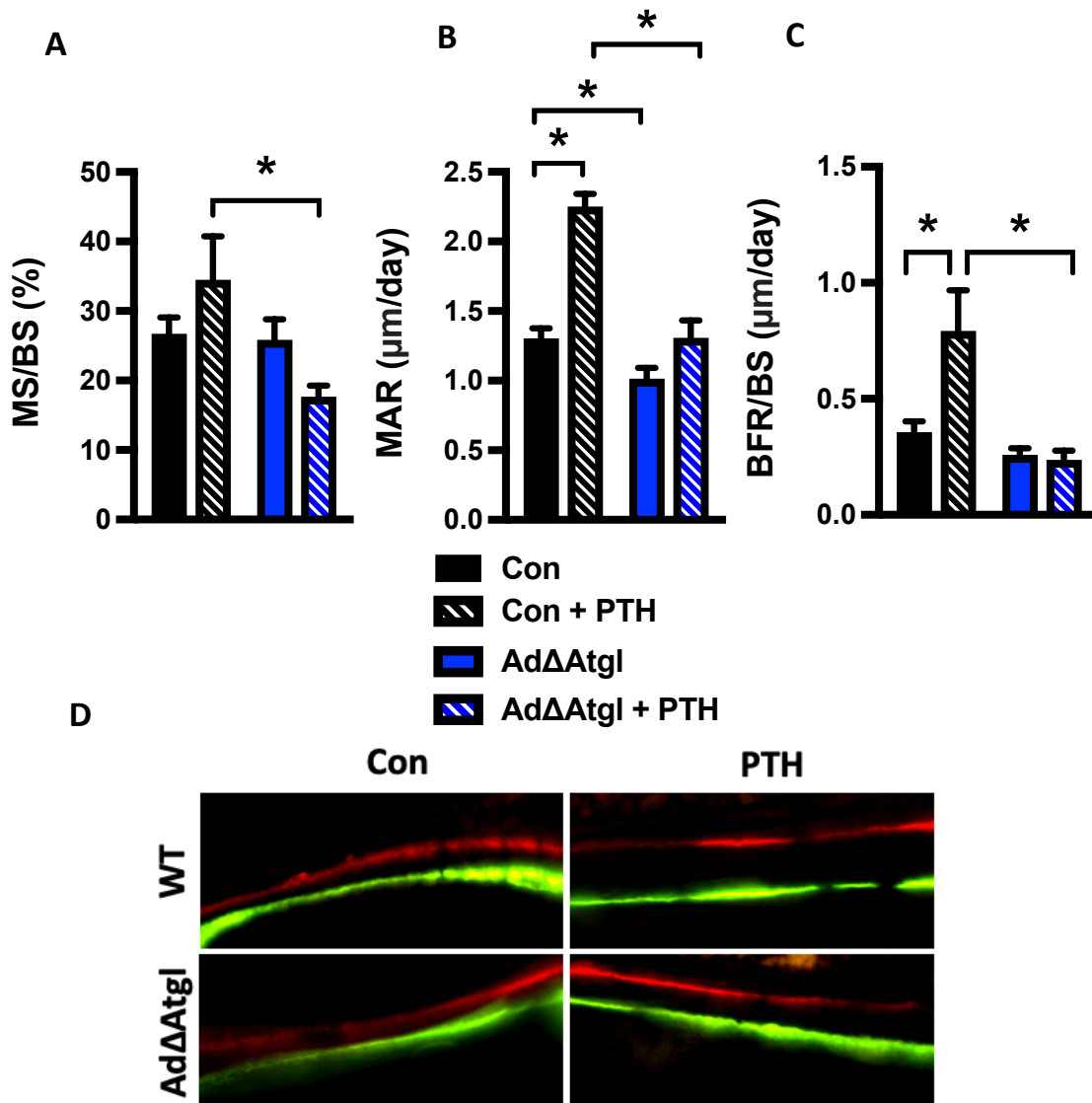
Figure 3.27 Dynamic histomorphometry analysis reveals Atgl deletion in adipose tissue abolishes PTH-induced increases in mineralization. 8-week-old control (Con) and AdΔAtgl male mice treated with PTH$_{1-34}$ (100ug/kg) or saline 5 days a week for 6 weeks have increased (A) mineralizing surface per bone surface (MS/BS (%)) (no significance), (B) mineral apposition rate (MAR μm/day), and (C) bone formation rate over bone surface (BFR/BS (μm/day). (D) Representative images indicate the abolished mineralizing response of trabecular bone to PTH when Atgl is abolished in adipocytes. All data are represented as mean ± SEM. *$p < .05$.

3.2 Materials and Methods

Animal models

Mouse lines were housed and maintained as described in Chapter 2. See chapter 2 for descriptions on the Cpt2$^{flox/flox}$ line. Pth1r$^{flox/flox}$ were kindly provided by Henry Kronenberg and have been previously described [144]. To generate an adipocyte-specific mutant, mice were crossed with AdipoQ-Cre mice [145]. The resulting Pth1r$^{flox/+}$; Cre$^{+/-}$ progeny were then backcrossed to Pth1r$^{flox/flox}$ mice to generate the tissue-specific knockouts. Breeding pairs of Pth1r$^{flox/flox}$; Cre$^{+/-}$ and Pth1r$^{flox/flox}$ were used to generate control mice (Pth1r$^{flox/flox}$) and knockout littermates (Pth1r$^{flox/flox}$; Cre$^{+/-}$). Genotyping primers for AdipoQ-Cre$^{TG/+}$ mice were 5'- GAA CCT GAT GGA CAT GTT CAGG-3' (forward) and 5'-AGT GCG TTC GAA CGC TAG AGC CTG T-3' (reverse). Genotyping primers for Pth1r$^{flox/flox}$ mice were 5'-TGG ACG CAG ACG ATG TCT TTA CCA-3' (forward) and 5'-ACA TGG CCA TGC CTG GGT CTG AGA-3' (reverse). All mice were maintained on a C57Bl/6 background.

Atgl$^{flox/flox}$ were kindly provided by Erin Kershaw and have been described previously [140]. To generate an adipocyte-specific mutant, mice were crossed with AdipoQ-Cre mice [145]. The resulting Atgl$^{flox/+}$; Cre$^{+/-}$ progeny were then backcrossed to Atgl$^{flox/flox}$ mice to generate the tissue-specific knockouts. Breeding pairs of Atgl$^{flox/flox}$; Cre$^{+/-}$ and Atgl$^{flox/flox}$ were used to generate control mice (Atgl$^{flox/flox}$) and knockout littermates (Atgl$^{flox/flox}$; Cre$^{+/-}$). Genotyping primers for AdipoQ-Cre$^{TG/+}$ mice were 5'- GAA CCT GAT GGA CAT GTT CAGG-3' (forward)

and 5'-AGT GCG TTC GAA CGC TAG AGC CTG T-3' (reverse). Genotyping primers for Atgl$^{flox/flox}$ mice were 5'-CAG GGG GCG AGG CGG TCA GA-3' (forward) and 5'-CGG TGA GGG TGG GGA ACG GAG TC-3' (reverse). All mice were maintained on a C57Bl/6 background.

For intermittent PTH injections, male mice were injected subcutaneously with PTH$_{1-34}$ (BACHEM, H-4835) resuspended in culture grade PBS (Corning) and injected at 100μg/kg, 5 days a week for 6 weeks. PBS was used as the control.

Western blot analysis and gene expression studies

Inguinal white adipose tissue (iWAT) was collected and flash frozen in liquid nitrogen 30 minutes post PTH or saline control administration. Western blot analyses were carried out according to standard technique using the primary antibodies phosphorylated-HSL S660 (Cell Signaling Technologies-4126S), HSL (Cell Signaling Technologies- 4107S), ATGL (Cell Signaling Technology- 2138S), and ACTIN (Cell Signaling Technology- 3700S). Gene expression studies were carried out as described in chapter 3. Sequences for Pthr were 5'-CAG GCG CAA TGT GAC AAG C-3' (forward) and 5'-TTT CCC GGT GCC TTC TCT TTC-3' (reverse). Reactions were normalized to endogenous 18S reference transcripts.

Metabolic profiling and bioassays

Animals at 8 weeks of age were individually house in a Comprehensive Laboratory Animal Monitoring System (Columbus Instruments) located in the

Johns Hopkins Center for Metabolism and Obesity Research. Calorimetry, daily body weight, and daily food intake data were acquired during a 4-day experimental period. Animals were allowed to acclimate for the 2 days before saline or PTH_{1-34} (100μg/kg) subcutaneous injections on day 3 and day 4 occurred. Oxygen consumption (VO_2, ml/kg/hr), and carbon dioxide production (VCO_2) were measured for each chamber every 20 minutes throughout the study. Respiratory exchange ratio ($RER = VCO_2 / VO_2$) was calculated by Oxymax software (v 4.90) to estimate relative oxidation of carbohydrates (RER=1.0) compared to fat (RER approaching 0.7), not accounting for protein oxidation. Energy expenditure was calculated [EE = VO2 x (3.815 + (1.232 x RER))] and normalized for lean body mass (kcal/kg/hr) assessed by qNMR (Echo MRI). Plasma free fatty acids (Sigma-Aldrich), triglycerides (Sigma-Aldrich), and cholesterol (Sigma-Aldrich) were measured colormetrically in plasma collected 30 minutes after administration of the final PTH injection.

Fluorescence microcopy and histology

Mouse adipose tissue and femur samples were fixed in 4% paraformaldehyde for 24 hours at 4°C and washed with PBS. Adipose tissue samples were paraffin-embedded and stained with H&E using standard methods. Femurs were decalcified using 14% EDTA and paraffin embedded. After embedding, 5μm sections were cut and stained with hematoxylin and eosin (H&E) using standard methods for bone marrow adipose tissue analysis. Bone marrow

adipocytes and inguinal and gonadal analysis was completed using ImageJ software.

For immunofluorescence, femurs were fixed in 4% formaldehyde for 24 hours at 4°C and washed with PBS. Femurs were decalcified using 14% EDTA and paraffin embedded in OCT. After embedding, $10\mu m$ sections were cut and stained following standard protocols and were imaged under a fluorescent microscope (Nikon Eclipse Ci with Photofluor LM75 light source). Primary antibodies used for this study were PTHR (Millipore 05-517) and PLIN1 (Cell Signaling Technology-9349S).

Skeletal phenotyping

Skeletal phenotyping was performed as described in chapter 2.

Statistical analysis

Quantitative data are shown as bar graphs produced using Prism Graphpad software. All results are expressed as mean $\pm$ SEM. Statistical analyses were performed using unpaired, two-tailed Student's t-tests or ANOVA tests followed by Tukey post-hoc tests using Prism Graphpad software. A p-value <0.05 was considered significant.

Chapter 4
Discussion

The simultaneous dysfunction in metabolism and the skeleton seen in diseases like osteoporosis, primary hyperparathyroidism, and diabetes mellitus, demonstrates key interactions between maintenance of bone integrity and metabolic homeostasis. Understanding the nuances of the utilization of fuel sources in osteoblasts may be essential to identifying the extent of the relationship between metabolic and skeletal dysfunction. This dissertation aimed to investigate how the utilization and the availability of fatty acids affects bone accrual in response to an anabolic stimulus. We demonstrate that β-oxidation of fatty acid is necessary for PTH-induced bone formation and that PTH must signal through osteoblasts but also through adipose tissue, inducing a lipolytic response, allowing for skeletal anabolism (Fig 4.1).

Much of the focus around the bioenergetics of osteoblasts was centered around the utilization of glucose. Recently, compounding evidence has highlighted the necessity for lipids and their derivatives, specifically fatty acids in osteoblast function. Previous work from our laboratory addressed this importance. In vitro studies identified that oxidation of $[^{14}C]$ Oleate to CO_2 and genes involved in fatty acid oxidation increase during osteoblast differentiation [56]. Osteoblasts treated with etomoxir, an irreversible inhibitor of fatty acid oxidation, decreased oleate oxidation to CO_2 and impacted differentiation, an indication of the importance of this lipid. In a later study, Cpt2, an obligate enzyme in beta oxidation was specifically deleted in mature osteoblasts and osteocytes which decreased bone

post-natal bone acquisition in female mice. Male mice only expressed a transient loss in bone, as their ability to shift their energetic requirements to glucose utilization rescued the phenotype [39]. Together with data identifying the significant uptake of postprandial lipid in the skeleton, the importance of the role in satisfying the energetic demands of osteoblasts is revealed. A next step in continuing to understand the role for fatty acids in the skeleton was to determine this requirement during a heightened state of anabolism.

In chapter 2, we demonstrated the in vitro effects of PTH on fatty acid oxidation in osteoblasts. RNA sequencing data from PTH-treated osteoblast cultures revealed dramatic changes in the gene profile of osteoblasts. Sequencing showed that PTH-induced increases in genes involved in fatty acid metabolism which were already highly expressed. PTH increased only a few genes involved in glucose oxidation, which was somewhat expected [104]. Interestingly, these alterations in glucose metabolism occurred to a lesser extent relative to fatty acid oxidation. PTH treatment increased release of $^{14}CO_2$ in primary cells treated with ^{14}C-oleate but not ^{14}C-glucose indicating PTH preferentially increases oxidation of fatty acids relative to glucose. In support of the data, Seahorse analysis demonstrated that PTH increased the oxygen consumption rate, which was attenuated by etomoxir. Together these data indicate that fatty acids are the substates responsible for the increase in mitochondrial respiration pointing to a preferential utilization of these lipids to satisfy the increase in fuel demand. Because these in vitro studies were evidence of the substrate-specific utilization in

response to PTH administration, we asked whether fatty acid oxidation was a requirement for PTH's effects on osteoblasts. PTH increased collagen deposition and alkaline phosphatase activity but the effects were blunted in cells lacking Cpt2 indicating a necessity for long chain fatty acid β-oxidation in the deposition of matrix in response to PTH treatment. These in vitro studies revealed specifics about the changes in osteoblast metabolism in response to PTH and that fatty acids are a critical substrate involved in these alterations. Most importantly, it was an initial indication that fatty acid β-oxidation may be critical for PTH-induced bone formation in vivo. The in vivo data presented in chapter 2 revealed this necessity. Intermittent PTH$_{1-34}$ treatment of Cpt2$^{flox/flox}$; Oc-Cre$^{TG/+}$ (OcnΔCpt2) and littermate controls, Cpt2$^{flox/flox}$; Oc-Cre$^{+/+}$ (Con) for 6 weeks led to increases in trabecular bone volume that was abolished or diminished in Cpt2 mutants, indicating in vivo that fatty acid β-oxidation is essential for the anabolic response of bone to PTH. Dynamic histomorphometric analysis showed on a cellular level that abolishing Cpt2 leads to dysfunction in PTH-induced mineralization. TRAP staining confirmed that the lack of mineralization when impairing long chain fatty acid β-oxidation in osteoblasts is due to an impairment in osteoblastic bone formation independent of osteoclasts.

In addition to PTH's induced changes in the metabolism of osteoblasts, Chapter 3 investigated the alterations in lipid in homeostasis. Our data revealed that acute PTH treatment induced a lipolytic response in a peripheral adipose depot of mice, increasing serum free fatty acids. Moreover, an indirect calorimetric

study showed PTH rapidly decreased the respiration exchange rations indicative of an increase in the utilization of lipid relative to glucose. With evidence that PTH induces changes in whole body lipid metabolism and that fatty acid are essential for osteoblasts for PTH-induced bone formation, we wanted to further address the possible role of fat as a major fuel source for this response. Pth1r$^{flox/flox}$; AdipoQ-Cre$^{TG/-}$ (AdΔPth1r) and littermate controls (Pth1r$^{flox/flox}$; AdipoQ-Cre$^{+/-}$) were used to begin to address this possibility. Specifically deleting the Pthr in adipocytes showed that acute PTH-induced increases in serum free fatty acids and increases in lipolytic enzymes in adipose tissue are necessary for this response. Prolonged PTH treatment revealed changes in adipocyte morphology in various fat depots including inguinal and gonadal white adipose tissue and bone marrow adipose tissue. These changes where blunted or abolished in AdΔPth1r mice relative to littermate controls. In line with a single acute PTH treatment, acute treatment after 6 weeks of intermittent administration also triggered an increase in serum free fatty acids that was abolished in Pth1r mutants. Dynamic and static histomorphometric analysis revealed that Pth1r expression in adipocytes is necessary for PTH anabolism in the femur. PTH-induced increases in trabecular bone volume seen in control mice were abolished or greatly diminished in Pth1r mutants. Additional analysis revealed that the there was a defect in mineralization but that this was due to an impairment in osteoblasts, independent of osteoclasts, in line with the analysis of the Cpt2 mutants in Chapter 2. However, there were no differences in bone density between saline treated control and mutants. These findings disrupt

the classical way of thinking of PTH's mechanism of anabolism. Not only must PTH signal through osteoblasts but signaling through adipose tissue is essential to induce increased bone formation.

Further investigation into the role of adipose tissue in PTH's anabolic response revealed the necessity for adipose lipolysis. In Chapter 3 we used another genetic model in which Atgl, the rate limiting enzyme in lipolysis, was specifically deleted in adipocytes. Acute PTH administration of Atgl$^{flox/flox}$; AdipoQ-Cre$^{+/+}$ (Controls) and Atgl$^{flox/flox}$; AdipoQ-Cre$^{TG/+}$ (AdΔAtgl) revealed the necessity for this enzyme in the lipolytic response to PTH. PTH-induced increases in serum free fatty acids were abolished in Atgl mutants. Alterations in inguinal fat pads evident in control mice after 6 weeks of treatment was abolished in mutants. Trabecular femoral analysis after intermittent treatment showed that the increases in bone volume and increases in mineralization were abolished in AdΔAtgl animals. This resistance to PTH-induced skeletal alterations demonstrates that the lipolytic response in adipose tissue is essential for these responses. The utilization of this third genetic model allowed us to confirm that PTH's anabolic affects are dependent on signaling through adipose tissue, releasing fatty acids, that are then utilized by osteoblasts during matrix deposition and mineralization.

Our studies reveal an expanded mechanism for PTH's mode of action on bone, identifying adipose tissue as key to this response. In our analysis we investigated the changes in various adipose tissue depots including peripheral depots (inguinal and gonadal adipose tissue) as well as bone marrow adipocytes.

102

However, a limitation of our study was in our ability to identify and characterize whether a specific adipose depot is the primary source of fatty acids for osteoblasts. Development of a bone marrow adipocytes specific conditional model would be necessary to address this. In a series of in vitro studies by Maridas et. al, acute PTH treatment increases mitochondrial respiration of bone marrow adipocytes, but prolonged PTH treatment revealed that PTH-liberated fatty acids were not being used for respiration but instead being shuttled out of marrow adipocytes. Furthermore, cultured stromal cells were able to uptake these liberated fatty acids suggesting BMAT are capable of supplying lipid to osteoblasts acting as a fuel source [105]. This study used a co-culture system of bone marrow adipocytes and osteoblast progenitors and may not be representative of what is occurring in vivo. Perhaps, both bone marrow adipocytes and peripheral adipose depots are supplying fatty acids for osteoblasts, altering utilization depending on external stimuli. There is a paradoxical increase in BMAT in clinical cases of anorexia nervosa which exhibits decreases in overall fat mass [146] or with rodent models of caloric restriction [105]. Conversely, a high fat diet also results in a significant increase in marrow adiposity while increasing peripheral fat depots [147].These findings could suggest that BMAT functions as lipid storage and provides a local source of lipid for bone cell in time systemic stress. Evidence from our study and others demonstrates that BMAT and peripheral adipose tissue both respond to PTH so additional experiments will need to be performed to further understand contributions of each fat depot.

The relationship between adipose tissue and the skeleton is further highlighted by effects of or caloric restriction or a high fat diet (HFD) leading to obesity on the functions and integrity of the bone. The availability of nutrients is critical to osteoblast function as caloric restriction during gestation or during postnatal life strongly influences the trajectory of the accrual and the maintenance of bone mass [23-25]. Caloric restriction decreases fat mass and induces changes in bone microarchitecture leading to decreased bone mineral density [148]. In extreme cases of caloric restriction as seen in anorexia nervosa, low-weight and fat mass is accompanied by bone loss and increase in fracture risk [149, 150]. Despite caloric restriction, intermittent PTH treatment still significantly increased bone formation and bone mass when diet and treatment were started simultaneously or when the caloric restricted diet began before treatment [105]. However, caloric restriction affected the skeletal response to another anabolic stimulus. Exercise increased bone mass for mice on a normal diet however failed to do so in animals with caloric restriction [151]. This highlights the heterogeneity in the response of bone to various stimuli as the diet used in both studies involved decreasing caloric intake but not altering fat content. However, the interventions began at different ages and lasted for different lengths of time. Perhaps if the PTH study began at the same or older timepoint as the exercise study and continued for longer, the PTH responsiveness may be impacted. A study suggested that aged animals have a greater skeletal response to intermittent PTH treatment [152]. More

studies are necessary to further address the relationship between low fat intake and impact on PTH responsiveness.

Our studies have uncovered a pathway necessary for PTH-induced skeletal anabolism. PTH signals through adipose tissue, releasing fatty acids which are utilized by osteoblasts to fuel the anabolic response. This concept can be extended to additional studies of disease such as primary hyperparathyroidism (PHPT). PHPT is caused by the excessive synthesis secretion of PTH by one or more of the parathyroid glands which induces a hypercalcemic state [153]. The continuous elevated levels of PTH have deleterious effects on numerous organs including the skeleton [154, 155]. Unlike the anabolic effects of intermittent PTH administration, chronically elevated levels lead to catabolic effects in bone [156]. There are increases in bone remodeling, but resorption is favored in part by increasing expression of RANKL and inhibition of OPG [119]. PHPT leads to bone structure deficits in patients by decreasing bone mineral density [157-159], and increasing fracture risks [160-162] . By using a mouse model of PHPT, which exhibits skeletal deficits [163], we could determine if PTH signaling through adipose tissue improves the alterations in the bone in Pth1r$^{flox/flox}$; AdipoQ-Cre$^{TG/-}$ animals. If signaling through adipose tissue is necessary for the anabolic effect of intermittent PTH treatment, perhaps it is necessary for its catabolic affects providing further insight into the molecular mechanisms of disease.

Another possibility of our study would be to use an ovariectomized (OVX) mouse model. This clinically relevant model simulates the menopausal phase in

females triggering estrogen deficiency and triggering bone loss, modeling osteoporosis [164, 165]. Similarly, to patients, intermittent PTH treatment diminishes bone loss in the OVX model [166-168]. Performing the ovariectomy on our three mouse models, OcnΔCpt2, AdΔPth1r, and AdΔAtgl would give us insight into how β-oxidation of fatty acids in osteoblast and adipose tissue plays a role in bone loss associated with estrogen deficiency. Our studies revealed that male saline-treated knockouts had no impaired post-natal bone accrual compared to littermate controls as indicated by micro-CT. It would be informative to identify whether a baseline phenotype is exacerbated with an ovariectomy in female mice. Additionally, intermittent treatment of OVX mutant animals would further reveal whether β-oxidation of fatty acids in osteoblast, PTH signaling through adipose tissue, or lipolysis is necessary for the hormone's therapeutic effects. All studies would give further understanding into the bioenergetics of PTH's actions on bone in a clinical setting.

Discovering new details into the bioenergetics of PTH on osteoblasts further highlights the relationship between adipose tissue and osteoblasts. Using three different genetic models we were able to demonstrate that fatty acid β-oxidation in osteoblasts (Cpt2$^{flox/flox}$; Oc-Cre), PTH signaling through adipose tissue (Pth1r$^{flox/flox}$; AdipoQ-Cre), and adipose tissue lipolysis (Atgl$^{flox/flox}$; AdipoQ-Cre) are required for PTH induced bone formation. PTH signals through osteoblasts but also signals through adipose tissue, liberating fatty acids which are then utilized by osteoblasts fueling the anabolic response. Although further studies are necessary,

this expanded understanding of a commonly used anabolic therapeutic provides insight and clarity into the molecular mechanism of PTH and the connection between metabolism and the skeleton.
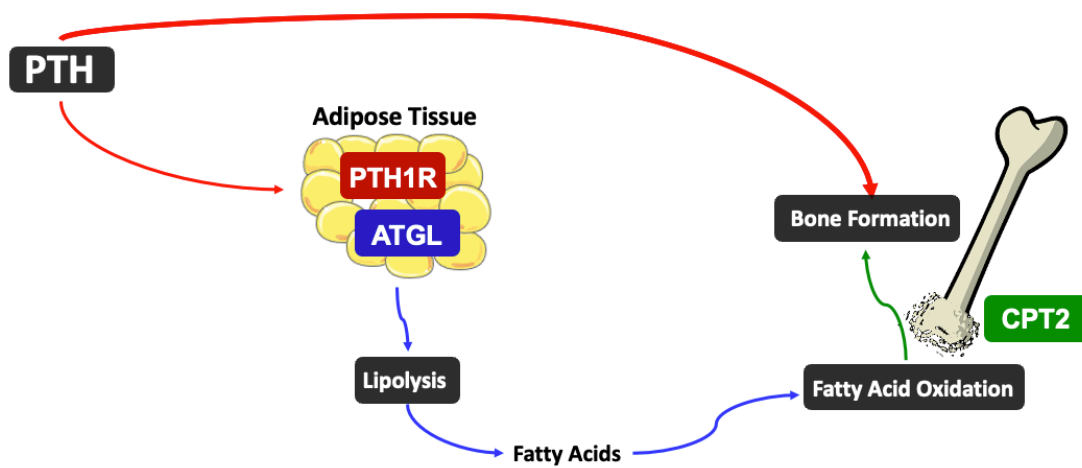

Figure 4.1 Schematic overview of β-oxidation of adipose-derived fatty acids fuel PTH-induced bone formation.

References

1. Teitelbaum, S.L., *Bone resorption by osteoclasts.* Science, 2000. 289(5484): p. 1504-8.
2. Tang, Y., et al., *TGF-beta1-induced migration of bone mesenchymal stem cells couples bone resorption with formation.* Nat Med, 2009. 15(7): p. 757-65.
3. Xian, L., et al., *Matrix IGF-1 maintains bone mass by activation of mTOR in mesenchymal stem cells.* Nat Med, 2012. 18(7): p. 1095-101.
4. Dudley, H.R. and D. Spiro, *The Fine Structure of Bone Cells.* J Biophys Biochem Cytol, 1961. 11(3): p. 627-49.
5. Khosla, S., S. Amin, and E. Orwoll, *Osteoporosis in men.* Endocr Rev, 2008. 29(4): p. 441-64.
6. Syed, F.A. and A.C. Ng, *The pathophysiology of the aging skeleton.* Curr Osteoporos Rep, 2010. 8(4): p. 235-40.
7. Borgstrom, F., et al., *Fragility fractures in Europe: burden, management and opportunities.* Arch Osteoporos, 2020. 15(1): p. 59.
8. Lewiecki, E.M., et al., *Healthcare Policy Changes in Osteoporosis Can Improve Outcomes and Reduce Costs in the United States.* JBMR Plus, 2019. 3(9): p. e10192.
9. Tatangelo, G., et al., *The Cost of Osteoporosis, Osteopenia, and Associated Fractures in Australia in 2017.* J Bone Miner Res, 2019. 34(4): p. 616-625.
10. Edelmuth, S., et al., *Comorbidities, clinical intercurrences, and factors associated with mortality in elderly patients admitted for a hip fracture.* Rev Bras Ortop, 2018. 53(5): p. 543-551.
11. Pedersen, A.B., et al., *Hip Fracture, Comorbidity, and the Risk of Myocardial Infarction and Stroke: A Danish Nationwide Cohort Study, 1995-2015.* J Bone Miner Res, 2017. 32(12): p. 2339-2346.
12. Roche, J.J., et al., *Effect of comorbidities and postoperative complications on mortality after hip fracture in elderly people: prospective observational cohort study.* BMJ, 2005. 331(7529): p. 1374.
13. Pavlova, N.N. and C.B. Thompson, *The Emerging Hallmarks of Cancer Metabolism.* Cell Metab, 2016. 23(1): p. 27-47.
14. Yi, M., et al., *Emerging role of lipid metabolism alterations in Cancer stem cells.* J Exp Clin Cancer Res, 2018. 37(1): p. 118.
15. Currie, E., et al., *Cellular fatty acid metabolism and cancer.* Cell Metab, 2013. 18(2): p. 153-61.
16. Lee, N.K., et al., *Endocrine regulation of energy metabolism by the skeleton.* Cell, 2007. 130(3): p. 456-69.
17. Oury, F., et al., *Endocrine regulation of male fertility by the skeleton.* Cell, 2011. 144(5): p. 796-809.
18. Wei, J. and G. Karsenty, *An overview of the metabolic functions of osteocalcin.* Rev Endocr Metab Disord, 2015. 16(2): p. 93-8.
19. Guntur, A.R. and C.J. Rosen, *Bone as an endocrine organ.* Endocr Pract, 2012. 18(5): p. 758-62.

20. Lee, W.C., et al., *Energy Metabolism of the Osteoblast: Implications for Osteoporosis.* Endocr Rev, 2017. 38(3): p. 255-266.

21. Dirckx, N., et al., *The role of osteoblasts in energy homeostasis.* Nat Rev Endocrinol, 2019. 15(11): p. 651-665.

22. Buttgereit, F. and M.D. Brand, *A hierarchy of ATP-consuming processes in mammalian cells.* Biochem J, 1995. 312 (Pt 1): p. 163-7.

23. Knight, B.S., et al., *The impact of murine strain and sex on postnatal development after maternal dietary restriction during pregnancy.* J Physiol, 2007. 581(Pt 2): p. 873-81.

24. Devlin, M.J., et al., *Caloric restriction leads to high marrow adiposity and low bone mass in growing mice.* J Bone Miner Res, 2010. 25(9): p. 2078-88.

25. Miller, K.K., et al., *Determinants of skeletal loss and recovery in anorexia nervosa.* J Clin Endocrinol Metab, 2006. 91(8): p. 2931-7.

26. Shum, L.C., et al., *Energy Metabolism in Mesenchymal Stem Cells During Osteogenic Differentiation.* Stem Cells Dev, 2016. 25(2): p. 114-22.

27. Shares, B.H., et al., *Active mitochondria support osteogenic differentiation by stimulating beta-catenin acetylation.* J Biol Chem, 2018. 293(41): p. 16019-16027.

28. Guntur, A.R., et al., *Bioenergetics during calvarial osteoblast differentiation reflect strain differences in bone mass.* Endocrinology, 2014. 155(5): p. 1589-95.

29. Chen, C.T., et al., *Coordinated changes of mitochondrial biogenesis and antioxidant enzymes during osteogenic differentiation of human mesenchymal stem cells.* Stem Cells, 2008. 26(4): p. 960-8.

30. Nichols, F.C. and W.F. Neuman, *Lactic acid production in mouse calvaria in vitro with and without parathyroid hormone stimulation: lack of acetazolamide effects.* Bone, 1987. 8(2): p. 105-9.

31. Neuman, W.F., M.W. Neuman, and R. Brommage, *Aerobic glycolysis in bone: lactate production and gradients in calvaria.* Am J Physiol, 1978. 234(1): p. C41-50.

32. Borle, A.B., N. Nichols, and G. Nichols, Jr., *Metabolic studies of bone in vitro. I. Normal bone.* J Biol Chem, 1960. 235: p. 1206-10.

33. Cohn, D.V. and B.K. Forscher, *Aerobic metabolism of glucose by bone.* J Biol Chem, 1962. 237: p. 615-8.

34. Felix, R., W.F. Neuman, and H. Fleisch, *Aerobic glycolysis in bone: lactic acid production by rat calvaria cells in culture.* Am J Physiol, 1978. 234(1): p. C51-5.

35. Wei, J., et al., *Glucose Uptake and Runx2 Synergize to Orchestrate Osteoblast Differentiation and Bone Formation.* Cell, 2015. 161(7): p. 1576-1591.

36. Komarova, S.V., F.I. Ataullakhanov, and R.K. Globus, *Bioenergetics and mitochondrial transmembrane potential during differentiation of cultured osteoblasts.* Am J Physiol Cell Physiol, 2000. 279(4): p. C1220-9.

37. Yu, Y., et al., *Glutamine Metabolism Regulates Proliferation and Lineage Allocation in Skeletal Stem Cells.* Cell Metab, 2019. 29(4): p. 966-978 e4.

38. Karner, C.M., et al., *Increased glutamine catabolism mediates bone anabolism in response to WNT signaling.* J Clin Invest, 2015. 125(2): p. 551-62.

39. Kim, S.P., et al., *Fatty acid oxidation by the osteoblast is required for normal bone acquisition in a sex- and diet-dependent manner.* JCI Insight, 2017. 2(16).

40. van Gastel, N., et al., *Lipid availability determines fate of skeletal progenitor cells via SOX9.* Nature, 2020. 579(7797): p. 111-117.

41. Singh, L., et al., *Good, Bad, or Ugly: the Biological Roles of Bone Marrow Fat.* Curr Osteoporos Rep, 2018. 16(2): p. 130-137.

42. Tintut, Y. and L.L. Demer, *Effects of bioactive lipids and lipoproteins on bone.* Trends Endocrinol Metab, 2014. 25(2): p. 53-9.

43. Tso, P. and J.A. Balint, *Formation and transport of chylomicrons by enterocytes to the lymphatics.* Am J Physiol, 1986. 250(6 Pt 1): p. G715-26.

44. Kersten, S., *Physiological regulation of lipoprotein lipase.* Biochim Biophys Acta, 2014. 1841(7): p. 919-33.

45. Windler, E., Y. Chao, and R.J. Havel, *Determinants of hepatic uptake of triglyceride-rich lipoproteins and their remnants in the rat.* J Biol Chem, 1980. 255(11): p. 5475-80.

46. Eichmann, T.O., et al., *Studies on the substrate and stereo/regioselectivity of adipose triglyceride lipase, hormone-sensitive lipase, and diacylglycerol-O-acyltransferases.* J Biol Chem, 2012. 287(49): p. 41446-57.

47. Schonfeld, P. and L. Wojtczak, *Short- and medium-chain fatty acids in energy metabolism: the cellular perspective.* J Lipid Res, 2016. 57(6): p. 943-54.

48. Richieri, G.V., A. Anel, and A.M. Kleinfeld, *Interactions of long-chain fatty acids and albumin: determination of free fatty acid levels using the fluorescent probe ADIFAB.* Biochemistry, 1993. 32(29): p. 7574-80.

49. Adeva-Andany, M.M., et al., *Mitochondrial beta-oxidation of saturated fatty acids in humans.* Mitochondrion, 2019. 46: p. 73-90.

50. Reddy, J.K. and T. Hashimoto, *Peroxisomal beta-oxidation and peroxisome proliferator-activated receptor alpha: an adaptive metabolic system.* Annu Rev Nutr, 2001. 21: p. 193-230.

51. Enlow, D.H., J.L. Conklin, and S. Bang, *Observations on the occurrence and the distribution of lipids in compact bone.* Clin Orthop Relat Res, 1965. 38: p. 157-69.

52. Rendina-Ruedy, E., A.R. Guntur, and C.J. Rosen, *Intracellular lipid droplets support osteoblast function.* Adipocyte, 2017. 6(3): p. 250-258.

53. Niemeier, A., et al., *Uptake of postprandial lipoproteins into bone in vivo: impact on osteoblast function.* Bone, 2008. 43(2): p. 230-237.

54. Newman, P., et al., *The uptake of lipoprotein-borne phylloquinone (vitamin K1) by osteoblasts and osteoblast-like cells: role of heparan sulfate proteoglycans and apolipoprotein E.* J Bone Miner Res, 2002. 17(3): p. 426-33.

55. Brodeur, M.R., et al., *Scavenger receptor of class B expressed by osteoblastic cells are implicated in the uptake of cholesteryl ester and estradiol from LDL and HDL3.* J Bone Miner Res, 2008. 23(3): p. 326-37.

56. Frey, J.L., et al., *Wnt-Lrp5 signaling regulates fatty acid metabolism in the osteoblast.* Mol Cell Biol, 2015. 35(11): p. 1979-91.

57. Bartelt, A., et al., *Quantification of Bone Fatty Acid Metabolism and Its Regulation by Adipocyte Lipoprotein Lipase.* Int J Mol Sci, 2017. 18(6).

58. Niemeier, A., et al., *Expression of LRP1 by human osteoblasts: a mechanism for the delivery of lipoproteins and vitamin K1 to bone.* J Bone Miner Res, 2005. 20(2): p. 283-93.

59. Grey, A., et al., *The low-density lipoprotein receptor-related protein 1 is a mitogenic receptor for lactoferrin in osteoblastic cells.* Mol Endocrinol, 2004. 18(9): p. 2268-78.

60. Chen, X., et al., *Reduced femoral bone mass in both diet-induced and genetic hyperlipidemia mice.* Bone, 2016. 93: p. 104-112.

61. Okayasu, M., et al., *Low-density lipoprotein receptor deficiency causes impaired osteoclastogenesis and increased bone mass in mice because of defect in osteoclastic cell-cell fusion.* J Biol Chem, 2012. 287(23): p. 19229-41.

62. Zhang, N., et al., *Low-density lipoprotein receptor deficiency impaired mice osteoblastogenesis in vitro.* Biosci Trends, 2018. 11(6): p. 658-666.

63. Catherwood, B.D., et al., *Growth of rat osteoblast-like cells in a lipid-enriched culture medium and regulation of function by parathyroid hormone and 1,25-dihydroxyvitamin D.* J Bone Miner Res, 1988. 3(4): p. 431-8.

64. Sims, A.M., et al., *Genetic analyses in a sample of individuals with high or low BMD shows association with multiple Wnt pathway genes.* J Bone Miner Res, 2008. 23(4): p. 499-506.

65. Bartelt, A., et al., *Lrp1 in osteoblasts controls osteoclast activity and protects against osteoporosis by limiting PDGF-RANKL signaling.* Bone Res, 2018. 6: p. 4.

66. Teufel, S. and C. Hartmann, *Wnt-signaling in skeletal development.* Curr Top Dev Biol, 2019. 133: p. 235-279.

67. Kim, D.H., et al., *A new low density lipoprotein receptor related protein, LRP5, is expressed in hepatocytes and adrenal cortex, and recognizes apolipoprotein E.* J Biochem, 1998. 124(6): p. 1072-6.

68. Fujino, T., et al., *Low-density lipoprotein receptor-related protein 5 (LRP5) is essential for normal cholesterol metabolism and glucose-induced insulin secretion.* Proc Natl Acad Sci U S A, 2003. 100(1): p. 229-34.

69. Shen, W.J., et al., *Scavenger receptor class B type I (SR-BI): a versatile receptor with multiple functions and actions.* Metabolism, 2014. 63(7): p. 875-86.

70. Ackert-Bicknell, C.L., *HDL cholesterol and bone mineral density: is there a genetic link?* Bone, 2012. 50(2): p. 525-33.

71. Martineau, C., et al., *The atherogenic Scarb1 null mouse model shows a high bone mass phenotype.* Am J Physiol Endocrinol Metab, 2014. 306(1): p. E48-57.

72. Isales, C.M., M. Zaidi, and H.C. Blair, *ACTH is a novel regulator of bone mass.* Ann N Y Acad Sci, 2010. 1192: p. 110-6.

73. Tourkova, I.L., et al., *The high-density lipoprotein receptor Scarb1 is required for normal bone differentiation in vivo and in vitro.* Lab Invest, 2019. 99(12): p. 1850-1860.

74. Martineau, C., et al., *Scavenger receptor class B, type I (Scarb1) deficiency promotes osteoblastogenesis but stunts terminal osteocyte differentiation.* Physiol Rep, 2014. 2(10).

75. Blair, H.C., et al., *Apolipoprotein A-1 regulates osteoblast and lipoblast precursor cells in mice.* Lab Invest, 2016. 96(7): p. 763-72.

76. Glatz, J.F., J.J. Luiken, and A. Bonen, *Membrane fatty acid transporters as regulators of lipid metabolism: implications for metabolic disease.* Physiol Rev, 2010. 90(1): p. 367-417.

77. Kevorkova, O., et al., *Low-bone-mass phenotype of deficient mice for the cluster of differentiation 36 (CD36).* PLoS One, 2013. 8(10): p. e77701.

78. Anderson, C.M. and A. Stahl, *SLC27 fatty acid transport proteins.* Mol Aspects Med, 2013. 34(2-3): p. 516-28.

79. Bao, M., et al., *Therapeutic potentials and modulatory mechanisms of fatty acids in bone.* Cell Prolif, 2020. 53(2): p. e12735.

80. Mark, H., et al., *Microvascular invasion during endochondral ossification in experimental fractures in rats.* Bone, 2004. 35(2): p. 535-42.

81. Thompson, Z., et al., *A model for intramembranous ossification during fracture healing.* J Orthop Res, 2002. 20(5): p. 1091-8.

82. Kronenberg, H.M., *Developmental regulation of the growth plate.* Nature, 2003. 423(6937): p. 332-6.

83. Baryawno, N., et al., *A Cellular Taxonomy of the Bone Marrow Stroma in Homeostasis and Leukemia.* Cell, 2019. 177(7): p. 1915-1932 e16.

84. Steinberg, S.J., et al., *Zellweger Spectrum Disorder*, in *GeneReviews((R))*, M.P. Adam, et al., Editors. 1993: Seattle (WA).

85. Brosius, U. and J. Gartner, *Cellular and molecular aspects of Zellweger syndrome and other peroxisome biogenesis disorders.* Cell Mol Life Sci, 2002. 59(6): p. 1058-69.

86. Heymans, H.S., et al., *Rhizomelic chondrodysplasia punctata: another peroxisomal disorder.* N Engl J Med, 1985. 313(3): p. 187-8.

87. Braverman, N., et al., *A Pex7 hypomorphic mouse model for plasmalogen deficiency affecting the lens and skeleton.* Mol Genet Metab, 2010. 99(4): p. 408-16.

88. Brites, P., et al., *Impaired neuronal migration and endochondral ossification in Pex7 knockout mice: a model for rhizomelic chondrodysplasia punctata.* Hum Mol Genet, 2003. 12(18): p. 2255-67.

89. Huybrechts, Y., et al., *WNT Signaling and Bone: Lessons From Skeletal Dysplasias and Disorders.* Front Endocrinol (Lausanne), 2020. 11: p. 165.

90. Zhong, Z., N.J. Ethen, and B.O. Williams, *WNT signaling in bone development and homeostasis.* Wiley Interdiscip Rev Dev Biol, 2014. 3(6): p. 489-500.

91. Moorer, M.C. and R.C. Riddle, *Regulation of Osteoblast Metabolism by Wnt Signaling.* Endocrinol Metab (Seoul), 2018. 33(3): p. 318-330.

92. Chen, H., et al., *Increased glycolysis mediates Wnt7b-induced bone formation.* FASEB J, 2019. 33(7): p. 7810-7821.

93. Esen, E., et al., *WNT-LRP5 signaling induces Warburg effect through mTORC2 activation during osteoblast differentiation.* Cell Metab, 2013. 17(5): p. 745-55.

94. Riddle, R.C., et al., *Lrp5 and Lrp6 exert overlapping functions in osteoblasts during postnatal bone acquisition.* PLoS One, 2013. 8(5): p. e63323.

95. Frey, J.L., et al., *beta-Catenin Directs Long-Chain Fatty Acid Catabolism in the Osteoblasts of Male Mice.* Endocrinology, 2018. 159(1): p. 272-284.

96. Holmen, S.L., et al., *Essential role of beta-catenin in postnatal bone acquisition.* J Biol Chem, 2005. 280(22): p. 21162-8.

97. Chen, J., et al., *WNT7B promotes bone formation in part through mTORC1.* PLoS Genet, 2014. 10(1): p. e1004145.

98.   Neer, R.M., et al., *Effect of parathyroid hormone (1-34) on fractures and bone mineral density in postmenopausal women with osteoporosis.* N Engl J Med, 2001. 344(19): p. 1434-41.

99.   Jilka, R.L., et al., *Increased bone formation by prevention of osteoblast apoptosis with parathyroid hormone.* J Clin Invest, 1999. 104(4): p. 439-46.

100.   Dobnig, H. and R.T. Turner, *Evidence that intermittent treatment with parathyroid hormone increases bone formation in adult rats by activation of bone lining cells.* Endocrinology, 1995. 136(8): p. 3632-8.

101.   Kim, S.W., et al., *Intermittent parathyroid hormone administration converts quiescent lining cells to active osteoblasts.* J Bone Miner Res, 2012. 27(10): p. 2075-84.

102.   Wu, X., et al., *Inhibition of Sca-1-positive skeletal stem cell recruitment by alendronate blunts the anabolic effects of parathyroid hormone on bone remodeling.* Cell Stem Cell, 2010. 7(5): p. 571-80.

103.   Adamek, G., et al., *Fatty acid oxidation in bone tissue and bone cells in culture. Characterization and hormonal influences.* Biochem J, 1987. 248(1): p. 129-37.

104.   Esen, E., et al., *PTH Promotes Bone Anabolism by Stimulating Aerobic Glycolysis via IGF Signaling.* J Bone Miner Res, 2015. 30(11): p. 2137.

105.   Maridas, D.E., et al., *Progenitor recruitment and adipogenic lipolysis contribute to the anabolic actions of parathyroid hormone on the skeleton.* FASEB J, 2019. 33(2): p. 2885-2898.

106.   Larsson, S., et al., *Parathyroid hormone induces adipocyte lipolysis via PKA-mediated phosphorylation of hormone-sensitive lipase.* Cell Signal, 2016. 28(3): p. 204-213.

107.   Fan, Y., et al., *Parathyroid Hormone Directs Bone Marrow Mesenchymal Cell Fate.* Cell Metab, 2017. 25(3): p. 661-672.

108.   Cameron, D.A., *The fine structure of osteoblasts in the metaphysis of the tibia of the young rat.* J Biophys Biochem Cytol, 1961. 9: p. 583-95.

109.   Borle, A.B., N. Nichols, and G. Nichols, Jr., *Metabolic studies of bone in vitro. II. The metabolic patterns of accretion and resorption.* J Biol Chem, 1960. 235: p. 1211-4.

110.   Peck, W.A., S.J. Birge, Jr., and S.A. Fedak, *Bone Cells: Biochemical and Biological Studies after Enzymatic Isolation.* Science, 1964. 146(3650): p. 1476-7.

111.   Esen, E., et al., *PTH Promotes Bone Anabolism by Stimulating Aerobic Glycolysis via IGF Signaling.* J Bone Miner Res, 2015. 30(11): p. 1959-68.

112.   Regan, J.N., et al., *Up-regulation of glycolytic metabolism is required for HIF1alpha-driven bone formation.* Proc Natl Acad Sci U S A, 2014. 111(23): p. 8673-8.

113.   Stegen, S., et al., *Glutamine Metabolism in Osteoprogenitors Is Required for Bone Mass Accrual and PTH-Induced Bone Anabolism in Male Mice.* J Bone Miner Res, 2021. 36(3): p. 604-616.

114.   Finkelstein, J.S., et al., *Parathyroid hormone for the prevention of bone loss induced by estrogen deficiency.* N Engl J Med, 1994. 331(24): p. 1618-23.

115. Dobnig, H. and R.T. Turner, *The effects of programmed administration of human parathyroid hormone fragment (1-34) on bone histomorphometry and serum chemistry in rats.* Endocrinology, 1997. 138(11): p. 4607-12.

116. Martin, T.J., N.A. Sims, and E. Seeman, *Physiological and Pharmacological Roles of PTH and PTHrP in Bone Using Their Shared Receptor, PTH1R.* Endocr Rev, 2021. 42(4): p. 383-406.

117. Yang, D., et al., *Contributions of parathyroid hormone (PTH)/PTH-related peptide receptor signaling pathways to the anabolic effect of PTH on bone.* Bone, 2007. 40(6): p. 1453-61.

118. Lee, S.K. and J.A. Lorenzo, *Parathyroid hormone stimulates TRANCE and inhibits osteoprotegerin messenger ribonucleic acid expression in murine bone marrow cultures: correlation with osteoclast-like cell formation.* Endocrinology, 1999. 140(8): p. 3552-61.

119. Ma, Y.L., et al., *Catabolic effects of continuous human PTH (1--38) in vivo is associated with sustained stimulation of RANKL and inhibition of osteoprotegerin and gene-associated bone formation.* Endocrinology, 2001. 142(9): p. 4047-54.

120. Kanzawa, M., et al., *Involvement of osteoprotegerin/osteoclastogenesis inhibitory factor in the stimulation of osteoclast formation by parathyroid hormone in mouse bone cells.* Eur J Endocrinol, 2000. 142(6): p. 661-4.

121. Fu, Q., et al., *Parathyroid hormone stimulates receptor activator of NFkappa B ligand and inhibits osteoprotegerin expression via protein kinase A activation of cAMP-response element-binding protein.* J Biol Chem, 2002. 277(50): p. 48868-75.

122. Rejnmark, L. and H. Ejlsmark-Svensson, *Effects of PTH and PTH Hypersecretion on Bone: a Clinical Perspective.* Curr Osteoporos Rep, 2020. 18(3): p. 103-114.

123. Nakchbandi, I.A., et al., *The role of the receptor activator of nuclear factor-kappaB ligand/osteoprotegerin cytokine system in primary hyperparathyroidism.* J Clin Endocrinol Metab, 2008. 93(3): p. 967-73.

124. Man, K.C. and J.T. Brosnan, *Inhibition of medium and short-chain fatty acid oxidation in rat heart mitochondria by dichloroacetate.* Metabolism, 1982. 31(7): p. 744-8.

125. Stacpoole, P.W. and J.M. Felts, *Diisopropylammonium dichloroacetate (DIPA) and sodium dichloracetate (DCA): effect on glucose and fat metabolism in normal and diabetic tissue.* Metabolism, 1970. 19(1): p. 71-8.

126. McAllister, A., S.P. Allison, and P.J. Randle, *Effects of dichloroacetate on the metabolism of glucose, pyruvate, acetate, 3-hydroxybutyrate and palmitate in rat diaphragm and heart muscle in vitro and on extraction of glucose, lactate, pyruvate and free fatty acids by dog heart in vivo.* Biochem J, 1973. 134(4): p. 1067-81.

127. Kim, D., B. Langmead, and S.L. Salzberg, *HISAT: a fast spliced aligner with low memory requirements.* Nat Methods, 2015. 12(4): p. 357-60.

128. Pertea, M., et al., *StringTie enables improved reconstruction of a transcriptome from RNA-seq reads.* Nat Biotechnol, 2015. 33(3): p. 290-5.

129. Lee, J., J.M. Ellis, and M.J. Wolfgang, *Adipose fatty acid oxidation is required for thermogenesis and potentiates oxidative stress-induced inflammation.* Cell Rep, 2015. 10(2): p. 266-79.

130. Lee, J., et al., *Hepatic Fatty Acid Oxidation Restrains Systemic Catabolism during Starvation.* Cell Rep, 2016. 16(1): p. 201-212.

131. Zhang, M., et al., *Osteoblast-specific knockout of the insulin-like growth factor (IGF) receptor gene reveals an essential role of IGF signaling in bone matrix mineralization.* J Biol Chem, 2002. 277(46): p. 44005-12.

132. Bouxsein, M.L., et al., *Guidelines for assessment of bone microstructure in rodents using micro-computed tomography.* J Bone Miner Res, 2010. 25(7): p. 1468-86.

133. Dempster, D.W., et al., *Standardized nomenclature, symbols, and units for bone histomorphometry: a 2012 update of the report of the ASBMR Histomorphometry Nomenclature Committee.* J Bone Miner Res, 2013. 28(1): p. 2-17.

134. Taniguchi, A., et al., *Parathyroid hormone-induced lipolysis in human adipose tissue.* J Lipid Res, 1987. 28(5): p. 490-4.

135. Zhong, L., et al., *Single cell transcriptomics identifies a unique adipose lineage cell population that regulates bone marrow environment.* Elife, 2020. 9.

136. Kir, S., et al., *PTH/PTHrP Receptor Mediates Cachexia in Models of Kidney Failure and Cancer.* Cell Metab, 2016. 23(2): p. 315-23.

137. Ahmadian, M., et al., *Desnutrin/ATGL is regulated by AMPK and is required for a brown adipose phenotype.* Cell Metab, 2011. 13(6): p. 739-48.

138. Kim, S.J., et al., *AMPK Phosphorylates Desnutrin/ATGL and Hormone-Sensitive Lipase To Regulate Lipolysis and Fatty Acid Oxidation within Adipose Tissue.* Mol Cell Biol, 2016. 36(14): p. 1961-76.

139. Pagnon, J., et al., *Identification and functional characterization of protein kinase A phosphorylation sites in the major lipolytic protein, adipose triglyceride lipase.* Endocrinology, 2012. 153(9): p. 4278-89.

140. Sitnick, M.T., et al., *Skeletal muscle triacylglycerol hydrolysis does not influence metabolic complications of obesity.* Diabetes, 2013. 62(10): p. 3350-61.

141. Schoiswohl, G., et al., *Impact of Reduced ATGL-Mediated Adipocyte Lipolysis on Obesity-Associated Insulin Resistance and Inflammation in Male Mice.* Endocrinology, 2015. 156(10): p. 3610-24.

142. Schreiber, R., H. Xie, and M. Schweiger, *Of mice and men: The physiological role of adipose triglyceride lipase (ATGL).* Biochim Biophys Acta Mol Cell Biol Lipids, 2019. 1864(6): p. 880-899.

143. D'Amelio, P., et al., *Effect of intermittent PTH treatment on plasma glucose in osteoporosis: A randomized trial.* Bone, 2015. 76: p. 177-84.

144. Kobayashi, T., et al., *PTHrP and Indian hedgehog control differentiation of growth plate chondrocytes at multiple steps.* Development, 2002. 129(12): p. 2977-86.

145. Eguchi, J., et al., *Transcriptional control of adipose lipid handling by IRF4.* Cell Metab, 2011. 13(3): p. 249-59.

146. Cawthorn, W.P., et al., *Bone marrow adipose tissue is an endocrine organ that contributes to increased circulating adiponectin during caloric restriction.* Cell Metab, 2014. 20(2): p. 368-375.

147. Tencerova, M., et al., *High-Fat Diet-Induced Obesity Promotes Expansion of Bone Marrow Adipose Tissue and Impairs Skeletal Stem Cell Functions in Mice.* J Bone Miner Res, 2018. 33(6): p. 1154-1165.

148. Zhu, J., et al., *Short-term caloric restriction induced bone loss in both axial and appendicular bones by increasing adiponectin.* Ann N Y Acad Sci, 2020. 1474(1): p. 47-60.

149. Fazeli, P.K. and A. Klibanski, *Effects of Anorexia Nervosa on Bone Metabolism.* Endocr Rev, 2018. 39(6): p. 895-910.

150. Chou, S.H. and C. Mantzoros, *Bone metabolism in anorexia nervosa and hypothalamic amenorrhea.* Metabolism, 2018. 80: p. 91-104.

151. McGrath, C., et al., *Exercise Degrades Bone in Caloric Restriction, Despite Suppression of Marrow Adipose Tissue (MAT).* J Bone Miner Res, 2020. 35(1): p. 106-115.

152. Knopp, E., et al., *The effect of aging on the skeletal response to intermittent treatment with parathyroid hormone.* Endocrinology, 2005. 146(4): p. 1983-90.

153. Bilezikian, J.P., et al., *Hyperparathyroidism.* Lancet, 2018. 391(10116): p. 168-178.

154. Silva, B.C., N.E. Cusano, and J.P. Bilezikian, *Primary hyperparathyroidism.* Best Pract Res Clin Endocrinol Metab, 2018. 32(5): p. 593-607.

155. Makras, P. and A.D. Anastasilakis, *Bone disease in primary hyperparathyroidism.* Metabolism, 2018. 80: p. 57-65.

156. Silva, B.C., et al., *Catabolic and anabolic actions of parathyroid hormone on the skeleton.* J Endocrinol Invest, 2011. 34(10): p. 801-10.

157. Silverberg, S.J., et al., *Skeletal disease in primary hyperparathyroidism.* J Bone Miner Res, 1989. 4(3): p. 283-91.

158. Chen, Q., et al., *Effects of an excess and a deficiency of endogenous parathyroid hormone on volumetric bone mineral density and bone geometry determined by peripheral quantitative computed tomography in female subjects.* J Clin Endocrinol Metab, 2003. 88(10): p. 4655-8.

159. Charopoulos, I., et al., *Effect of primary hyperparathyroidism on volumetric bone mineral density and bone geometry assessed by peripheral quantitative computed tomography in postmenopausal women.* J Clin Endocrinol Metab, 2006. 91(5): p. 1748-53.

160. Khosla, S., et al., *Primary hyperparathyroidism and the risk of fracture: a population-based study.* J Bone Miner Res, 1999. 14(10): p. 1700-7.

161. Vignali, E., et al., *Morphometric vertebral fractures in postmenopausal women with primary hyperparathyroidism.* J Clin Endocrinol Metab, 2009. 94(7): p. 2306-12.

162. Yeh, M.W., et al., *The Relationship of Parathyroidectomy and Bisphosphonates With Fracture Risk in Primary Hyperparathyroidism: An Observational Study.* Ann Intern Med, 2016. 164(11): p. 715-23.

163. Li, J.Y., et al., *IL-17 Receptor Signaling in Osteoblasts/Osteocytes Mediates PTH-Induced Bone Loss and Enhances Osteocytic RANKL Production.* J Bone Miner Res, 2019. 34(2): p. 349-360.

164. Sophocleous, A. and A.I. Idris, *Rodent models of osteoporosis.* Bonekey Rep, 2014. 3: p. 614.

165. Roberts, B.C., et al., *The longitudinal effects of ovariectomy on the morphometric, densitometric and mechanical properties in the murine tibia: A comparison between two mouse strains.* Bone, 2019. 127: p. 260-270.

166. Alexander, J.M., et al., *Human parathyroid hormone 1-34 reverses bone loss in ovariectomized mice.* J Bone Miner Res, 2001. 16(9): p. 1665-73.

167. Pierroz, D.D., et al., *Combined treatment with a beta-blocker and intermittent PTH improves bone mass and microarchitecture in ovariectomized mice.* Bone, 2006. 39(2): p. 260-7.

168. Chen, J., et al., *PTHG2 Reduces Bone Loss in Ovariectomized Mice by Directing Bone Marrow Mesenchymal Stem Cell Fate.* Stem Cells Int, 2021. 2021: p. 8546739.

Curriculum Vitae

<h1 align="center">Nathalie Spita Alekos</h1>

<p align="center">spitana25@gmail.com</p>

EDUCATION

Johns Hopkins School of Medicine, Baltimore, MD
PhD Candidate, Cellular and Molecular Medicine, August 2016 – June 2022
- ***PhD Thesis: Investigating the role of β-oxidation in osteoblasts and adipose tissue lipolysis in fueling bone formation in response to intermittent parathyroid hormone treatment.***
- *Course Highlights*: Anatomy, Histology, and Physiology, Molecular Biology and Genomics, Principles of Genetics, Pathways of Regulation, Cell Structure and Dynamics, Cellular and Molecular Basis of Disease, Principles of Immunology, Grant Writing, Statistics for Laboratory Scientists, Neurobiology, Neurodegeneration.

Virginia Commonwealth University, Richmond, VA
Bachelor of Science, Biology, Minor in Chemistry, August 2010 – May 2014
- *Course Highlights*: Immunology I & II, Biology of Cancer I & II, Animal Physiology, Comparative Vertebrate Anatomy, Cell Biology, Genetics, Medicinal Botany, Biochemistry.

RESEARCH EXPERIENCE

Johns Hopkins School of Medicine, Department of Orthopaedic Surgery, Baltimore, MD
PhD Candidate, May 2019 – present
- *Investigating* bone and adipose tissue interaction during skeletal anabolism.
- *Mentoring* undergraduate trainees.
- *Techniques:* micro-computed tomography (micro-CT), dynamic histomorphometry analysis, mouse bone and adipose tissue dissections/processing/sectioning, immunohistochemistry, microscopy, osteoblast/osteoclast cell culture, enzyme-linked immunosorbent assay (ELISA), gene expression analysis (qPCR), lipid profiling, mouse handling/breeding/colony maintenance.

Johns Hopkins School of Medicine, Department of Neuroscience, Baltimore, MD
PhD Candidate, June 2017 – April 2019
- *Investigated* the mechanisms underlying Glycerophosphodiester Phosphodiesterase 2 (GDE2) dysfunction in neurodegeneration.
- *Techniques:* mouse brain and spinal cord dissections/processing/sectioning, confocal microscopy, neuronal cultures.

Georgetown University, Department of Biology, Washington, DC
Research Technician, Sept. 2014 – July 2016
- *Investigated* the molecular coordination and regulation of axon guidance during cochlear development.
- *Assisted with laboratory training* of undergraduate and graduate students.
- *Managed and organized* all laboratory ordering and supplies.
- *Maintained* mouse colonies.

- *Assisted* advisor with initial laboratory set up.
- *Techniques:* mouse cochlear dissections, cochlear wholemounts, cochlear ganglion neuronal analysis using Imaris, molecular cloning, in-situ hybridization.

Virginia Commonwealth University School of Medicine
Department of Anatomy and Neurobiology, Richmond, VA
Undergraduate Research Assistant, Oct. 2012 – April 2014
- *Conducted research* to identify novel biomarkers to assess clinical outcome of TBI patients. Urinary molecular byproducts were analyzed to study the evolution of neuroplasticity during inpatient rehabilitation.
- *Techniques:* operation, maintenance, and solvent preparation for nanoAcquity chromatography system (Symmetry C18 trapping column & HSS T3 nanoAcquity capillary column), Synapt G2 hybrid ion mobility/ mass spectrometer (Waters), and Teague TE-10 smoke exposure system, neuronal cell densitometry, rat handling and behavioral testing.

Virginia Commonwealth University School of Medicine
Department of Anatomy and Neurobiology, Richmond, VA
Undergraduate Research Assistant, June 2011 – Oct. 2012
- *Investigated* the effect of nandrolone treatment on neuromuscular regeneration after denervated atrophy.
- *Techniques:* mouse muscle dissection/processing/sectioning, cell quantification and analysis of muscle fibers and satellite cells.

HONORS & AWARDS

ASBMR President's Award, American Society for Bone and Mineral Research Annual Meeting, October 2021.

ASMBR Young Investigator Award for the ECTS Masterclass for PhD Students, Trainees, and Young Investigators, August 2021.

Finalist, Johns Hopkins Graduate Consulting Club 9th Annual Healthcare Competition, April 2019

Summer Research Fellow, Virginia Commonwealth University Undergraduate Research Opportunities Program, May 2013

Scholar, Initiative for Maximizing Student Diversity, Virginia Commonwealth University Division for Health Sciences Diversity, June 2011

MEMBERSHIP IN PROFESSIONAL SOCIETIES

The American Society for Bone and Mineral Research, **Member**, May 2021- present

PRESENTATIONS

Invited Speaker, *β-oxidation of adipose-derived fatty acids fuel PTH-induced bone formation,* National Institutes of Health, Matrix Biology Scientific Interest Group, January 2022.

Oral Presentation, *β-oxidation of adipose-derived fatty acids fuel PTH-induced bone formation,* American Society for Bone and Mineral Research Annual Meeting, October 2021.

Presentation, *β-oxidation of adipose-derived fatty acids fuel PTH-induced bone formation,* Fifteenth Fellow Forum on Osteoporosis and Metabolic Bone Diseases, Endocrine Fellows Foundation, September 2021.

Plenary Oral Presentation, *Adipose lipolysis is required for PTH-induced bone formation*, European Calcified Tissue Society Congress, May 2021.

Poster, *Control of Cochlear Innervation by Semaphorin Signaling*, Greater Baltimore Society of Neuroscience. Baltimore, MD, 2015.

Poster, *Diagnostics of Brain Rehabilitation,* Virginia Commonwealth University, Undergraduate Research Opportunities Poster Symposium for Research and Creativity, Richmond, VA 2014

Poster, *Assessing whether nandrolone increases satellite cells following denervated atrophy*, Central Virginia Chapter, Society of Neuroscience Annual Meeting, Richmond, VA 2011.

Presenter, *Assessing whether nandrolone increases satellite cells following denervated atrophy*, Virginia Commonwealth University, Department of Biochemistry and Molecular Biology Undergraduate Research Symposium, 2011.

PUBLICATIONS

Alekos NS, Moorer MC, Riddle RC. "Dual effects of lipid metabolism on osteoblast function." *Frontiers in Endocrinology* 2020; 11:578194.

Coate TM, **Spita NA**, Zhang KD, Isgrig KT, Kelley MW. "Neuropilin-2/Semaphorin-3F-mediated repulsion promotes inner hair cell innervation by spiral ganglion neurons*." eLIFE* 2015; 10.7554.

Isaacs J, Feher J, Shall M, Vota S, Fox MA, Mallu S, Razavi A, Friebe I, Shah S, **Spita N**. "Effects of nandrolone on recovery after neurotization of chronically denervated muscle in a rat model." *Journal of Neurosurgery* 2013; 119(4): 914-923.